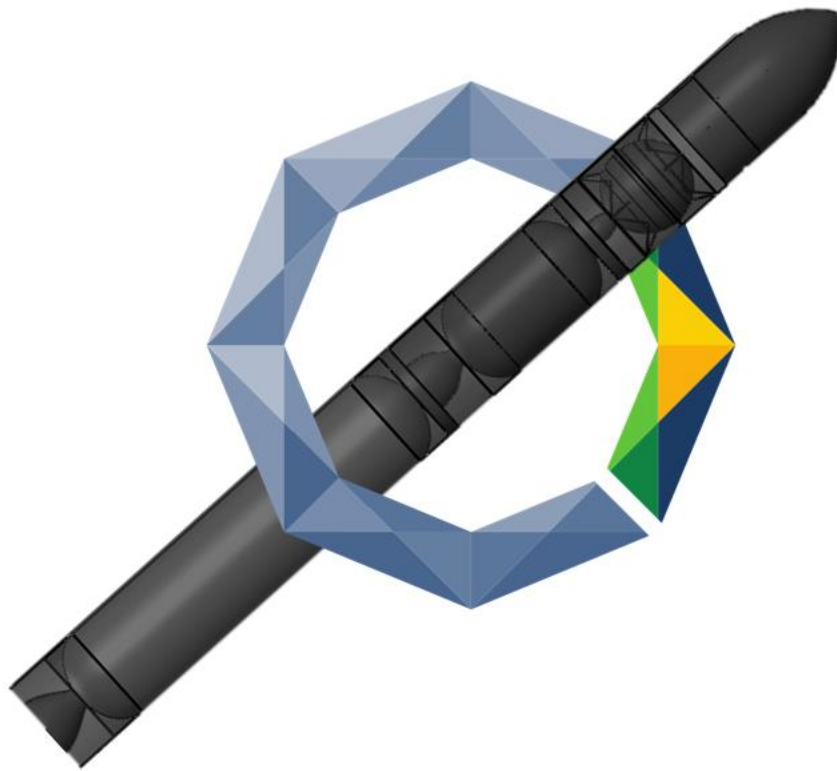


AIAA 2018-2019 Graduate Team Missile Systems Design Competition



Project Lance:

A Modernization of the United States' Intercontinental Ballistic Missile System

Design Proposal by

Joust Aerospace

California State Polytechnic University, Pomona



AIAA Member Numbers and Signatures









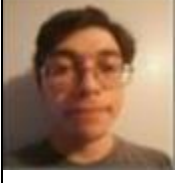


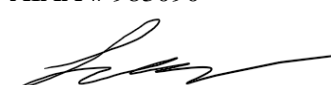



 <p>Rebecca M. Thomas Team Lead AIAA # 750106</p> 	 <p>David R. Hernandez Deputy Lead AIAA # 982944</p> 
 <p>Vishal D. Barkataki Inboard Profile AIAA # 983094</p> 	 <p>Tatsuya M. Danno Propulsion AIAA # 949568</p> 
 <p>Joshua Klyde Mission Design AIAA # 579760</p> 	 <p>Pablo C. Lopez Navigation and Stability AIAA # 983090</p> 
 <p>Jesus David Montes Trajectory AIAA # 890897</p> 	 <p>Dr. Donald Edberg Faculty Advisor AIAA # 22972</p> 

Table of Contents

1.0 Introduction.....	9
1.1 Mission Overview and Driving Requirements	9
1.2 Motivation	9
1.3 ΔV Required.....	10
2.0 Concept of Operations	11
3.0 Overview of Architectures.....	13
3.1 Architecture 1 Overview	13
3.2 Architecture 2 Overview	14
3.3 Architecture Down Select.....	15
4.0 Detailed Design.....	16
4.1 Propellant Selection.....	16
4.2 Optimum ΔV Ratio and Preliminary Mass Estimate.....	17
4.3 Inboard Profile.....	18
4.3.1 Missile Configuration.....	18
4.3.2 Post-Boost Vehicle.....	25
4.3.3 Re-entry Vehicles.....	26
4.3.4 Mass Statement	31
5.0 Performance Assessments.....	32
5.1 Trajectory Analysis.....	32
5.1.1 Free-flight Trajectory and Range Calculation.....	32
5.1.2 Atmospheric Trajectory Assumptions.....	34
5.1.3 Ascent Trajectory Method.....	38
5.1.4 Re-entry Trajectory Method.....	41
5.1.5 Simulation Results.....	43
5.2 Circular Error Probable	49
5.3 Ability to Hit all Targets.....	52
5.3.1 Thrust Termination System.....	52
5.3.2 Optimum Height of Burst.....	54
5.3.3 Deeply Buried Hardened Targets	54
5.3.4 Trajectory Considerations	55
6.0 Systems Analysis	56
6.1 Thermal Protection Systems	56
6.2 Flight Loads.....	57
6.3 Material Selection and Stress Analysis.....	60
6.3.1 Material Selection	60

6.3.2 Stress Analysis	61
6.4 Attitude Control System	62
6.5 Aerodynamic Stability	63
6.5.1 Static Stability	65
6.5.2 Closed Loop Stability	68
6.6 Software and Power Considerations	70
6.7 Reliability	71
6.8 Manufacturing and Maintenance	75
6.8.1 Manufacturing	75
6.8.2 Maintenance.....	75
6.9 Launch System	75
6.9.1 Fixed vs. Mobile Launch System	75
6.9.2 Silo Survivability.....	76
6.10 Mission Safety	78
6.11 Disposal Concepts	78
6.12 End of Mission Repurposing	78
6.13 Cost Analysis	79
6.13.1 United States Air Force Space Planners Guide	79
6.13.2 TRANSCOST Analysis.....	80
6.13.3 Additional Costs and Cost Comparison	81
6.14 Treaty Compliance	82
6.15 Development Schedule	83
6.16 Derived Requirements	84
7.0 Project Schedule.....	85
8.0 Compliance Matrix	86
9.0 Conclusion	87
References.....	88
Appendix A: Using Solver to Optimize ΔV Ratios	90
Appendix B: Trajectory Simulation MATLAB Script Listing	95

List of Figures

Figure 1.3-1 Symmetric Free-Flight Trajectory.....	10
Figure 2.0-1 Concept of Operations Ascent Sketch.....	12
Figure 2.0-2 Concept of Operations Descent Sketch.....	13
Figure 3.1-1 Architecture 1 Drawing.....	14
Figure 3.2-1 Architecture 2 Drawing.....	15
Figure 4.3.1.1-1 Solid Motor Sizing.....	19
Figure 4.3.1.1-2 Nozzle Sizing Drawings.....	20
Figure 4.3.1.1-3 ICBM Component Sizing.....	21
Figure 4.3.1.1-4 General Vehicle Configuration.....	22
Figure 4.3.1.1-5 Step Layout and Separation Planes.....	23
Figure 4.3.1.1-4 Frangible Joint Method courtesy of EBA&D.....	23
Figure 4.3.1.2-1 Payload Configurations.....	24
Figure 4.3.1.2-1 Payload Fairing Separation Method.....	25
Figure 4.3.2-1 Post-Boost Vehicle.....	26
Figure 4.3.3.1-1 Ballistic Re-entry Vehicle Overview.....	27
Figure 4.3.3.2-1 Conical Geometry Parameters for Waverider Sizing.....	28
Figure 4.3.3.2-2 Glide RV 3-D Model.....	29
Figure 4.3.3.2-3 Dimensioned Drawing of Designed Re-Entry Vehicle.....	30
Figure 4.3.3.2-4 Cross Section and Labeled View of Glide RV Internal Layout.....	30
Figure 4.3.4-1 Mass Breakdown without Propellant.....	31
Figure 4.3.4-2 Mass Breakdown with Propellant.....	31
Figure 5.3.1-1 Minuteman III Motor with TTS Assembly.....	53
Figure 5.3.1-2 Overview of Minuteman III TTS.....	53
Figure 5.3.4-1 Launch Velocity Difference for Southern Launch.....	55
Figure 6.2-1 Max-q Shear Loads.....	59
Figure 6.2-2 Max-q Bending Loads.....	59
Figure 6.2-3 Max-q Axial Loads.....	60
Figure 6.4-1 ICBM Attitude Control Block Diagram.....	63
Figure 6.5-1 $C_{N\alpha}$ vs. Mach number.....	64
Figure 6.5-2 C_L vs. Mach number.....	64
Figure 6.5-3 C_N vs. Mach number.....	64
Figure 6.5-4 CP vs. Mach number.....	65
Figure 6.5.1-1 Free Body Diagram of Launch Vehicle.....	66
Figure 6.5.1-2 ICBM Transfer Function.....	66
Figure 6.5.1-3 ICBM Closed Loop Root Locus with Rate Feedback Gain.....	67

Figure 6.5.1-4 ICBM Bode Diagram with Rate Feedback Gain..... 67

Figure 6.5.2-1 PID Controller Transfer Function 68

Figure 6.5.2-2 Root Locus with PID Controller 68

Figure 6.5.2-3 Step Response with PID Controller 69

Figure 6.5.2-4 Bode Diagram with PID Controller 70

Figure 6.7-1 Weibull Bathtub curve depicting 3 life-cycle phases 74

Figure 6.9.2-1 Silo Survivability 76

Figure 6.9.2-2 Probability of Kill Against Minuteman III Silo 77

Figure 7.0-1 Project Schedule 85

Figure A-1 Adding the Solver Add-in to Excel 90

Figure A-2 Launch Vehicle Properties 91

Figure A-3 Optimum Velocity Ratio Table 91

Figure A-4 Optimum Velocity Ratio Formulas 91

Figure A-5 Mass Ratios and GLOM Table..... 92

Figure A-6 Mass Ratios and GLOM Formulas..... 92

Figure A-7 Solver Parameters for a Three-Stage Vehicle 94

Figure A-8 Solver Results..... 94

List of Tables

Table 1.1-1 Driving Requirements.....	9
Table 3.3-1 Architecture Down Select Trade Study	15
Table 4.1-1 Propellant Trade Study	16
Table 4.2-1 Estimation of ΔV Losses	17
Table 4.2-2 Optimum ΔV Ratio.....	18
Table 4.3.1.1-1 Performance Assumptions	18
Table 4.3.1.1-2 Nozzle Sizing Results.....	20
Table 4.3.1.1-3 ICBM Sizing.....	21
Table 4.3.3.1-1 Ballistic Coefficient for Ballistic Re-entry Vehicle.....	27
Table 4.3.3.2-1 Glide Re-Entry Vehicle Mass Summary	29
Table 5.3.2-1 Optimum Height of Burst.....	54
Table 6.2-1 Max-q Parameters.....	57
Table 6.3.1-1 Carbon Epoxy Material Data.....	60
Table 6.3.2-1 Stress Analysis Results.....	61
Table 6.7-1 Electrical System Minimum Component Reliability Requirements.....	72
Table 6.7-2 Solid Propulsion System Minimum Component Reliability Requirements	73
Table 6.7-3 Subsystem Reliability and Total ICBM System Reliability	74
Table 6.9.1-1 Launch System Trade Study.....	76
Table 6.13-1 USAF Space Planners Guide Cost Estimation	80
Table 6.13-1 TRANSCOST Analysis.....	81
Table 6.13.3-1 Cost Estimation Comparison	82
Table 6.13.3-2 Unit Cost Estimation Comparison.....	82
Table 6.16-1 Derived Requirements	84
Table 8.0-1 Compliance Matrix.....	86
Table 9.0-1 ICBM Summary Sheet.....	87

List of Acronyms and Symbols

CEP	Circular Error Probable
CLS	Cold Launch System
CNS	Celestial Navigation System
ΔV	Change in velocity
EMP	Electromagnetic pulse
GPS	Global Positioning System
HoB	Height of Burst
HMX	High Melting Explosive (Octogen)
ICBM	Intercontinental Ballistic Missile
INS	Inertial Navigation System
I_{sp}	Specific Impulse
M	Mach number
Max-q	Maximum dynamic pressure
MMH	Monomethyl hydrazine
NTO	Nitrogen Tetroxide
PBV	Post-Boost Vehicle
RFP	Request for Proposals
RV	Re-entry Vehicle
TRL	Technical Readiness Level

1.0 Introduction

1.1 Mission Overview and Driving Requirements

The purpose of the competition was to design a long-range strategic missile system, or ICBM, capable of carrying two, independently guided, 1000 lb_m nuclear payloads with an objective range of 10,000 nmi (18,500 km). The payloads must be able to hit both soft targets, like cities, and deeply buried hardened targets, like a military bunker.

Table 1.1-1 outlines the driving requirements listed in the AIAA RFP. A full list of systems level requirements is provided in Section 8.0 Compliance Matrix.

Table 1.1-1 Driving Requirements

Driving Requirements		
Metric	Threshold	Objective
Maintenance	Minimum 20 years without maintenance	
Range	7,000 nmi (13,000 km)	10,000 nmi (18,500 km)
Flight Time	90 min	60 min
Circular Error Probable (CEP)	150 ft (45.7 m)	100 ft (30.5 m)
Launch Site Integration	Minuteman III silo <u>or</u> mobile launcher	
Payload Size	Each payload has a weight of 1000 lb _m (454 kg) with a 22 in (0.559 m) diameter and 80 in (2.03 m) length	

1.2 Motivation

The Minuteman III has been in use by the United States Air Force since it was first deployed in 1970. For about twenty years, the Peacekeeper missile was also put into use, but has since been disposed, so the 450 Minuteman III missiles are the only remaining component of the land-based portion of the nuclear triad as they approach 50 years in service. In the 50 years since their deployment, the technology on the Minuteman missiles has aged considerably as costs to maintain many of the systems on the missile have

grown too high. The United States needs a reliable nuclear deterrent on land, air, and sea, and the Minuteman III must be replaced with a newer system to maintain that reliability.

1.3 ΔV Required

The first step of the design process was to calculate the ΔV required to complete the worst-case launch scenario. This was to a target at the objective range of 10,000 nmi (18,520 km) and a burnout height of 86.4 nmi (160 km). It was also launched completely due west ($\beta = 270^\circ$) from a latitude of 32.7° N. A symmetric trajectory was assumed ($h_{bo} = h_{re-entry}$) and that the total range angle was equal to the free-flight range angle. This is depicted in Figure 1.3-1 which was obtained from *Fundamentals of Astrodynamics* (Ref 1.3-1).

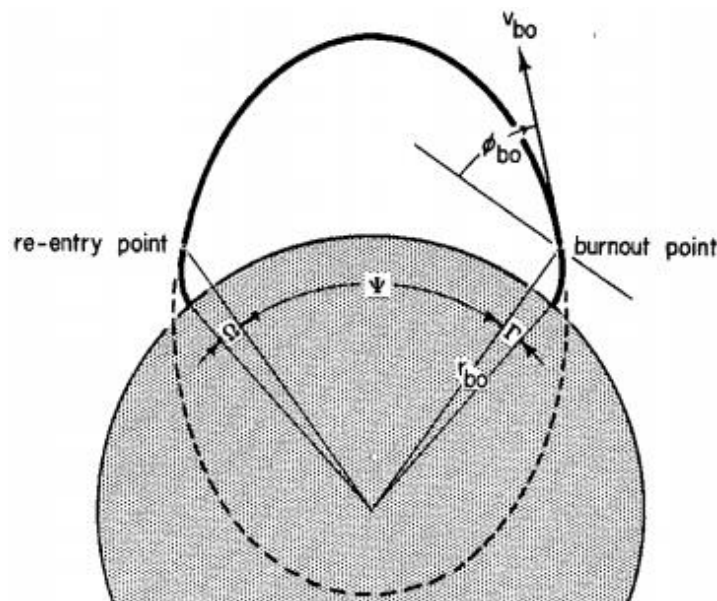


Figure 1.3-1 Symmetric Free-Flight Trajectory

The total ΔV required was calculated using Equation 1.3-1.

$$\Delta V_{req} = \Delta V_{bo} + \Delta V_{launch\ site} + \Delta V_{grav} + \Delta V_{drag} + \Delta V_{steer} \quad \text{(Equation 1.3-1)}$$

Where it was assumed that $\Delta V_{grav} = 3.61$ kft/s (1.1 km/s), $\Delta V_{drag} = 0.15$ kft/s (0.046 km/s), $\Delta V_{steer} = 0.11$ kft/s (0.034 km/s), and $\Delta V_{launch\ site} = 1.27$ kft/s (0.387 km/s). The ΔV at burnout, ΔV_{bo} , was calculated using Equations 1.3-2 and 1.3-3.

$$\Delta V_{bo} = \sqrt{Q_{bo} V_c^2}, V_c = 25.6 \text{ kft/s (7.79 km/s)} \quad (\text{Equation 1.3-2})$$

$$\sin\left(\frac{\varphi_{max}}{2}\right) = \frac{Q_{bo}}{2 - Q_{bo}} \quad (\text{Equation 1.3-3})$$

Given that 10,000 nmi (18,520 km) is equal to a 90° range angle, $\psi_{max} = 166.7^\circ$, and $Q_{bo} = 0.997$. This results in ΔV_{bo} of 26 kft/s (7.8 km/s) and a ΔV_{req} of 31 kft/s (9.3 km/s).

2.0 Concept of Operations

The operation of Project Lance will be broken up into several phases in a tactical scenario. These phases consist of the launch initiation, pre-launch, launch, ascent, and the descent phase terminated by the impact on target.

The launch initiation will be started with a presidential order to launch the ICBMs. Next, a quick, approximately 30 second, consultation and authorization to launch will occur, followed by the order to launch being sent to the designated command post(s) which should take approximately 2-3 minutes.

During pre-launch, the control center(s) will receive the order to launch and two of the designated crew members will verify the launch within 1 minute. Once authenticated, the crew members will turn the keys to initiate the launch, 30 seconds after the confirmation of the launch codes.

The launch sequence will be initiated with a final flight-readiness check and a start-up of the INS, this initial step shall take no longer than 2 minutes and will be immediately followed by the pressurization of the cold launch system (CLS). The silo doors will then open and once the CLS is pressurized, the electrical umbilicals will disconnect. Immediately after the missile clears the silo opening, the first step motor will ignite, and the ascent phase will begin.

A cold launch system is necessary for launch because of the ICBM's size. A reinforced steel canister houses the missile. A launch ejection gas generator is at the bottom of the canister which contains a small rocket motor fired into 100+ gallons of water. This generates steam pressure that pushes the ICBM out of

the canister. Teflon-coated urethan pads are used to protect and smoothly guide the missile during ejection.

During the ascent phase the missile will sequentially fire each step as shown in Figure 2.0-1

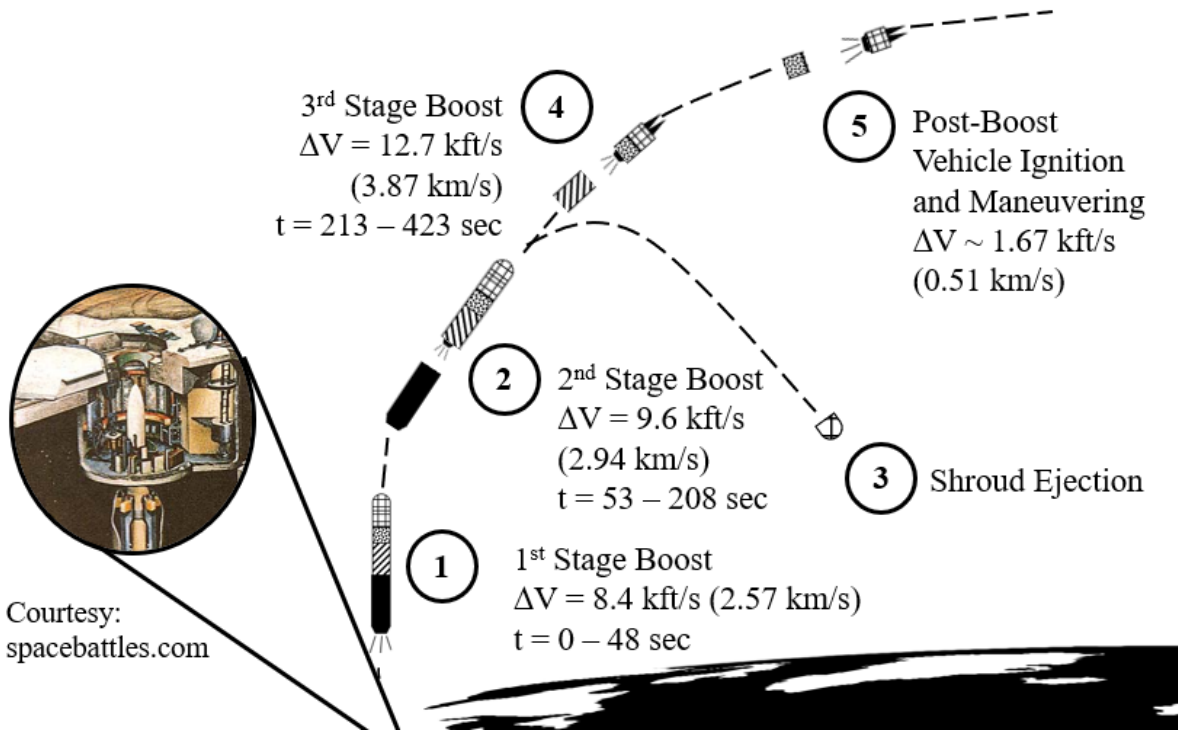


Figure 2.0-1 Concept of Operations Ascent Sketch

The missile is designed to have a 5 second delay between the separation of one step and the ignition of the following step's motor. The post-boost vehicle (PBV) will ignite and begin maneuvering to orient its warheads approximately 428 seconds after launch. After the PBV has positioned itself in the appropriate fashion for each warhead, they will be released, and the descent phase of the operation begins as shown in Figure 2.0-2.

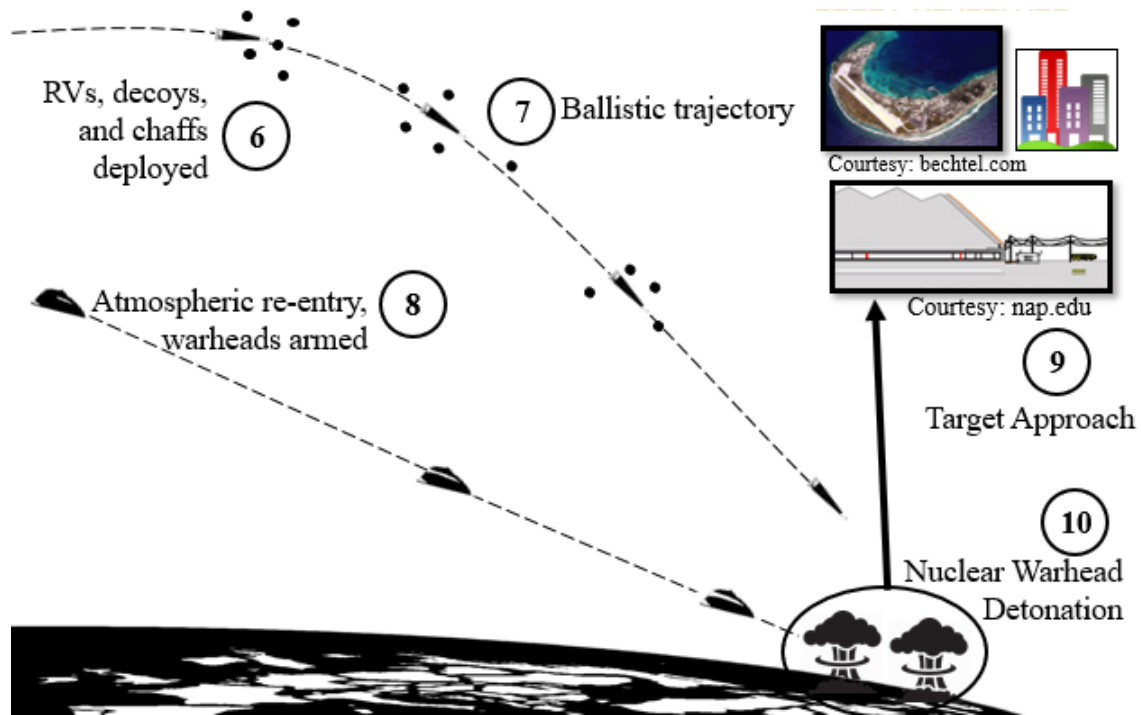


Figure 2.0-2 Concept of Operations Descent Sketch

The warheads will be released and travel to their respective targets on board either a ballistic re-entry vehicle (RV) or a hypersonic glide RV. Depending on the target type, the warhead detonation will occur at different altitudes to ensure the most effective execution of mission.

3.0 Overview of Architectures

3.1 Architecture 1 Overview

Architecture 1 is a two-stage, liquid-fueled ICBM. The ICBM utilizes both celestial and inertial navigation systems (CNS & INS). The RVs will use GPS and INS navigation systems. Hypergolic propellants, specifically MON-3/MMH were selected since it has a higher specific impulse than solid motors. Despite the performance boost, hypergolic propellants require more complex engine systems to transfer liquid propellants and are more toxic which requires more investment in safety, handling procedures, and maintenance thus increasing the development cost. To mitigate the cost issue, the liquid-fueled ICBM will be constructed using standard proven materials such as aluminum and steel. In addition,

Architecture 1 will only house conventional ballistic RVs. These changes will lower the cost and risk associated with using hypergolic propellants by limiting the amount of potential failure points as a result of implementing modern technologies.

Figure 3.1-1 show a CAD drawing of Architecture 1.

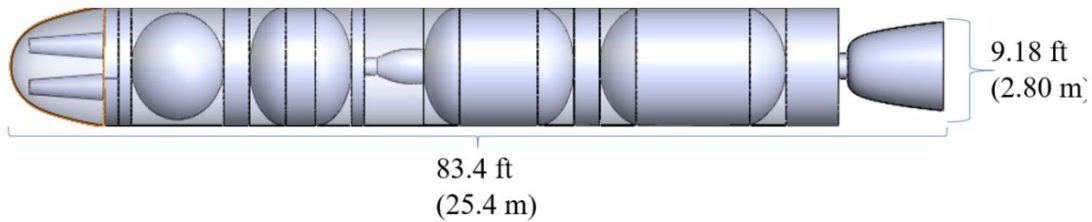


Figure 3.1-1 Architecture 1 Drawing

The required ΔV for this architecture is 30.6 kft/s (9.32 km/s).

3.2 Architecture 2 Overview

Architecture 2 is a three-stage, solid-fueled ICBM. The ICBM uses celestial and inertial navigation systems (CNS & INS). The RVs have both GPS and INS. The use of solid propellants allows for lower cost to develop and manufacture. It is constructed using composites to reduce the gross liftoff mass. All ICBMs will be launched using existing Minuteman III silos. This also helps lower the development and maintenance costs.

Furthermore, it includes both a conventional and gliding RV to improve survivability against enemy countermeasures. The glide RV avoids the post-boost and midcourse phases which would allow it to circumvent space-based ballistic missile defense systems. The ballistic RV would be less susceptible to air defenses that target glide RVs (Ref 3.2-1). Thus, the enemy would need to have both systems which increases costs.

Figure 3.2-1 shows a CAD drawing of Architecture 2.

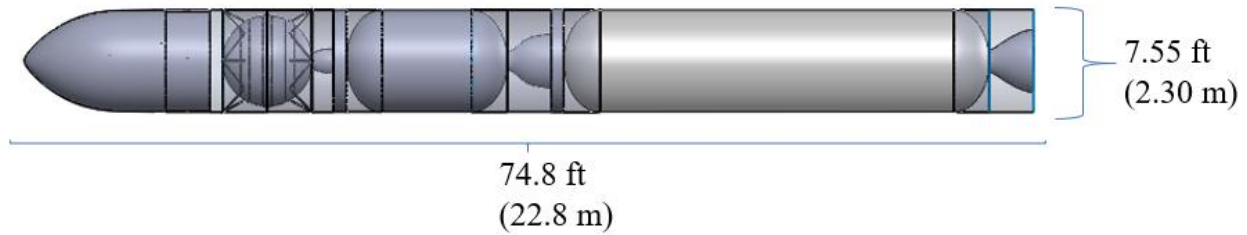


Figure 3.2-1 Architecture 2 Drawing

The required ΔV for this architecture is 30.8 kft/s (9.36 km/s).

3.3 Architecture Down Select

A trade study was completed in order to down select the architectures. The criteria of the trade study were the ability to meet the maintenance requirement, the cost per vehicle, and the ICBM diameter and length.

The trade study is shown in Table 3.3-1.

Table 3.3-1 Architecture Down Select Trade Study

Architecture Down Select Trade Study		
Criteria	Architecture 1	Architecture 2
Capable of no maintenance for 20 years?	No, high likelihood that NTO tanks would require maintenance	Yes, solid motors are capable of long-term storage without maintenance
Cost per vehicle	\$74.4 million (2019 dollars)	\$21.6 million (2019 dollars)
ICBM diameter	9.2 ft (2.8 m), less than 1.6 ft (0.5 m) between ICBM and launch canister which limits space for ground support equipment and personnel	7.55 ft (2.3 m), same diameter as the Peacekeeper
ICBM length	83.3 ft (25.4 m), length of Peacekeeper launch canister is 85.0 ft (25.9 m) so there is limited room for size increase	74.8 ft (22.8 m), length of the vehicle can increase by 10.2 ft (3.1 m) and still fit in launch canister

Architecture 2, the three-stage, solid ICBM was selected for further design work and will be the focus of the remainder of this proposal. It can be launch-ready at a moment’s notice without maintenance for over 20 years. Its use of solid motors results in a cost-effective ICBM, and its smaller size allows for future growth if analysis indicates an increase in size is needed.

4.0 Detailed Design

4.1 Propellant Selection

Solid propellants were selected for use because of their ease and safety of transport compared to liquid propellants. They also would occupy less volume than liquid propellants because of their high density. A trade study was conducted to choose between CMBD/HMX, PBAN/AP/Al, and a solid fuel ramjet. The trade study criteria are outlined below:

- I_{sp} – A higher I_{sp} will result in a lighter ICBM for a given required ΔV
- $I_{sp, vol}$ – The higher the volumetric specific impulse, the smaller the required propellant volume
- Storability – Motors must be storable without maintenance for at least 20 years
- Plume signature – Low plume signature helps to reduce the risk of early detection by reducing the infrared signature
- Technical Readiness Level (TRL) – A high TRL is needed to provide the reliability required by an ICBM

The propellant trade study is shown in Table 4.1-1.

Table 4.1-1 Propellant Trade Study

Propellant Trade Study			
	CMBD/ HMX	PBAN/AP/Al	Solid Fuel Ramjet
Sea Level I_{sp} (s)	270	242	1,000
Vacuum I_{sp} (s)	300	270	N/A
Density (lb/ft ³)	112	84.3	111
Sea Level $I_{sp, vol}$ (s)	486	327	1,770
Vacuum $I_{sp, vol}$ (s)	540	354	N/A
Storability (years)	25	25	25
Plume Signature	Med (min. smoke)	High	Low
TRL	9 (Actual system proven through successful mission operations)	9	7 (System prototype demonstration in an operational environment)

Information for CMBD/HMX was obtained from Ref 4.1-1, PBAN/AP/Al from Ref 4.1-2, and the solid fuel ramjet from Ref 4.1-3.

The final propellant selection is a solid propellant formulation similar to NEPE-75, which is used for all three stages of the Trident missile. It contains 75% fuel, including octogen (HMX), aluminum (Al), and ammonium perchlorate (AP). The binder is nitrate ester-plasticized polyethylene glycol (NEPE), and the plasticizer is nitroglycerin (NG). HMX is a powerful and insensitive high explosive, and by replacing most of the AP, the I_{sp} is increased (Ref 4.1-4). NEPE is more flexible than HTPB which allows for a high percentage of solid fuel (Ref 4.1-4). Finally, infrared irradiance can be reduced by adding potassium salt to the propellant (Ref 4.1-5)

4.2 Optimum ΔV Ratio and Preliminary Mass Estimate

The optimum ΔV ratio for the ICBM was found using Excel’s solver tool (see Appendix A). The drag, gravity, and steering losses were split unevenly between the stages (Table 4.2-1). This results in a more realistic distribution of ΔV losses.

Table 4.2-1 Estimation of ΔV Losses

Estimation of ΔV Losses				
	Total	1st Stage	2nd Stage	3rd Stage
ΔV_{grav} , ft/s (m/s)	3,610 (1,100)	2,640 (803)	722 (220)	253 (77)
ΔV_{drag} , ft/s (m/s)	131 (40)	125 (38)	6.6 (2)	0
ΔV_{steer} , ft/s (m/s)	98 (30)	3 (0.9)	92 (28)	3 (0.9)

Excel Solver minimized gross liftoff mass by varying the three velocity ratios. Then, the mass ratios were calculated by each stage’s ΔV . Table 4.2-2 outlines the optimum ΔV of each stage.

Table 4.2-2 Optimum ΔV Ratio

Optimum ΔV Ratio		
		Fraction of Total ΔV
$\Delta V_{1,}$ ft/s (m/s)	8,432 (2,570)	28%
$\Delta V_{2,}$ ft/s (m/s)	9,823 (2,944)	31%
$\Delta V_{3,}$ ft/s (m/s)	12,880 (3,867)	41%
$\Delta V_{total,}$ ft/s (m/s)	30,710 (9,361)	

The estimated gross liftoff mass, calculated using the mass ratios, was 115 Ton (104 Tonne).

4.3 Inboard Profile

4.3.1 Missile Configuration

4.3.1.1 Missile Sizing and Overview

The inboard profile of the ICBM itself followed the method outlined in *Elements of Space Launch Vehicle Design* (Ref 4.3.1-1). A body diameter of 7.55 ft. (2.3m) was selected due to the fact it is the same diameter as the Peacekeeper which can fit and be cold launched from existing Minuteman III silos as required by the request for proposal. The assumptions made are listed in Table 4.3.1.1-1.

Table 4.3.1.1-1 Performance Assumptions

Performance Assumptions			
Item	Step 1	Step 2	Step 3
T/W	2.3	1.25	1
I_{sp} (s)	270	285	300

Next the solid motor casings were sized, and the final results are shown in Figure 4.3.1.1-1. Assumptions made include elliptical domes, the inner diameter and outer diameter difference is negligible, an additional 10% propellant volume and 2% propellant ignitor volume were accounted for, and no start up time.

$$Vol_{propellant} = \frac{m_{propellant}}{\rho_{propellant}} \quad (\text{Equation 4.3.1-1})$$

$$Vol_{casing} = 1.12Vol_{propellant} \quad (\text{Equation 4.3.1-2})$$

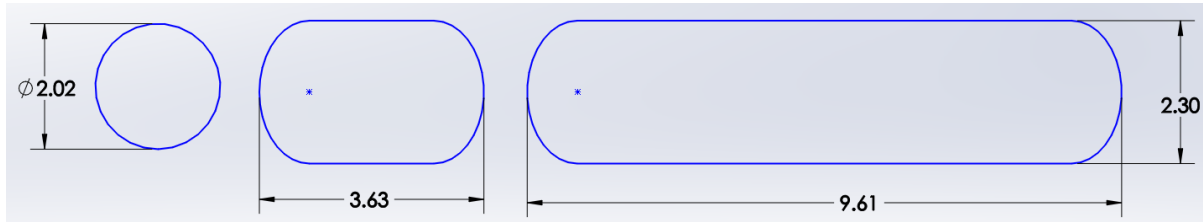


Figure 4.3.1.1-1 Solid Motor Sizing

The motor nozzles were sized, and the final results are shown in Table 4.3.1.1-2 and Figure 4.3.1.1-2.

$$L_{nozzle} = (D_{exit} - D_{throat})(\%length)(\tan 15^\circ) \quad (\text{Equation 4.3.1-3})$$

$$L_{comb\ chamber} = \left[\frac{4(L^*)(A_{throat})(LthRatio_{chamber})}{\pi} \right]^{\frac{1}{3}} \quad (\text{Equation 4.3.1-4})$$

$$D_{chamber} = \frac{L_{comb\ chamber}}{LthRatio_{chamber}} \quad (\text{Equation 4.3.1-5})$$

$$L_{conv\ section} = \frac{(D_{chamber} - D_{throat})}{[2\tan(\alpha_{conv\ section})]} \quad (\text{Equation 4.3.1-6})$$

Table 4.3.1.1-2 Nozzle Sizing Results

	Step 1	Step 2	Step 3	Comments
(T/W)	2.30	1.25	1.00	Similar to Peacekeeper
W, Ton (Tonne)	102 (104)	32.5 (33.0)	9.08 (9.23)	
T _{SL} , kips (kN)	526 (2,340)	90.8 (404)	20.3(90.5)	
P _c , atm (MPa)	78 (7.90)	78 (7.90)	78 (7.90)	Chamber pressure, average of Castor 120 (mod. Peacekeeper 1st stage)
ε _{nozzle}	12.0	12.0	12.0	LR 87
T _{Vac} , kips (kN)	611 (2,720)	107 (474)	20.3 (90.5)	
D _t , ft (m)	2.07 (0.630)	0.886 (0.270)	0.467 (0.130)	
D _e , ft (m)	7.12 (2.17)	3.05 (0.930)	1.48 (0.450)	
L _{nozzle} , ft (m)	7.81 (2.38)	3.64 (1.11)	1.94 (0.590)	
L _{conv} , ft (m)	0.262 (0.08)	0.394 (0.12)	0.328 (0.10)	30 deg angle

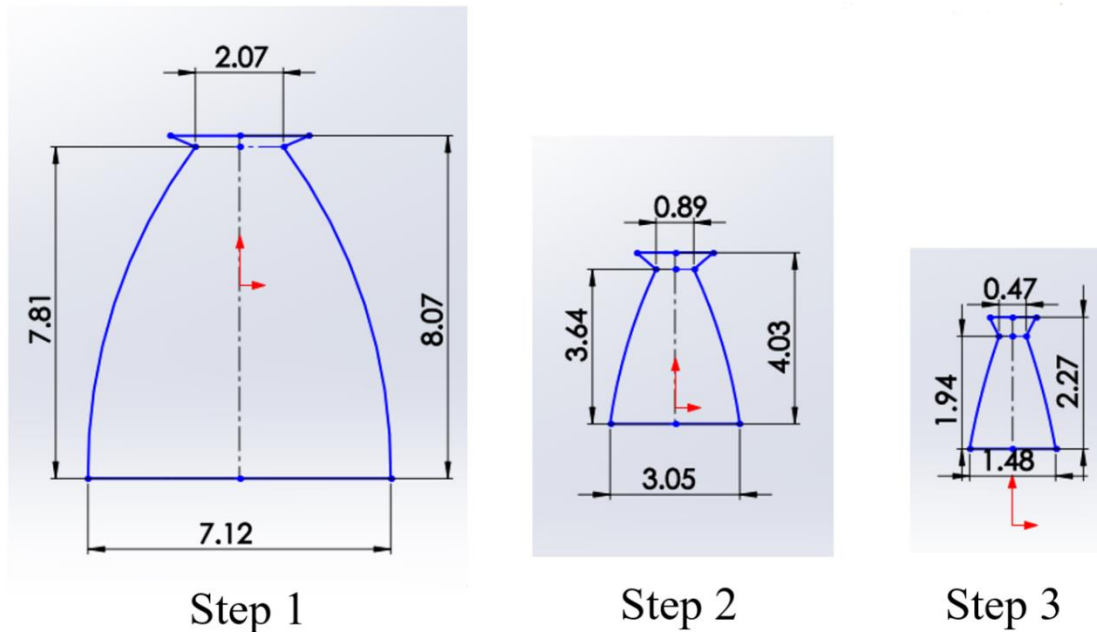


Figure 4.3.1.1-2 Nozzle Sizing Drawings

Figure 4.3.1.1-3 was used to size various miscellaneous components of the ICBM including the interstages, thrust structures, and fairings (Ref 4.3.1-1). Finally, a spreadsheet was created to show the finalized length of each part of the ICBM's inboard profile as show in Table 4.3.1.1-3.

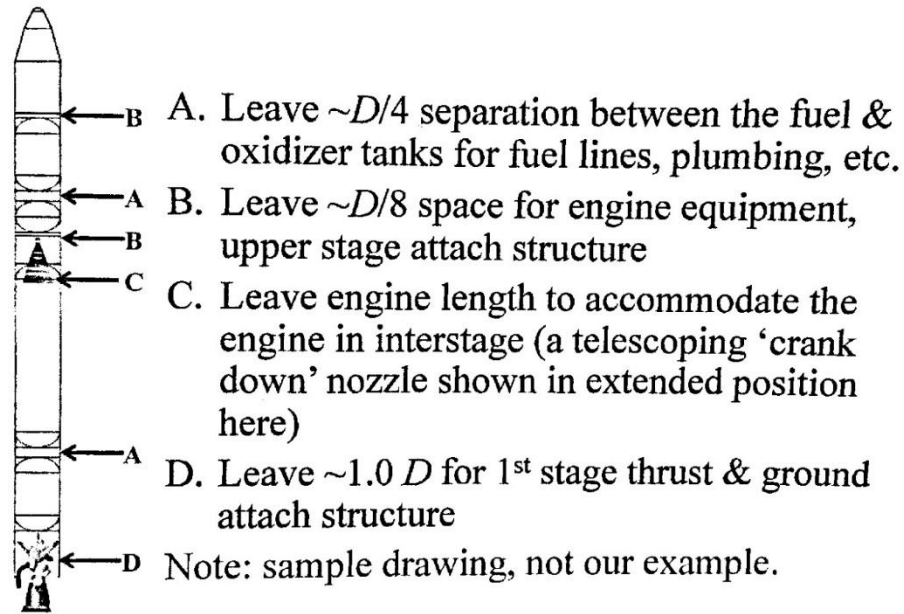


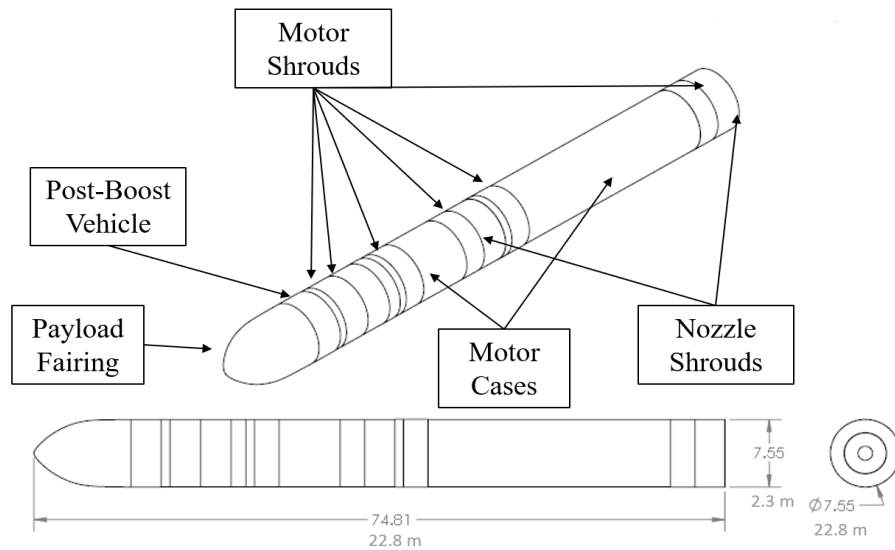
Figure structsize. Other required spaces and volumes on a typical LV.

Figure 4.3.1.1-3 ICBM Component Sizing

Table 4.3.1.1-3 ICBM Sizing

Item	Length ft (m)	Item	Length ft (m)
Payload fairing	10.5 (3.20)	Step 2 lower dome shroud	2.67 (0.81)
Payload + PAF	0.00 (0.00)	Step 2 gimbal	0.00 (0.00)
PBV	3.28 (1.00)	Step 2 nozzle shroud	3.25 (0.99)
Payload separation shroud	0.94 (0.29)	Step 2 nozzle	3.25 (0.99)
Step 3 upper dome shroud	3.32 (1.01)	Step 2 separation shroud	0.94 (0.29)
Step 3 Solid Motor Casing	6.64 (2.02)	Step 1 upper dome shroud	2.67 (0.81)
Step 3 lower dome shroud	3.32 (1.01)	Step 1 Solid Motor Casing	31.54 (9.62)
Step 3 gimbal	0.00 (0.00)	Step 1 lower dome shroud	2.67 (0.81)
Step 3 nozzle shroud	1.58 (0.48)	Step 1 ground attach shroud	3.25 (0.99)
Step 3 nozzle	1.58 (0.48)	Step 1 gimbal	0.00 (0.00)
Step 3 separation shroud	0.94 (0.29)	Step 1 nozzle	3.25 (0.99)
Step 2 upper dome shroud	2.67 (0.81)	Avionics	0.00 (0.00)
Step 2 Solid Motor Casing	11.94 (3.64)	Wiring	0.00 (0.00)

A general vehicle configuration can be seen in Figure 4.3.1.1-4 and Figure 4.3.1.1-5 shows the step layout and separation planes for each step. A Hollow-Form Frangible Joint method will be implemented for the stage separation method as shown in Figure 4.3.1.1-6. This method was selected since it is a proven and tested method by Ensign-Bickford Aerospace & Defense Company that is cost effective and allows improved reliability reducing the dependence on precision machining. Essentially when the inner sleeve expands the metal will fracture on both sides when stage separation is determined by the flight computer.



All dimension in feet
unless otherwise stated

Figure 4.3.1.1-4 General Vehicle Configuration

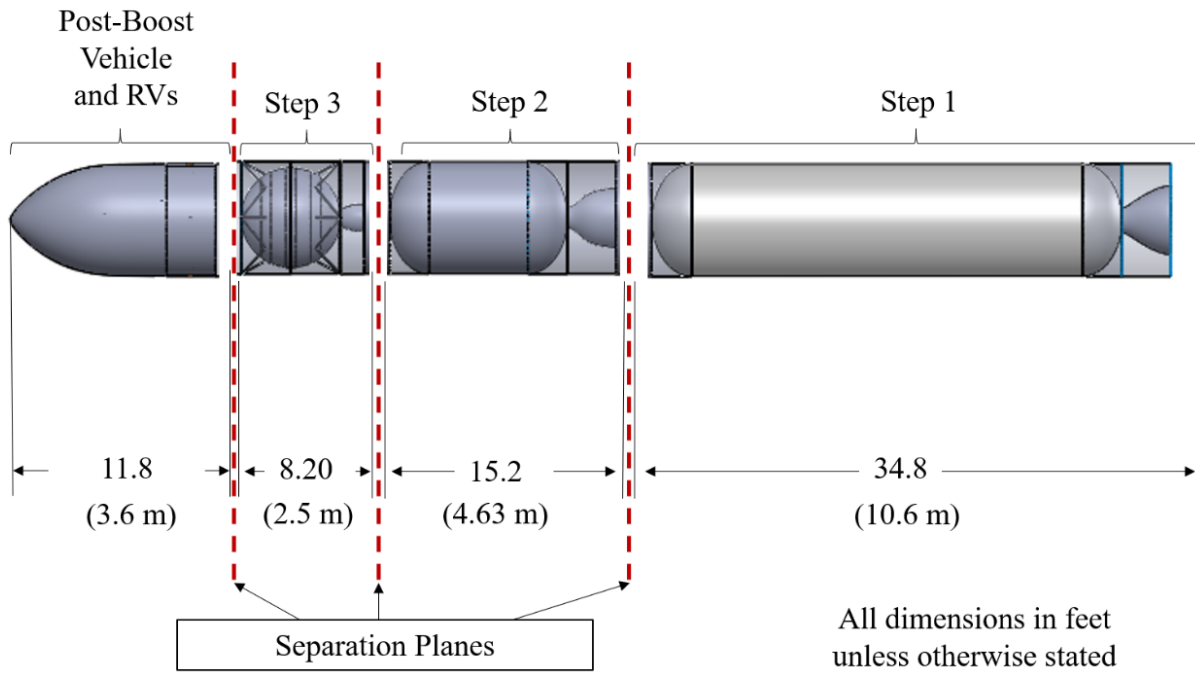


Figure 4.3.1.1-5 Step Layout and Separation Planes

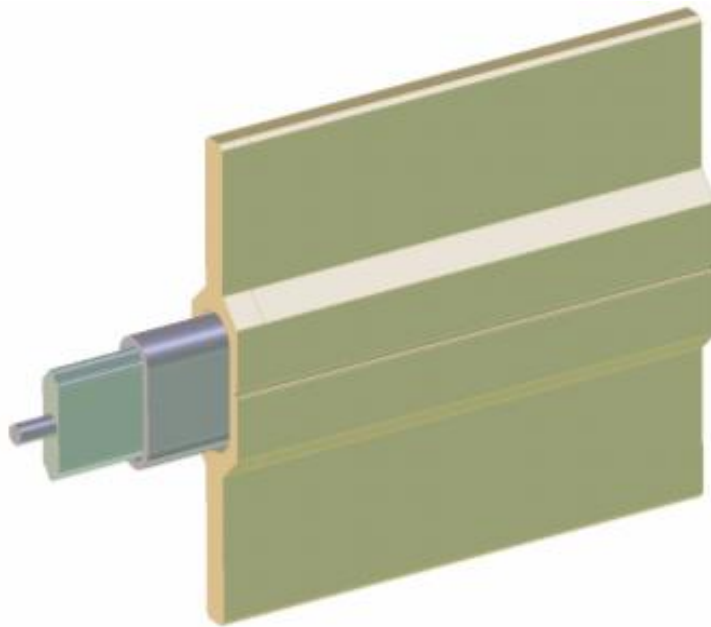


Figure 4.3.1.1-4 Frangible Joint Method courtesy of EBA&D

4.3.1.2 Payload Configuration

The ICBM is designed to have multiple payload bay configurations as depicted in Figure 4.3.1.2-1. The left most figures show the minimum payload configuration as defined by the RFP. The ICBM is designed to carry either ballistic or glide RVs or a combination of the two. For this report, the rightmost configuration will be analyzed which consists of one glide RV and two ballistic RVs, but one of the ballistic RVs will be a decoy in order to be treaty compliant. A Flexible Confined Detonating Cord with thrusting separation rails will be used to release deploy the fairing. Redundant detonators of equal length will be placed in order to increase reliability as shown in Figure 4.3.1.2-2.

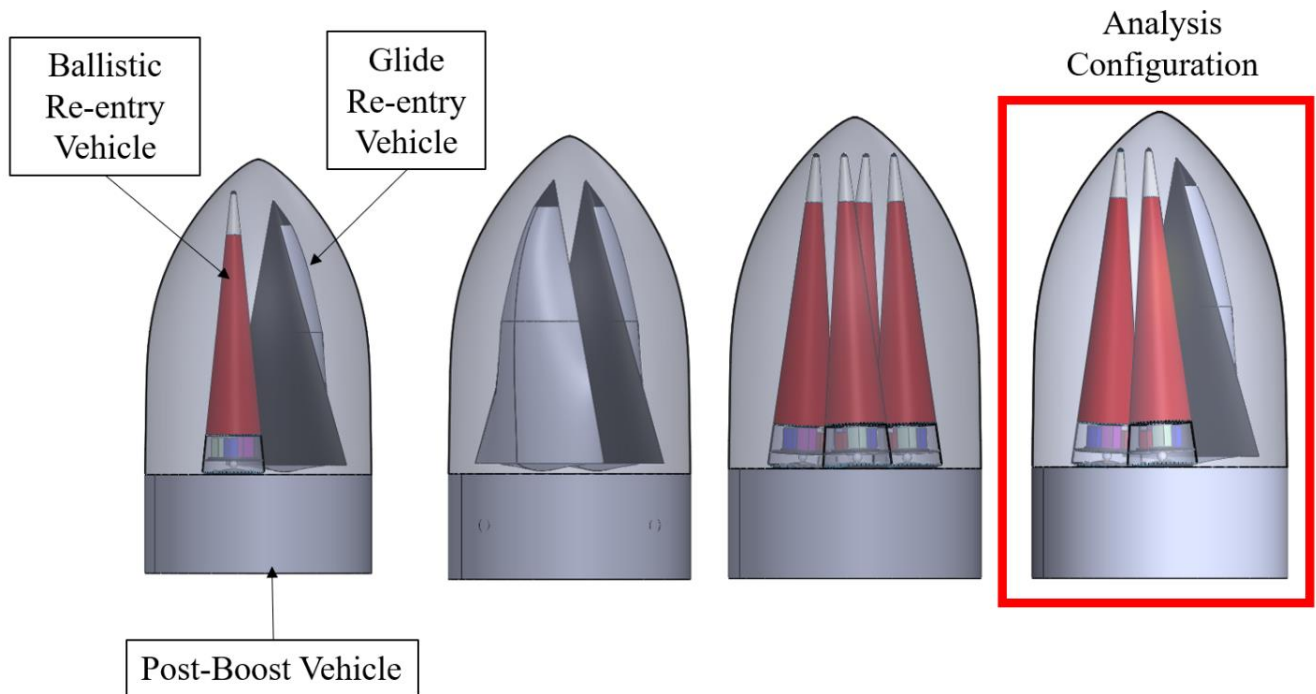


Figure 4.3.1.2-1 Payload Configurations

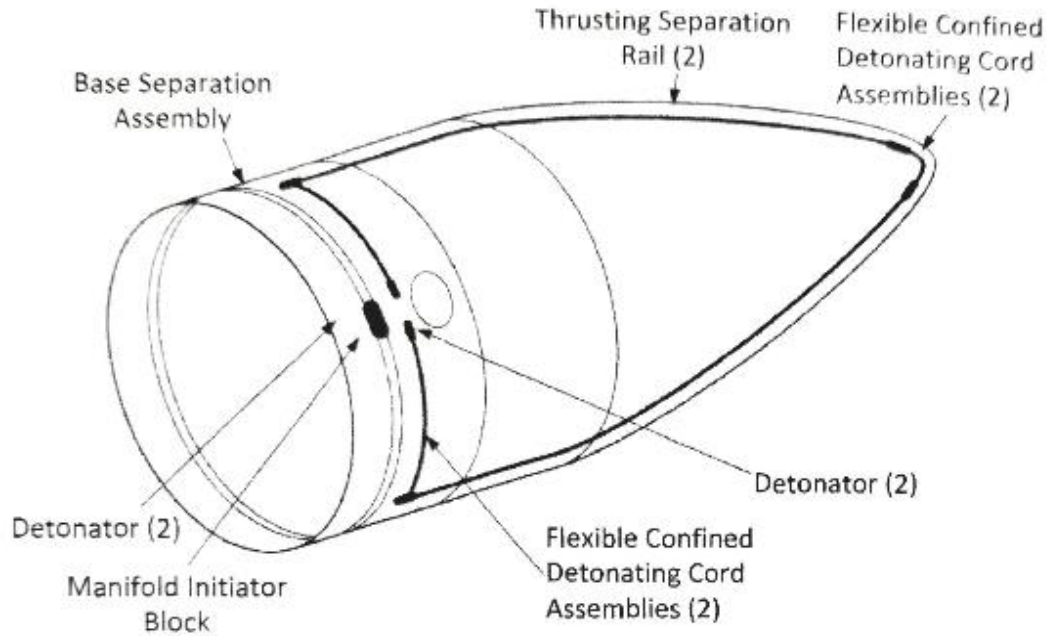


Figure 4.3.1.2-1 Payload Fairing Separation Method

4.3.2 Post-Boost Vehicle

The PBV is used to deploy the RVs and any decoys to different targets by providing precise attitude and velocity changes. The ΔV of the PBV is 1.67 kft/s (510 m/s). This was determined by the 100 nmi (186 km) footprint between the RV impact points. The calculated value was multiplied by six to allow for trajectory corrections and to reduce the accumulated error before RV release.

The PBV has NTO as an oxidizer and MMH as fuel. It includes an axial engine capable of thrust vectoring and eight attitude control engines. Figure 4.3.2-1 illustrates the inboard profile of the PBV. The units of the drawing are in feet.

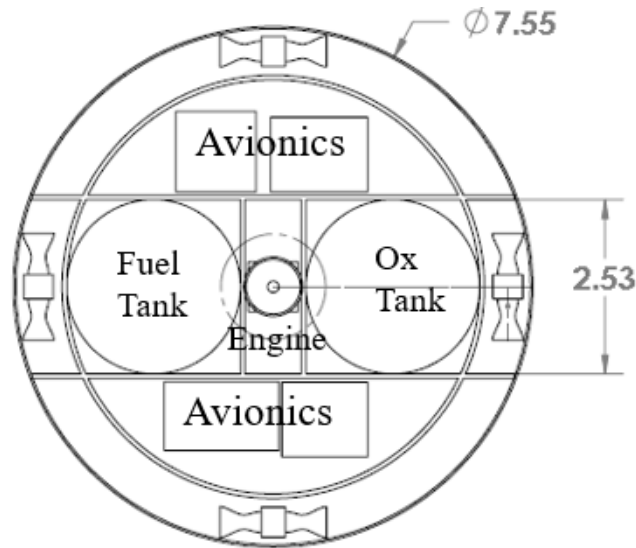


Figure 4.3.2-1 Post-Boost Vehicle

4.3.3 Re-entry Vehicles

Note that the term “payload” is used as the portion of the re-entry vehicle which includes the actual warhead, fuses, and arming devices. The RV encompasses the payload, avionics (including GPS), control actuators, motors, and any thermal protection system. The payload dimensions given by the proposal were significantly larger than that of the current Minuteman III W87 warheads, so a new RV design was considered. A conventional ballistic conical RV and a non-conventional glide vehicle were designed.

4.3.3.1 Ballistic Re-entry Vehicle

The ballistic RV (BRV) utilizes a shape based off previous RVs used on ICBMs. It has a conical shape with spherical blunt at the top. The material used is a hybrid ablative heat-resistant phenolic carbon-carbon. Kick motors are included to improve survivability and decrease time to target. Spin motors are included to improve accuracy and gyroscopic inertia. A diagram showing the layout and lengths of the vehicle is shown in Figure 4.3.3.1-1.

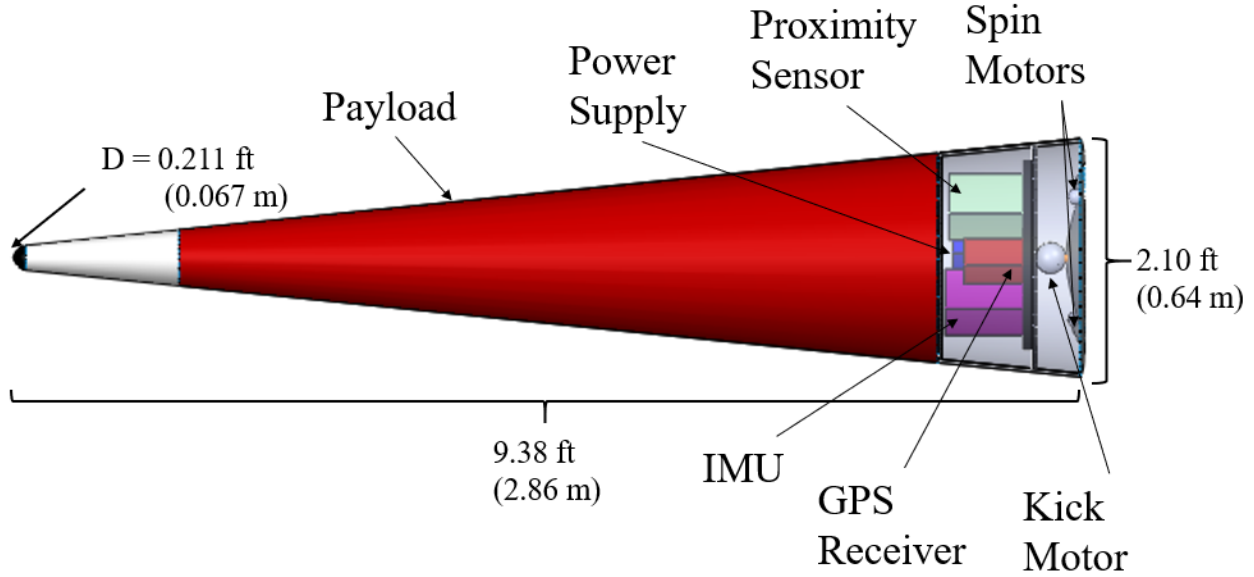


Figure 4.3.3.1-1 Ballistic Re-entry Vehicle Overview

The total mass of the re-entry vehicle is 1350 lb_m, of which 1000 lb_m is the payload. The ballistic coefficient was found to range from 0.43 to 0.92 atm, depending on the drag experienced by the vehicle.

The table below list the figures used for calculating the ballistic coefficient.

Table 4.3.3.1-1 Ballistic Coefficient for Ballistic Re-entry Vehicle

Ballistic Coefficient	
Min C _D	0.2
Max C _D	0.43
Area (ft ²)	3.46
Mass (lb _m)	1353
Max β (atm)	0.92
Min β (atm)	0.43

4.3.3.2 Hypersonic Glide Re-entry Vehicle

To have optimal maneuverability and glide potential, the waverider geometries were considered when designing the hypersonic glide RV. For this preliminary design, many assumptions were made and a baseline, non-optimized model was created. To begin, an assumption that the oncoming flow is deflected by a conical shock attached to the cone apex is made. If a body is considered which consists of only the lower portion of such a cone, the body will have the shape of a delta wing with a curved lower surface. (Ref 4.3.3.2-2). An overall shock cone was sized based on the estimated size of the re-entry vehicle. From here the remaining geometry was sized by constraining the cone angle and varying the cone and arc length of the trailing edge. The variables and initial parameters are shown in Figure 4.3.3.2-1 below.

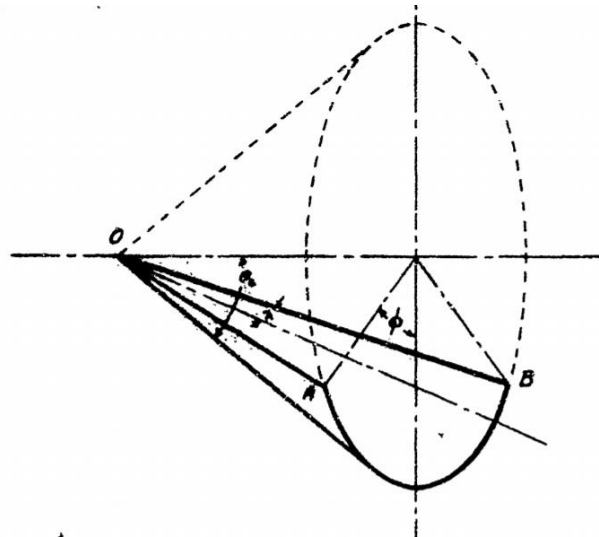


Figure 4.3.3.2-1 Conical Geometry Parameters for Waverider Sizing

From these assumptions, the lift to drag ratio of the sharp conical configuration of the figure above can be obtained as the ratio of surface area projected on a horizontal plane to that projected on a vertical plane normal to the flow. The lift to drag ratio becomes:

$$\frac{L}{D} = \left[\frac{1}{\tan \theta_c} \right] \left[\frac{\sin \phi}{\phi} \right] \quad \text{(Equation 4.3.3.2-1)}$$

where θ_c is the cone half-angle and ϕ is the meridian half-angle.

The L/D for a vehicle designed to optimally fit the given payload has the following parameters:

$\theta_c = 25^\circ$ and $\phi = 45^\circ$ which yields a L/D of 1.86.

Once the general shape and geometry were designed, space was allocated for components and sized based on typical avionics systems and data based off of ballistic RV components. Figures 4.3.3.2-2, 4.3.3.2-3, and 4.3.3.2-4 are the 3-D model, dimensioned view, and a cross-sectional view of the RV.

Table 4.3.3.2-1 Glide Re-Entry Vehicle Mass Summary

Glide Re-Entry Vehicle Mass Summary		
	Weight	Unit
Airframe	122	lb _m
Ablative shielding	10.5	lb _m
Ballast	157	lb _m
IMU/GPS	44.1	lb _m
Actuator	110	lb _m
Flight Computer & Mounting	4.41	lb _m
Control Surface(s)	11.0	lb _m
Payload	1000	lb _m
Total	1340	lb_m

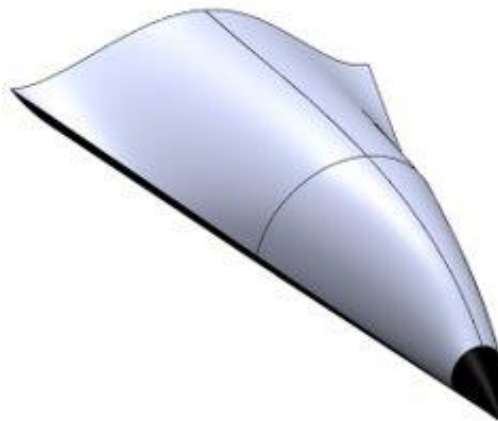


Figure 4.3.3.2-2 Glide RV 3-D Model

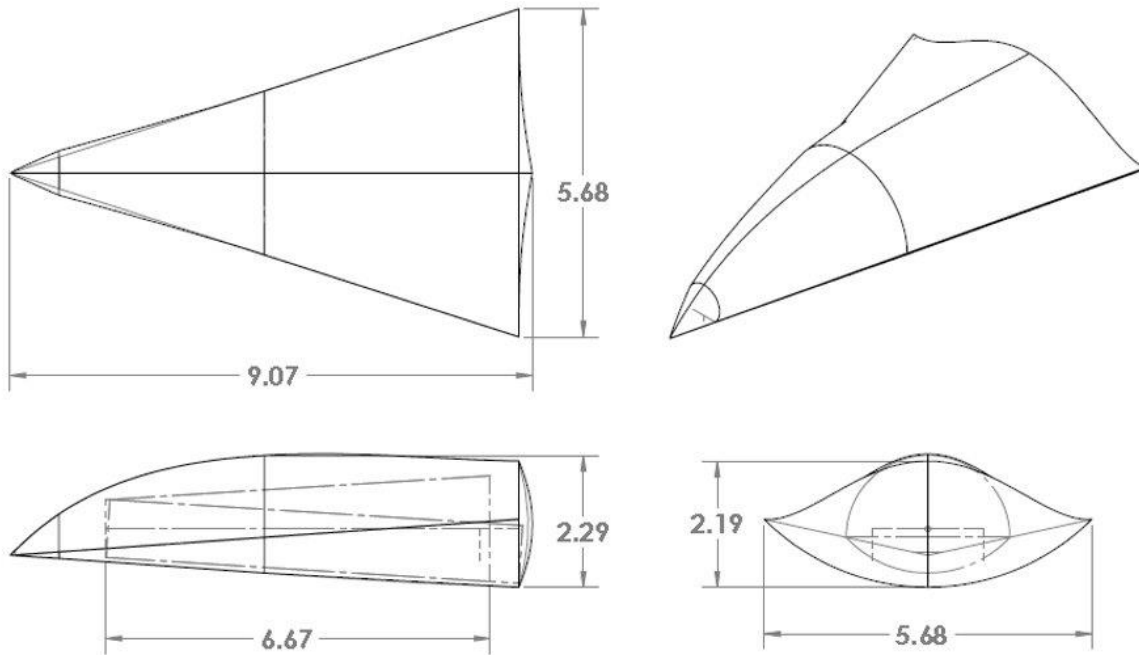


Figure 4.3.3.2-3 Dimensioned Drawing of Designed Re-Entry Vehicle

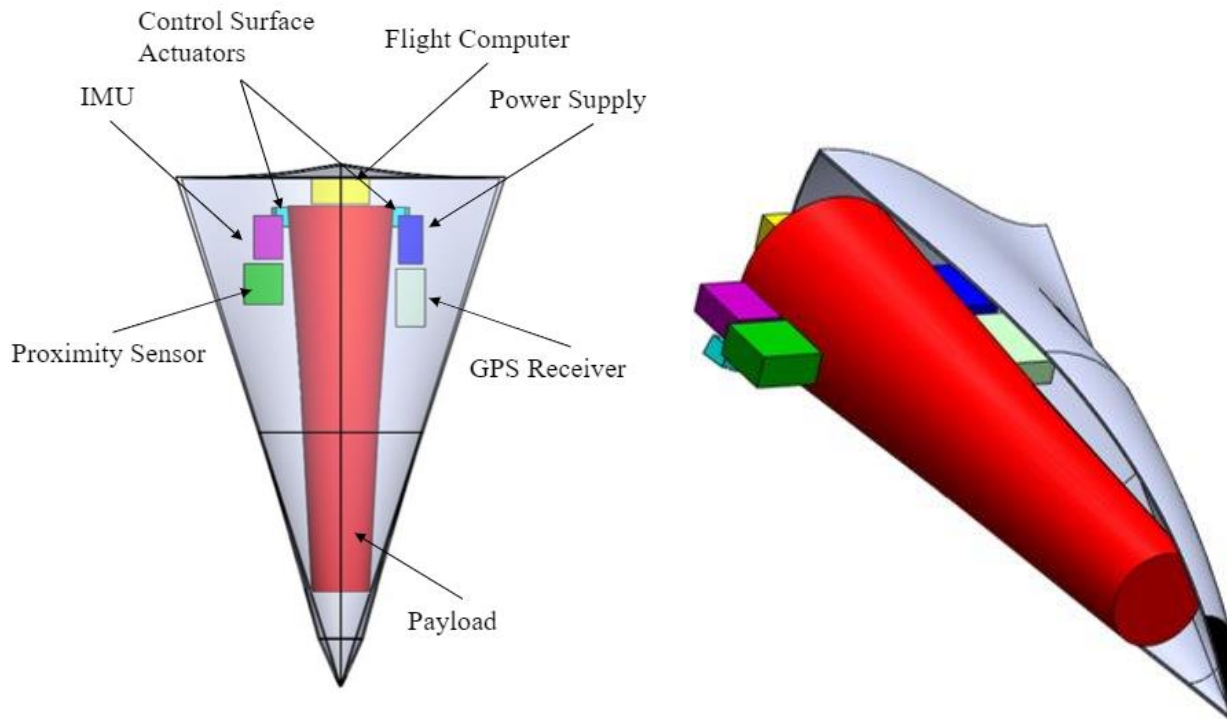


Figure 4.3.3.2-4 Cross Section and Labeled View of Glide RV Internal Layout

4.3.4 Mass Statement

The total mass of the vehicle without propellant is 6.42 tons and 107.5 tons with propellant. Figure 4.3.4-1 and 4.3.4-2 shows the breakdown of masses for the different components of the system.

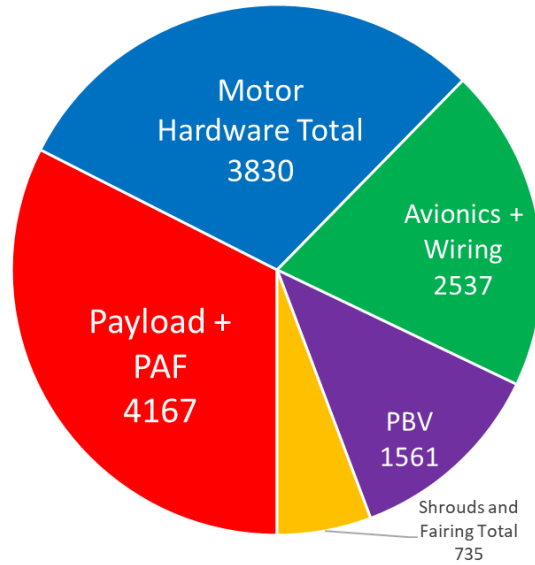


Figure 4.3.4-1 Mass Breakdown without Propellant

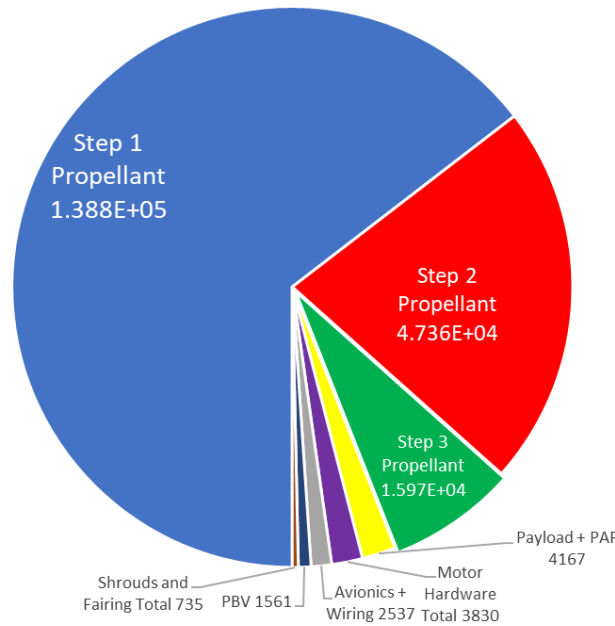


Figure 4.3.4-2 Mass Breakdown with Propellant

5.0 Performance Assessments

5.1 Trajectory Analysis

The primary goals of the trajectory analysis were to verify that the range, flight time, and CEP requirements will be met by the Lance ICBM system. This was done with Euler-integrated trajectory simulations and a Monte Carlo analysis, both implemented in MATLAB.

5.1.1 Free-flight Trajectory and Range Calculation

Most of an ICBM's flight is absent of any non-conservative forces. This phase is dubbed the "free-flight," and it is critical to the overall trajectory objectives. In a sense, the ascent phase's objective is to inject the PBV into the proper orbit, and the re-entry phase merely marks the end of the free-flight. Therefore, this section will deal with the orbital calculations and parameters that the atmospheric phases of ICBM flight will rely on.

In ballistic trajectory calculations, it is convenient to use a non-dimensional parameter called Q , which is defined by Equation 5.1-1.

$$Q = \left(\frac{v_o}{v_{circular}} \right)^2 = \frac{v_o^2 (R_{Earth} + h)}{\mu_{Earth}} \quad (\text{Equation 5.1-1})$$

As the equation suggests, Q can be described as the squared ratio of the velocity of an orbiting object and the corresponding circular orbit velocity at that altitude. The v_o in the equation is the velocity of the object, accounting for launch-site speed.

Calculating Q and the flight path angle (ϕ) at the burnout of the ICBM boost stages was critical to determining the free-flight trajectory of the PBV. These two values can be found with the ascent simulation method, described in Section 5.1.3, and the eccentricity of the free-flight orbit can be calculated with Equation 5.1-2.

$$e^2 = 1 + Q_{bo}(Q_{bo} - 2) \cos^2 \phi_{bo} \quad (\text{Equation 5.1-2})$$

Next, the semi-major axis of the orbit was found with Equation 5.1-3.

$$a = \frac{R_{Earth} + h_{bo}}{2 - Q_{bo}} \quad (\text{Equation 5.1-3})$$

Since “free-flight” is defined as the trajectory outside of atmospheric influence, the end of this portion of the flight was set as the limit of the 1976 standard atmosphere (85 km). Therefore, this gave both limits of the free flight:

$$(r_{ff} > R_{Earth} + h_{bo}) \ \& \ (r_{ff} > R_{Earth} + 85 \text{ km})$$

With this information, Equations 5.1-4 and 5.1-5 was used to solve for the free-flight range angle (Ψ).

$$r = \frac{a(1 - e^2)}{1 + e \cos \theta} \quad (\text{Equation 5.1-4})$$

$$\Psi = \theta_{re-entry} - \theta_{bo} \quad (\text{Equation 5.1-5})$$

Per the RFP requirement, it was necessary to calculate the free-flight time as well. This can be accomplished with Equations 5.1-6 and 5.1-7.

$$\cos E_1 = \frac{e - \cos \frac{\Psi}{2}}{1 - e \cos \frac{\Psi}{2}} \quad (\text{Equation 5.1-6})$$

$$t_{ff} = 2 \sqrt{\frac{a^3}{\mu}} (\pi - E_1 + e \sin E_1) \quad (\text{Equation 5.1-7})$$

The free-flight range angle and flight time can then be added to the ascent and re-entry values after the simulations are completed (described in Sections 5.1.3 and 5.1.4).

5.1.2 Atmospheric Trajectory Assumptions

A rocket launch through the atmosphere is an immensely complex dynamic problem. Therefore, the simulation of this process requires some simplifying assumptions

The first major simplification in the simulation method is the use of two-dimensional, point-mass equations of motion. Second, the ascent and re-entry assume a flat, non-rotating earth. However, the launch-site velocity is accounted for in range calculations. Finally, instantaneous motor start, stop, throttle, and pitch maneuvers were assumed, and steering losses were not accounted for.

The drag coefficients of both the launch vehicle and payload were varied with Mach number. Drag Models were generated using RASAero, a semi-empirical “combined aerodynamic analysis and flight simulation software.” (Ref 5.1.2-1) The drag profile for the ascent stages is shown in Figure 5.1-1 and the profile for re-entry is shown in 5.1-2. For simplicity, it was assumed that the glide re-entry vehicles would share the same drag characteristics.

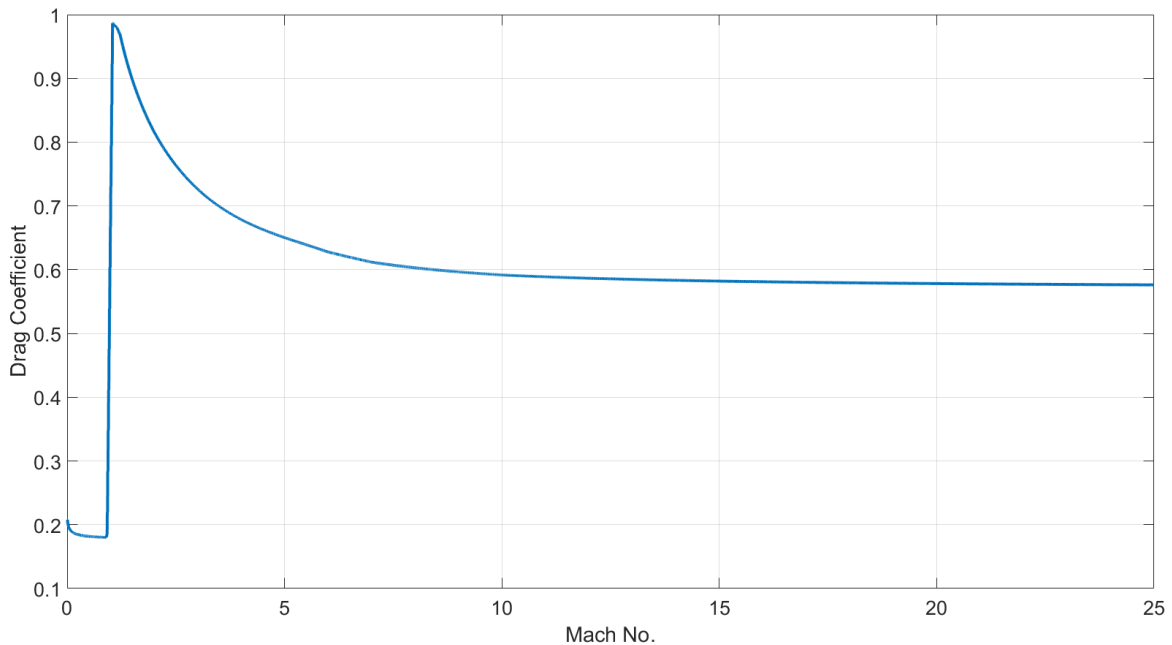


Figure 5.1-1 ICBM Drag Profile

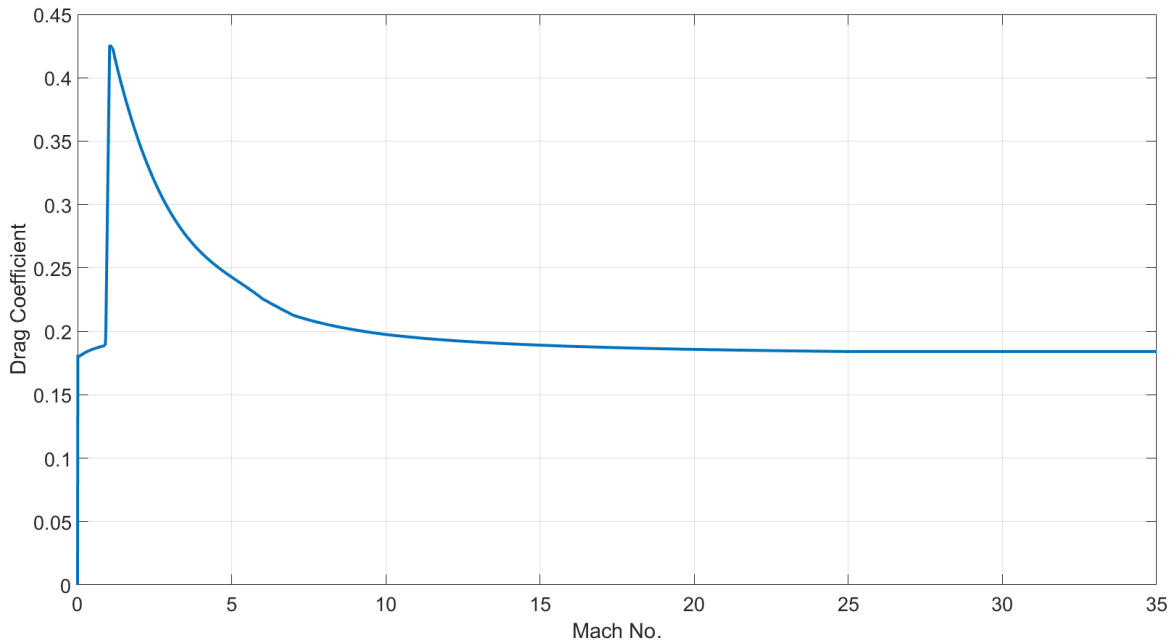


Figure 5.1-2 Re-entry Vehicle Drag Profile

In addition to drag variation with Mach number, thrust variation with altitude was included in the ascent simulation. This was done with vacuum and sea-level values for specific impulse and thrust. The first step in this process was to obtain the mass flow, c^* , and chamber pressure of the motors from the performance calculations. With these values known, it was convenient to define a constant motor parameter (Equation 5.1-8).

$$\lambda = \frac{c^* \left(\frac{A_e}{A_t} \right)}{g_0 p_c} \quad \text{(Equation 5.1-8)}$$

Using the sea-level and vacuum values previously mentioned, the motor exit pressure was approximated with a modified thrust equation (Equation 5.1-9).

$$p_e^{SL} = \frac{T_{SL} - \left(\frac{I_{sp}^{SL}}{I_{sp}^{Vac}} \right) T_{Vac}}{A_e} \quad \text{(Equation 5.1-9)}$$

$$p_e^{vac} = \frac{T_{Vac} - \left(\frac{I_{sp}^{vac}}{I_{sp}^{SL}}\right) T_{SL}}{A_e}$$

$$p_e \approx \frac{p_e^{SL} + p_e^{vac}}{2}$$

Then, the optimum specific impulse was estimated with Equation 5.1-10.

$$I_{sp,opt}^{vac} = I_{sp}^{vac} - \lambda p_e$$

$$I_{sp,opt}^{SL} = I_{sp}^{SL} - \lambda(p_e - p_{atm,SL})$$

$$I_{sp,opt} \approx \frac{(I_{sp,opt}^{SL} + I_{sp,opt}^{vac})}{2} \quad \text{(Equation 5.1-10)}$$

These approximate parameters could then be used to generate a thrust profile which varies with altitude (Equations 5.1-11 and 5.1-12).

$$I_{sp}[h] = I_{sp,opt} + \lambda(p_e - p_{atm}[h]) \quad \text{(Equation 5.1-11)}$$

$$T[h] = \dot{m}g_0 I_{sp}[h] \quad \text{(Equation 5.1-12)}$$

A visual representation of the motor performance for each stage is shown in Figures 5.1-3 and 5.1-4.

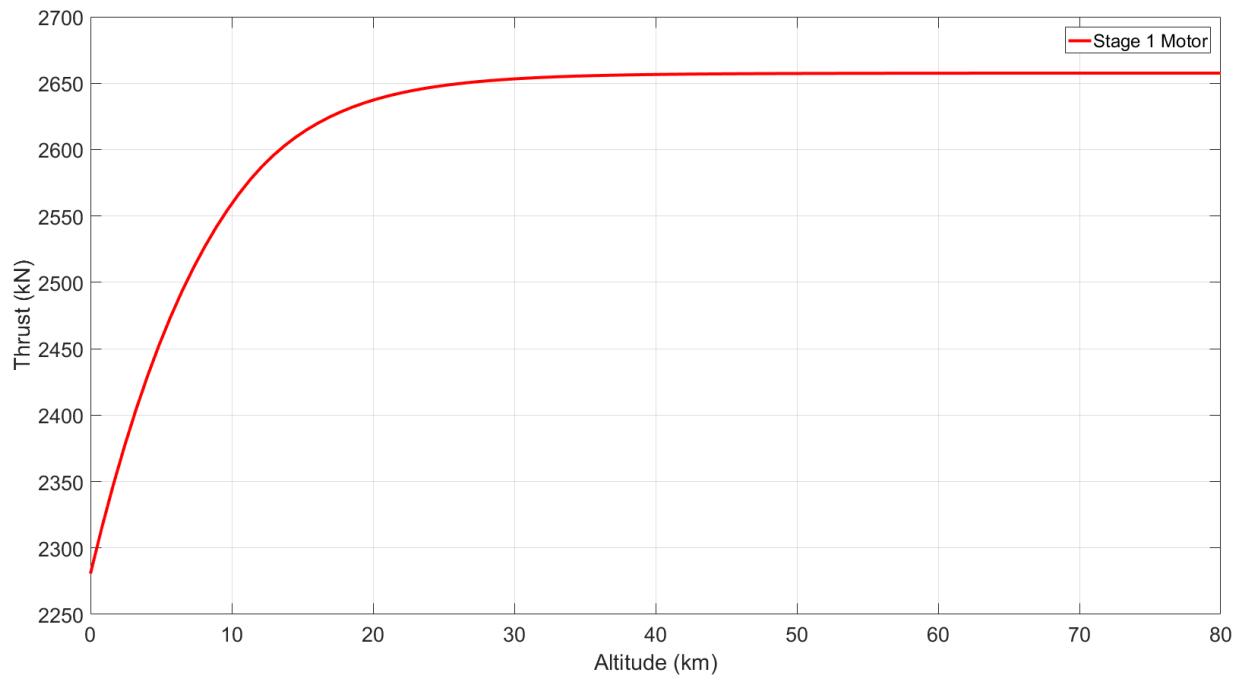


Figure 5.1-3 Thrust versus Altitude for the First Stage Motor

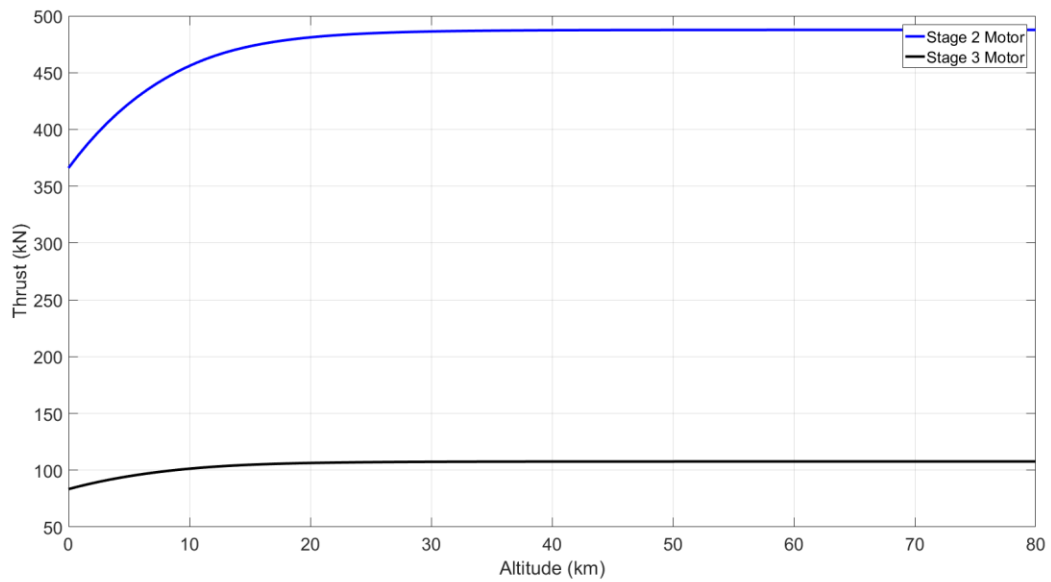


Figure 5.1-4 Thrust versus Altitude for the Second and Third Stage Motors

5.1.3 Ascent Trajectory Method

As previously mentioned, the simulation method uses two-dimensional equations of motion for a point mass (equations 5.1-13 to 5.1-30), and the equations are Euler integrated. Therefore, the velocity, altitude, down-range distance, and flight path angle are integrated with their derivative from the previous time-step. In addition, forces on the body are only accounted for in the velocity direction. In other words, altitude and down-range distance integration was only dependent on the velocity and flight path angle.

The “method of shooting” was the primary procedure for determining the optimum trajectories. Inputs to the MATLAB tool were pitch kick magnitude, kick time, coast time, stage separation time, launch-site latitude, and launch direction. The most efficient way to determine the correct trajectory was to vary the pitch kick magnitude, while every other input parameter remained constant. The kick time was set to three seconds, the coast and separation time were set to five and two seconds, the launch site latitude was set to 41°N (Warren AFB), and the direction was due West. All simulations ran with a Westward launch, since this would be a worst-case scenario. In this case, the Earth’s rotational velocity would subtract from the total Δv produced by the launch vehicle, lowering the orbital parameter (Q). Meeting the range requirement in this worst-case scenario ensures the ICBM can meet the range in any direction.

The Euler-integrated ascent simulation contains 16 major parameters which are tracked throughout the flight. To start the simulation, only six of these need to be defined at the time of liftoff ($t = 0$). The required initial conditions are listed in Table 5.1-1, and every other parameter can be set equal to zero.

Table 5.1-1 Initial Conditions to Begin Ascent Euler Integration

Initial Conditions to Begin Ascent Euler Integration	
Flight Parameter at Liftoff	Equation/Definition
Mass (m)	Gross Liftoff Mass (GLOM)
Thrust (T)	Thrust at sea-level (T_{SL})
Acceleration (\dot{v})	$\frac{T_{SL}}{m_1} - g_0$
Flight path angle (ϕ)	$\frac{\pi}{2}$ (90°)
Air density (ρ)	Air density at sea-level (ρ_{SL})
Acceleration due to gravity (g)	Accel. due to gravity at sea-level (g_0)

Integration Procedure:

The index (i) goes from 1 to N , where 1 denotes conditions at liftoff, and N is roughly the total flight time divided by the time-step (dt).

Step One: Calculate the parameters that rely on the previous time-step

$$v_i = v_{i-1} + dt(\dot{v}_{i-1}) \quad \text{(Equation 5.1-13)}$$

$$h_i = h_{i-1} + dt(\dot{h}_{i-1}) \quad \text{(Equation 5.1-14)}$$

$$X_i = X_{i-1} + dt(\dot{X}_{i-1}) \quad \text{(Equation 5.1-15)}$$

If the flight time is equal to the time of the pitch maneuver:

$$\phi_i = \phi_{i-1} - \Delta\phi_{kick} \quad \text{(Equation 5.1-16)}$$

At all other points in the simulation:

$$\phi_i = \phi_{i-1} + dt(\dot{\phi}_{i-1}) \quad (\text{Equation 5.1-17})$$

Step Two: Calculate the Parameters that rely on the current time step

Note: stdatm.x[h] denotes the standard atmosphere table look-up function, where x is the property desired (pressure, temperature, density, or speed of sound).

Density: $\rho_i = \text{stdatm.}\rho[h_i]$ (Equation 5.1-18)

Mach number: $M_i = \frac{v_i}{\text{stdatm.sos}[h_i]}$ (Equation 5.1-19)

Thrust: $T_i = \dot{m}[\text{stage}]g_0I_{sp}[h_i, \text{stage}]$ (Equation 5.1-20)

Dynamic pressure: $q_i = \frac{1}{2}\rho_i v_i^2$ (Equation 5.1-21)

Drag: $D_i = q_i S_{ref}^{ICBM} C_D^{ICBM} [M_i]$ (Equation 5.1-22)

Gravity: $g_i = g_0 \left(\frac{R_{Earth}}{R_{Earth} + h_i} \right)^2$ (Equation 5.1-23)

Flight path angle: $\dot{\phi}_i = - \left(\frac{g_i}{v_i} - \frac{v_i}{R_{Earth} + h_i} \right) \cos \phi_i$ (Equation 5.1-24)

Vertical velocity: $\dot{h}_i = v_i \sin \phi_i$ (Equation 5.1-25)

Horiz. velocity: $\dot{X} = \left(\frac{R_{Earth}}{R_{Earth} + h_i} \right) v_i \cos \phi_i$ (Equation 5.1-26)

Orbital parameter: $Q_i = (v_i - v_{Earth}[\text{Latitude}])^2 \frac{R_{Earth} + h_i}{\mu_{Earth}}$ (Equation 5.1-27)

*For a launch directly West

Step Three: Calculate the mass and acceleration, based on staging conditions

In general, the simulation follows Equation 5.1-28 when the launch vehicle is not coasting.

$$m_i = m_{i-1} - dt(\dot{m}[stage]) \quad (\text{Equation 5.1-28})$$

When the separation time for a stage is reached, Equation 5.1-29 is used.

$$m_i = m_{i-1} - m_{structure}[stage] \quad (\text{Equation 5.1-29})$$

Otherwise, the mass during the coast is held constant. Additionally, the thrust is set equal to zero during the coast. This allows the acceleration to be calculated with Equation 5.1-30, outside of any logical statements.

$$\dot{v}_i = \frac{T_i - D_i}{m_i} - g_i \sin \phi_i \quad (\text{Equation 5.1-30})$$

When the simulation ends, the burnout conditions are used for the orbital calculation described in Section 5.1.1.

5.1.4 Re-entry Trajectory Method

The re-entry trajectory simulation uses the same Euler integration technique as the ascent portion. Therefore, the integration procedure described in Section 5.1.3 applies to this section as well. However, there are some key details that differentiate the calculations.

First, the initial conditions are more complex since they are defined by the end of the free-flight trajectory. Therefore, less parameters than the ascent can be set to zero. Table 5.1-2 lists the relevant initial conditions.

Table 5.1-2 Initial Conditions to Begin Re-entry Euler Integration

Flight Parameter at Re-entry	Equation/Definition
Altitude (h)	85 km
Velocity (v)	$\sqrt{2\mu_{Earth} \left(\frac{1}{R_{Earth} + 85 \text{ km}} - \frac{1}{2a} \right)}$
Orbit parameter (Q)	$2 - \frac{R_{Earth} + 85 \text{ km}}{a}$
Flight path angle (ϕ)	$-\cos^{-1} \frac{\sqrt{e^2 - 1}}{\sqrt{Q_{re}(Q_{re} - 2)}}$
Density (ρ)	<i>stdatm.</i> ρ [85 km]
Dynamic Pressure (q)	$\frac{1}{2} \rho_{re} v_{re}^2$
Acceleration due to gravity (g)	$g_0 \left(\frac{R_{Earth}}{R_{Earth} + 85 \text{ km}} \right)^2$
Rate of Descent (\dot{h})	$v_{re} \sin \phi_{re}$
Down-range velocity (\dot{X})	$\left(\frac{R_{Earth}}{R_{Earth} + 85 \text{ km}} \right) v_{re} \cos \phi_{re}$
Mach number (M)	$\frac{v_{re}}{\text{stdatm. } \text{sos}[85 \text{ km}]}$
Drag (D)	$q_{re} S_{ref}^{RV} C_D^{RV} [M_{re}]$
Time derivative of flight path angle ($\dot{\phi}$)	$-\left(\frac{g_{re}}{v_{re}} - \frac{v_{re}}{R_{Earth} + 85 \text{ km}} \right) \cos \phi_{re}$
Acceleration (\dot{v})	$\frac{D_{re}}{m_{RV}} - g_{re} \sin \phi_{re}$

In addition, equations for mass change and thrust can be disregarded (ablation rate not accounted for).

Therefore, the acceleration calculation in the integration is completed with Equation 5.1-31.

$$\dot{v}_i = \frac{D_i}{m_{RV}} - g_i \sin \phi_i \quad (\text{Equation 5.1-31})$$

It is also worth noting that the drag term is now dependent on the drag profile in Figure 5.1-2, and the reference area is the base area of the RV.

The re-entry simulation runs until an “impact” condition, rather than a “burnout.” Therefore, the time is stepped until the altitude reaches a pre-defined value. For the simulations described in Section 5.1.5, 50 meters was chosen to avoid integrating to a point where the standard atmosphere is not defined.

Finally, the re-entry simulation includes calculations for a lifting body. To avoid overcomplication, it was assumed that the lift on the glide re-entry vehicle is only dependent on L/D and drag. This is shown by the lift calculation through Equation 5.1-32.

$$L_i = q_i S_{ref}^{RV} (L/D)_{RV} C_D^{RV} [M_i] \quad (\text{Equation 5.1-32})$$

From initial runs, it was found that allowing the lift to remain constant throughout the simulation will cause the re-entry vehicle to “bounce” off the atmosphere and return to orbit. To correct this, the simulation allows for a maneuver in which the lift is reversed. The effect of lift on the flight path angle is shown in Equation 5.1-33.

$$\dot{\phi}_i = \frac{L_i}{m_{RV} v_i} - \left(\frac{g_i}{v_i} - \frac{v_i}{R_{Earth} + h_i} \right) \cos \phi_i \quad (\text{Equation 5.1-33})$$

5.1.5 Simulation Results

To demonstrate the flexibility of the Lance missile, two simulations were performed. These scenarios will be referred to as the “low-arc” and “high-arc” trajectories. The low-arc implemented a higher pitch-kick magnitude to improve range, and according to the simulation, this method meets the 10,000 nautical mile objective. As shown in Table 5.1-3, all simulations also fell below the objective time of 60 minutes, so

the low-arc trajectory meets both the objective flight time and range. Therefore, the low-arc was set as the primary trajectory, and the remainder of this section will deal with the results from its analysis.

Figures 5.1-5 and 5.1-8 are visual comparisons of the low-arc and high-arc trajectories during ascent and free-flight. Figures 5.1-6 and 5.1-7 describe the ascent performance of the ICBM. Figures 5.1-9, 5.1-10, and 5.1-11 are ballistic and glide re-entry vehicle performance comparisons. Figure 5.1-12 shows the lift and drag performance of the glide re-entry vehicle.

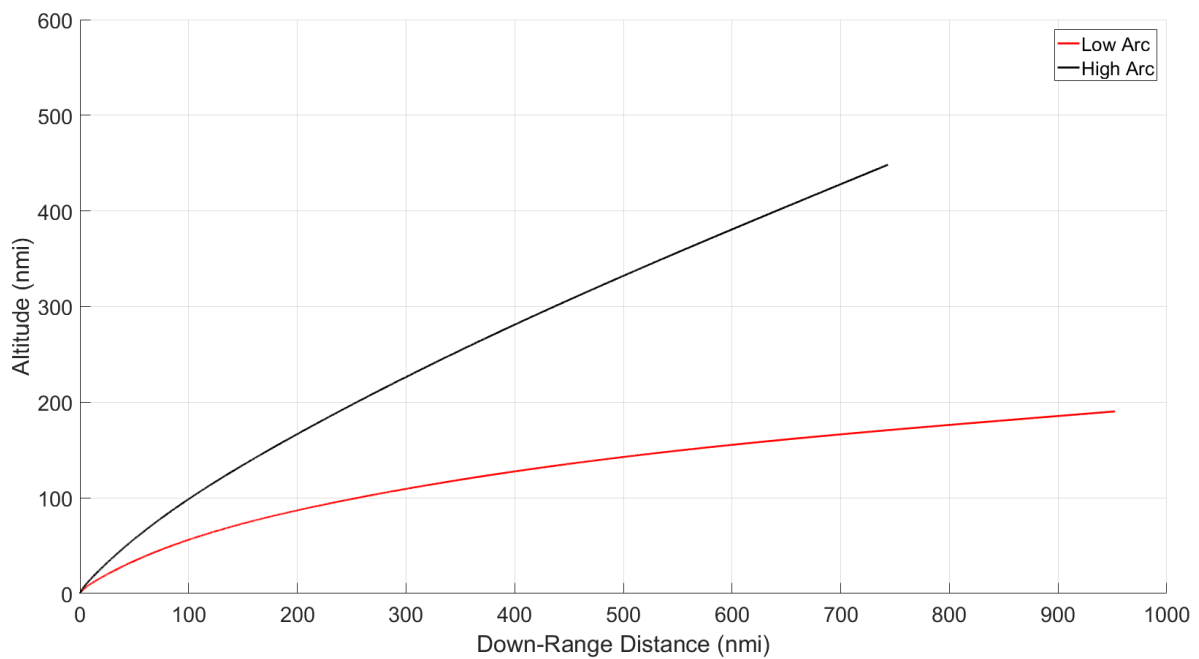


Figure 5.1-5 Ascent Profiles for Low-Arc and High-Arc Trajectories

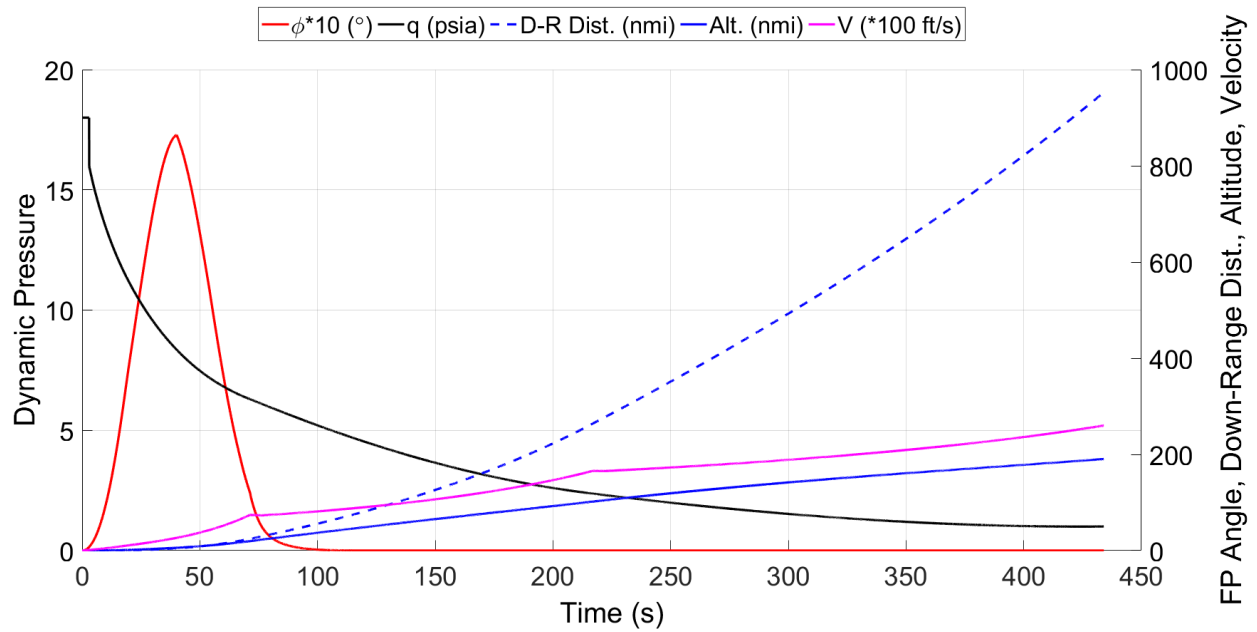


Figure 5.1-6 Ascent Flight Performance for Low-Arc Trajectory

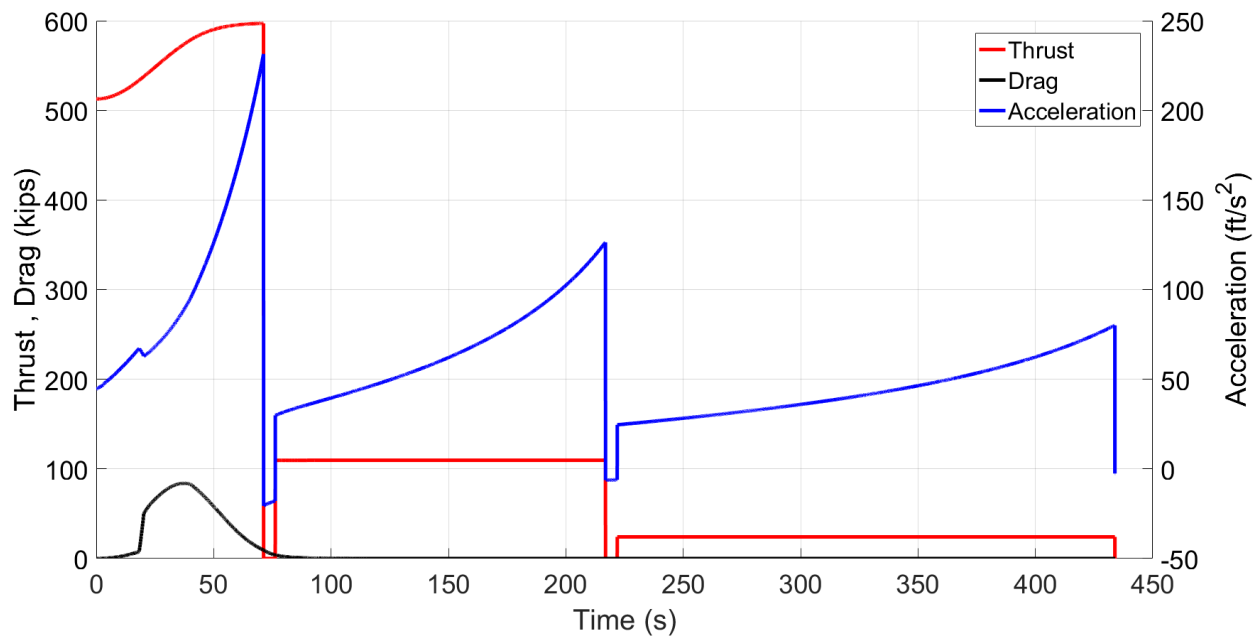


Figure 5.1-7 Ascent Thrust, Drag, and Acceleration for Low-Arc Trajectory

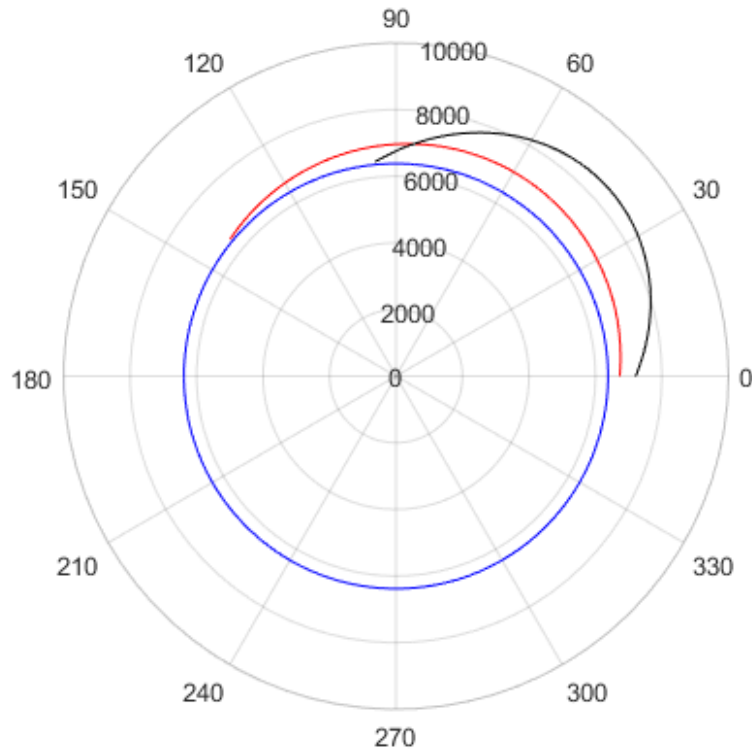


Figure 5.1-8 Free-Flight for Low-Arc (Red) and High-Arc (Black) Trajectories

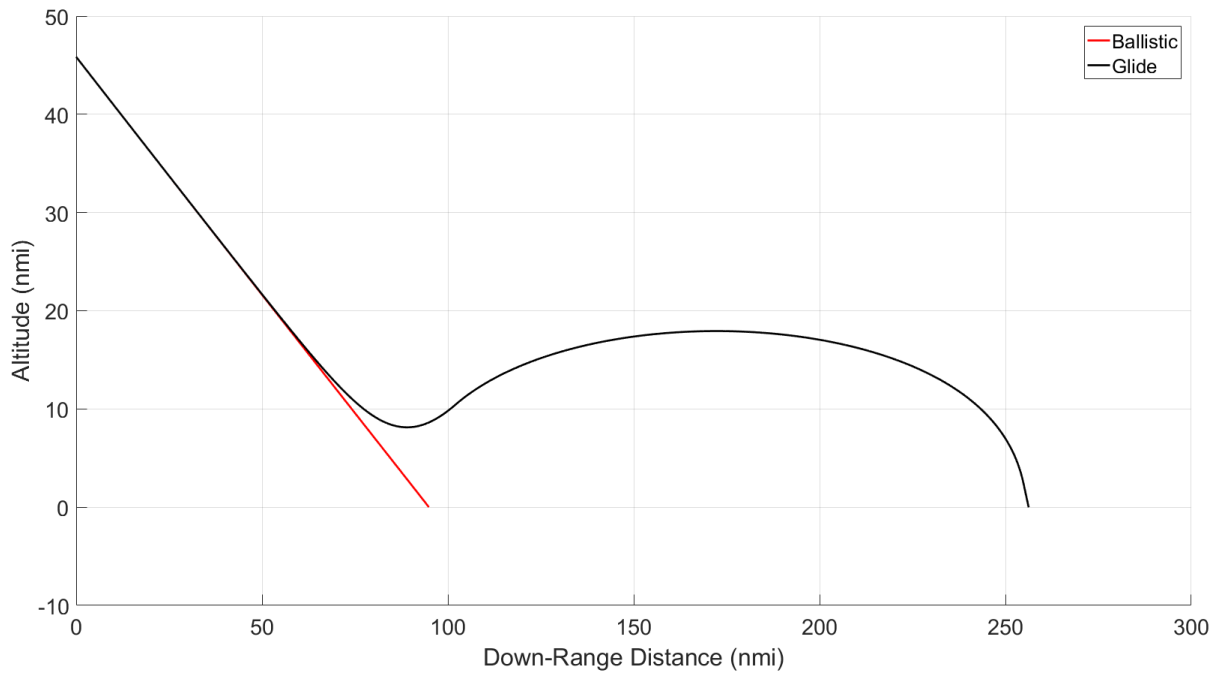


Figure 5.1-9 Re-entry Profiles for Ballistic and Glide Re-entry Vehicles (Low-Arc)

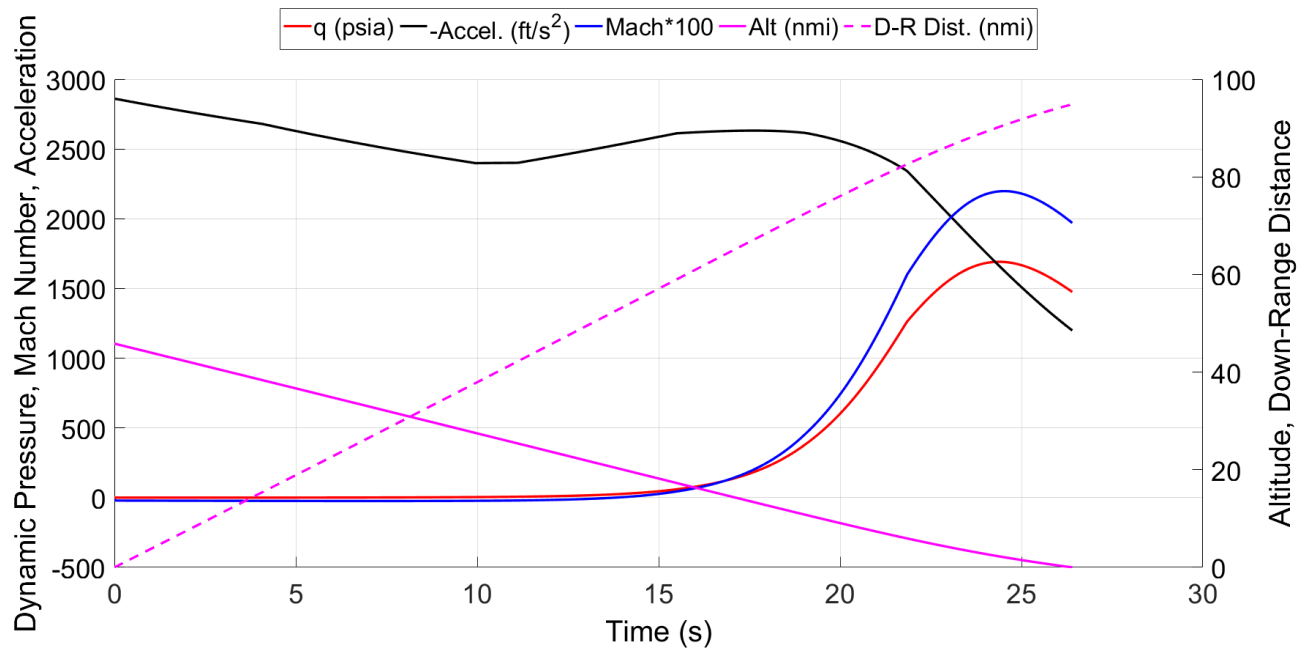


Figure 5.1-10 Flight Performance for Ballistic Re-Entry (Low-Arc)

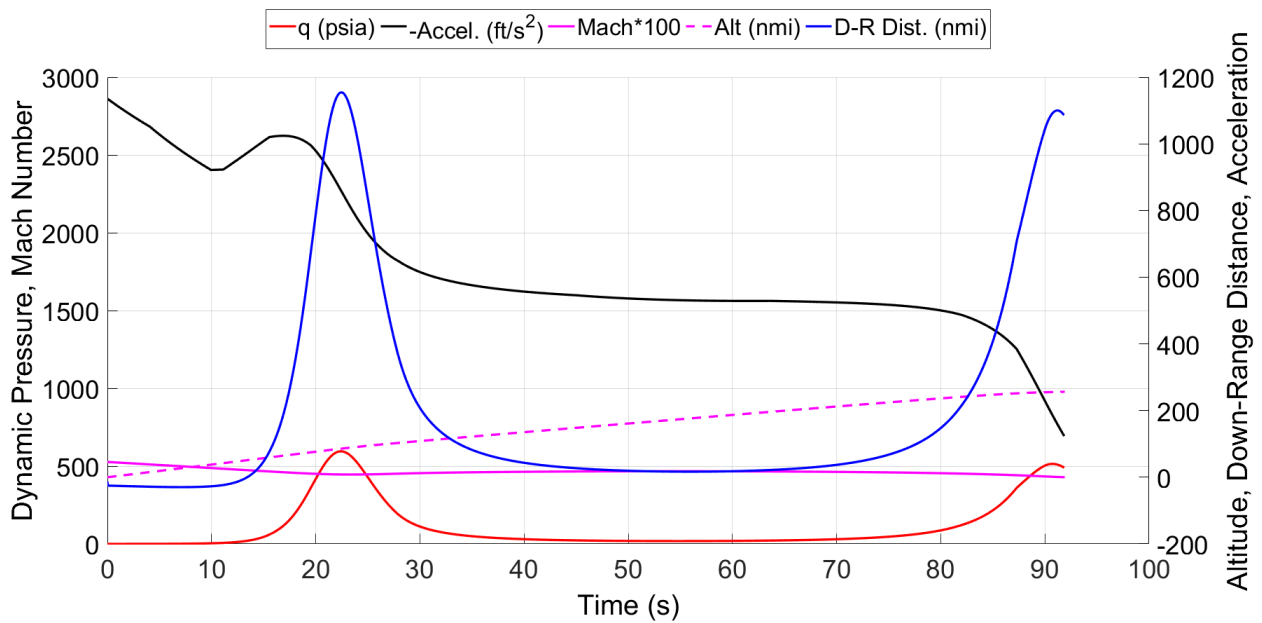


Figure 5.1-11 Flight Performance for Glide Re-Entry (Low-Arc)

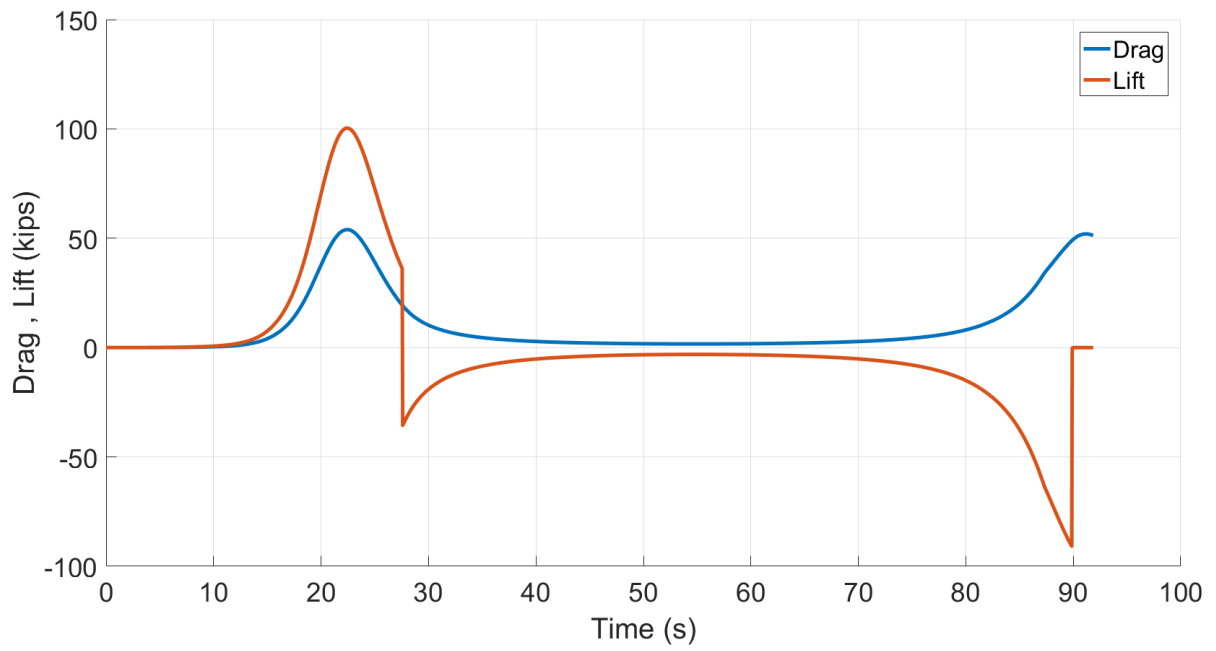


Figure 5.1-12 Transient Lift and Drag for Glide Re-entry

Table 5.1-3 Summary of Trajectory Simulation Results

Low Arc Trajectory				High Arc Trajectory			
Ascent Max q (psia)		17.28		Ascent Max q (psia)		14.05	
Ballistic Re-entry		Glide Re-entry		Ballistic Re-entry		Glide Re-entry	
Max q (psia)	1691	Max q (psia)	595	Max q (psia)	2299	Max q (psia)	1183
Mach at Impact	12.09	Mach at Impact	6.93	Mach at Impact	15.12	Mach at Impact	4.28
Time to Target (min)	46	Time to Target (min)	47	Time to Target (min)	47	Time to Target (min)	47
Range (km)	18659	Range (km)	18958	Range (km)	13199	Range (km)	13279
Range (nm)	10064	Range (nm)	10225	Range (nm)	7119	Range (nm)	7162

5.2 Circular Error Probable

Once the primary trajectory simulations were completed, the method could be adjusted and used to perform a circular error probable calculation. When discussing ballistic missiles, the circular error probable denotes the radius of a circle into which 50% of the fired ordnance will fall (Ref 5.2-1).

Therefore, the simplest way to estimate the CEP without testing is to vary the flight conditions with a statistical distribution and perform a Monte Carlo simulation.

Since the PBV is designed to provide Δv corrections to keep the warheads on the correct trajectory, the initial conditions for the Monte Carlo simulation was set at the beginning of the re-entry phase.

Unfortunately, information on the accuracy of PBV systems could not be acquired, so it was assumed that the velocity and flight path angle would not vary from the target values.

Instead, a Gaussian distribution for relative density and temperature fluctuations in the upper atmosphere was applied to the simulation (Ref 5.2-2). Random fluctuations (confined by the distributions in Figures 5.1-13 and 5.1-14) were applied to each run in the Monte Carlo simulation.

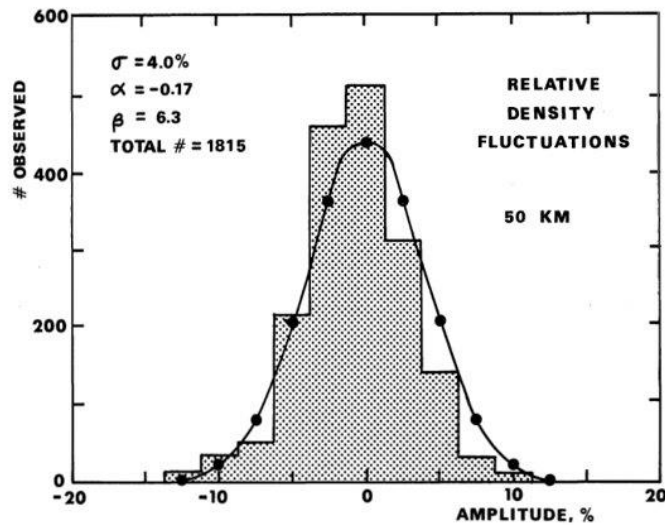


Figure 5.1-13 Distribution of the 1969 MRN Relative Density Fluctuations in the 45 to 55 km Range

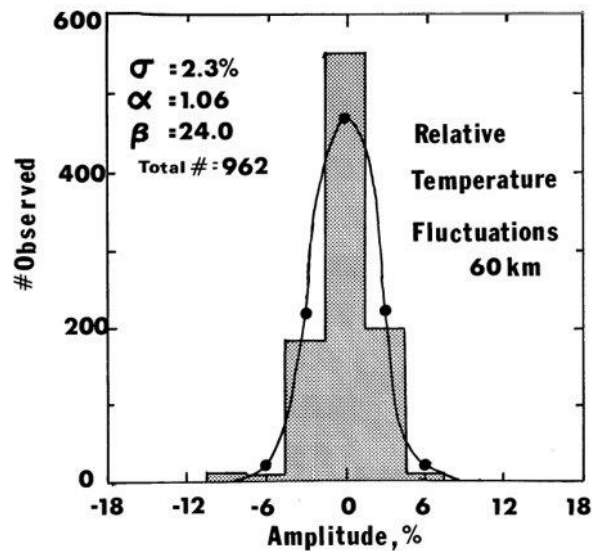


Figure 5.1-14 Distribution of the 1969 MRN Relative Temp. Fluctuations in the 45 to 55 km Range

Before the Monte Carlo analysis was implemented, a simulation ran to obtain a “target” value for the re-entry down-range distance. The deviation from the target for all data points is defined by Equation 5.1-34.

$$\Delta X_i = |X_{target} - X_i^{MonteCarlo}| \quad \text{(Equation 5.1-34)}$$

The circular error probable is a function of standard deviation (σ), and the equation for a 50% ring is shown by 5.1-35.

$$CEP_{50\%} = \sigma[\Delta X_i] \sqrt{-2 \ln(1 - 0.5)} \quad \text{(Equation 5.1-34)}$$

Table 5.1-4 shows the results of 500 simulations for each trajectory. The high CEP for the glide re-entry vehicles is due to the lack of control surface correction in the simulation. In addition, the glide maneuvers make the re-entry vehicles more susceptible to atmospheric variance.

Table 5.1-4 CEP Results Summary

Trajectory	CEP
Low-arc, ballistic	142 ft (43.2 m)
Low-arc, glide	2,820 ft (859 m)
High-arc, ballistic	123 ft (37.4 m)
High-arc, glide	2,500 ft (762 m)

5.3 Ability to Hit all Targets

The key result from the trajectory simulations is that Project Lance demonstrates the capability to engage any desired target. This is due to the ICBM's design for a worst-case launch scenario (Warren AFB, silo N-07, to target 10,000 nmi [18,500 km] due west). Targets below the maximum range of the missile can be hit by adjusting the magnitude of the pitch-kick maneuver (increasing the trajectory altitude). It has been demonstrated that this engagement method is viable to at least 7,000 nmi.

For testing, and trajectories closer to the minimum ICBM range of 2,970 nmi (5,500 km), a thrust termination system will be used.

5.3.1 Thrust Termination System

A Thrust Termination System (TTS) is an essential component of solid-fueled motors since they cannot be terminated once ignited. The ICBM needs to be able to stop producing thrust in order to deploy the PBV and the payload. The ICBM is designed such that TTS is always implemented by the third stage when the PBV needs to be deployed. TTS is comprised of a receiver, Safe & Arm Device in addition to the termination system. The receiver obtains a signal in order to enable thrust termination to start. This component of termination will only be used during testing in order to prevent any potential interference during actual missile launch scenarios. The Safe Arm Device will use a set of electronics that determine when to initiate the firing of the payload (Ref 5.3.1-1). Figure 5.3.1-1 and Figure 5.3.1-2 depicts the termination method that will be used for the TTS which is similar to that of the Minuteman III TTS (Ref 5.3.1-2). Explosive bolts will be used at angled thrust termination ports and will be placed evenly around the circumference in order to ensure even cut off. Furthermore, redundant detonation cords of equal length and leading to each thrust termination port will be implemented to improve reliability (Ref 5.3.1-3).

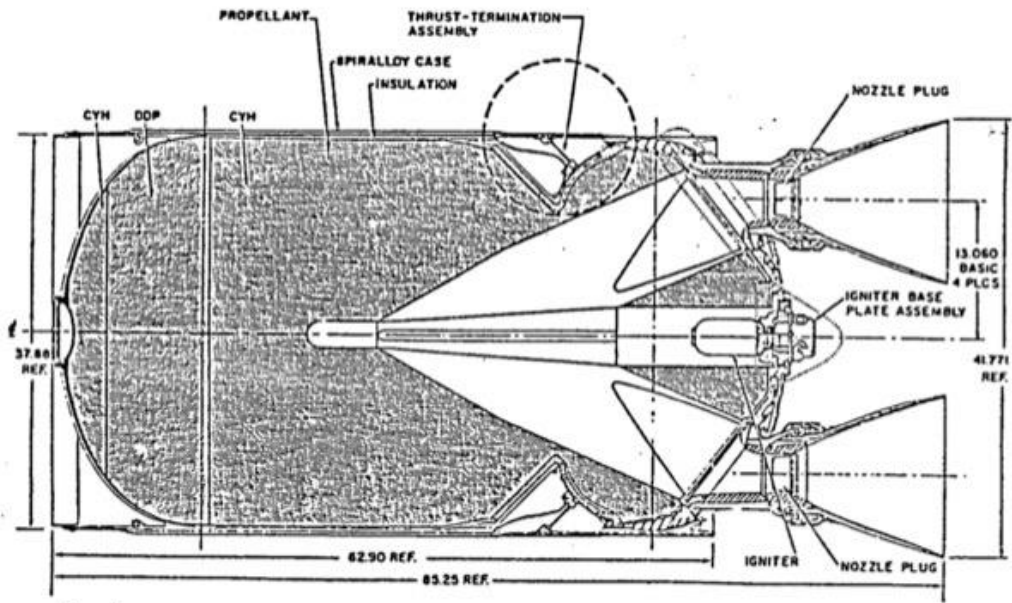


Figure 5.3.1-1 Minuteman III Motor with TTS Assembly

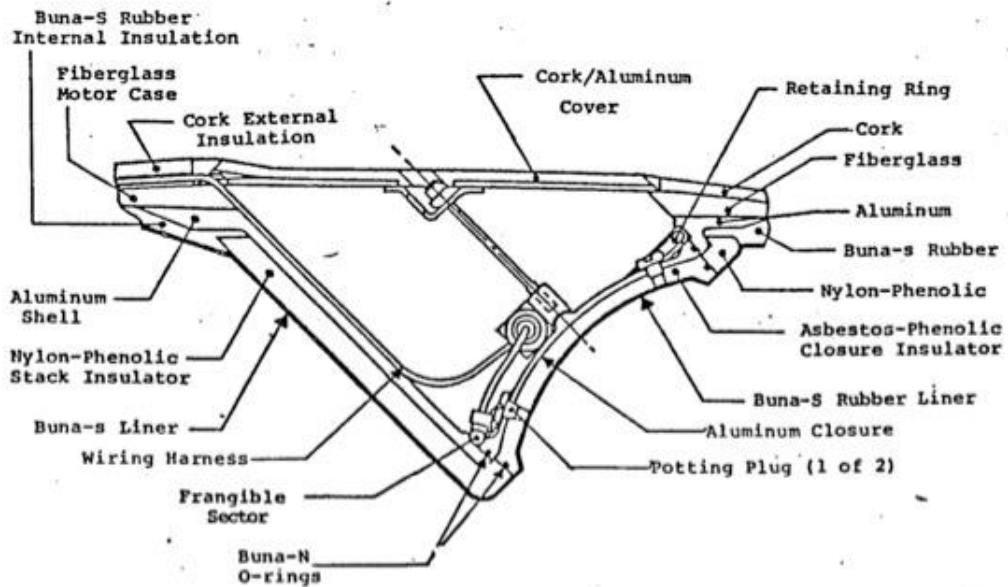


Figure 5.3.1-2 Overview of Minuteman III TTS

5.3.2 Optimum Height of Burst

Both the glide re-entry vehicle and the ballistic re-entry vehicle are equipped with a height of burst sensor. This allows for the detonation of the nuclear payload at its optimum height of burst. The optimum height of burst is dependent on the yield of the nuclear payload and the desired overpressure.

Table 5.3.2-1 outlines the optimum height of burst for a 300-kiloton nuclear payload at overpressures that represent both soft and hard targets, and the overpressure effects. Data was obtained from the NUKEMAP website (Ref 5.3.2-1).

Table 5.3.2-1 Optimum Height of Burst

Overpressure, psi	Air Blast Radius, kft (km)	Optimum HoB, kft (km)	Overpressure Effects
1	43.3 (13.2)	10.3 (3.13)	Light damage to cities
5	15.5 (4.71)	6.86 (2.09)	Medium damage to cities
20	4.99 (1.52)	4.00 (1.22)	Heavy damage to cities
200	1.80 (0.55)	1.05 (0.32)	Extreme damage to civilian structures, some damaged to hardened structures
3,000	0.459 (0.14)	0.230 (0.07)	Damage to missile silos

5.3.3 Deeply Buried Hardened Targets

The re-entry vehicles are also required to engage deeply buried hardened targets. To determine the effectiveness of both RVs in meeting this requirement, the penetration thickness of each RV into a concrete element was calculated using Equation 5.3.3-1. The equation is known as the Ballistic Research Laboratory Formula (Ref 5.3.3-1).

$$T = \frac{427}{\sqrt{f'_c}} \left(\frac{W}{D^{1.8}} \right) \left(\frac{V_s}{1000} \right)^{1.33} \quad \text{(Equation 5.3.3-1)}$$

T is the penetration thickness (in), F'_c is the compressive strength of concrete (3,000 psi), W is the weight of the RV (lb_m), D is the diameter of the RV (in), and V_s is the striking velocity (ft/s).

The penetration thickness is 83 ft for the ballistic RV, and 32 ft for the Glide RV. The impact angle should be greater than 30° to prevent ricochet.

5.3.4 Trajectory Considerations

There are certain targets where the minimum-energy trajectory should be avoided. This is the case for any trajectory that would fly over Russia or China, which would occur for a target in Southeast Asia. A trajectory over Russia or China could trigger their early warning systems.

Two primary options exist to avoid this trajectory. The first is an ICBM capable of a plane-change. This should also be avoided because this option could be destabilizing. If an ICBM can perform a plane-change, any country might perceive any launch as an attack.

The second, and preferred, option is a southern launch (launch over the Southern hemisphere). This requires a higher ΔV , but it is possible with the Joust Aerospace ICBM. Figure 5.3.4-1, courtesy of the RAND Corporation, highlights the launch velocity difference between a direct launch and opposite launch (Ref 5.3.4-1). For a 10,000 nmi range, which is within the ICBM’s capabilities, there is no launch velocity difference, so the ICBM could hit any target with either trajectory.

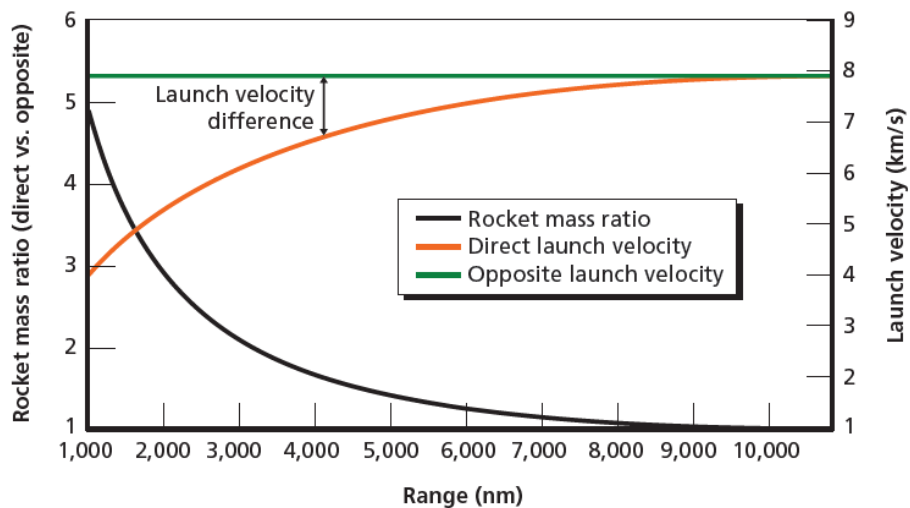


Figure 5.3.4-1 Launch Velocity Difference for Southern Launch

6.0 Systems Analysis

6.1 Thermal Protection Systems

There are three notable thermal protection systems aboard the missile: ablative coating on the leading edge of the re-entry vehicles, payload fairing, and the motor casing. This section will go over the sizing of thermal protection systems.

For the payload fairing, a standard P-50 cork sheet will be used, based on the fairing of Antares. From that fairing, an average thickness of the insulation is ½” and has a density of 29.97 lb_m/ft³ was assumed (Ref 6.1-1), which adds an additional 92.6 lb_m to the fairing.

The motor casing will have a 0.2-inch (50 mm) coating of SLA-561 ablative (density of 14.2 lb_m/ft³) (Ref 6.1-2) to ensure the casing material will not burn through due to high and unexpected combustion temperatures. This adds an additional 17.4 lb_m on the first step, 6.57 lb_m on the second step, and 10.8 lb_m to the third step solid motor case.

Preliminary thermal analysis was conducted on the RV. The maximum heat rate of the RV during its descent phase was obtained through the Sutton-Graves stagnation heating model (Ref 6.1-3), shown in the equation below:

$$q_s = k \left(\frac{\rho}{R_n} \right)^{\frac{1}{2}} V^3 \quad \text{(Equation 6.1-1)}$$

Where $k = 1.7415 \times 10^{-4}$ for Earth.

This yields an approximate heat rate of 20,000 W/cm². Plugging the heat rate into Stefan-Boltzmann Law (shown below), the approximate maximum temperature can be found.

$$T = \left(\frac{q}{\epsilon * \sigma} \right)^{0.25} \quad \text{(Equation 6.1-1)}$$

Note, a grey body assumption with an emissivity of 0.85 was made on the re-entry vehicle. The expected maximum temperature to be observed during re-entry is 14,900 R (8,300 K). Assuming an ablation rate of 0.7 mm/s at 14,900 R and an atmospheric flight time of 26.4 seconds, the minimum required thickness for Reinforced Carbon-Carbon (RCC) ablative is, 0.738 inches (18.5 mm). Adding a factor of safety of 1.5 and accounting for ease of manufacturing, the final design ablative becomes 1.18 inches (30 mm) on the stagnation point. On the tangential skin portion, it is safe to assume half the thickness (0.59 inches / 15 mm). For the RCC, this is an additional weight of 10.5 lb_m to the ballistic RV. The glide RV was assumed to have an identical thickness and weight of ablative material.

6.2 Flight Loads

While there are many types of loads that the ICBM is exposed to before and during launch, only flight loads during max-q were considered at this stage of the design process. Ground loads did not need to be calculated because the ICBM is protected from winds by the silo.

The analysis assumed quasi-static loading, no friction drag, and $C_{N\alpha} = 0$ for cylindrical sections. The max-q parameters are listed in Table 6.2-1.

Table 6.2-1 Max-q Parameters

Max-q Parameters	
Max-q, atm (kPa)	1.15 (117)
$t_{\max-q}$, s	40.0
$h_{\max-q}$, nmi (km)	5.94 (11.0)
$v_{\max-q}$, ft/s (m/s)	2,630 (803)
$\rho_{\max-q}$, lb /ft ³ (kg/m ³)	0.022 (0.36)
$a_{\max-q}$, ft/s (m/s)	968 (295)
M _{max-q}	2.72

At max-q, 30.4 Ton (27.6 Tonne) of the first step's propellant is remaining, and the 2nd and 3rd step propellants are unused. The vehicle has a longitudinal acceleration of 2.95 g₀.

During max-q, the ICBM is in a region of high wind speeds. The AMR 95% wind profile envelope was used to predict a wind velocity of 271 ft/s (82.6 m/s) at the ICBM's height during max-q, 5.94 nmi (11.0 km). The sideways gusts induce a relative angle of attack of 5.9°.

In order to find the normal force on the vehicle, the aerodynamic load coefficient, $C_{n\alpha}$, was required. The $C_{n\alpha}$ was found to be 0.06/deg, using an aerodynamic chart (Ref 4.3.1-1). This results in a C_N of 0.35.

With respect with the wind axes, there is a lift force of 33.9 kips (151 kN) acting on the fairing and a drag force of 72.6 kips (323 kN), assuming a C_D of 0.7. These forces were resolved into 41.1 kips (183 kN) shear force and 68.8 kips (306 kN) axial force.

The shear force on the fairing is destabilizing so the nozzle needs to gimble to trim the ICBM. In order for a zero-net moment about the center of gravity, a gimbal force of 29.5 kips (131 kN) is required at a gimbal angle of 3.22°. This is feasible with solid rocket motor nozzles.

Inertial loads from propellants and structural mass oppose the air loads. The lateral load factor during max-q was 0.52 g₀.

Figure 6.2-1 shows the max-q shear loads along the ICBM. The maximum shear load occurs at the fairing. The shear load is negative at the bottom of the first step because of the lateral component of thrust.

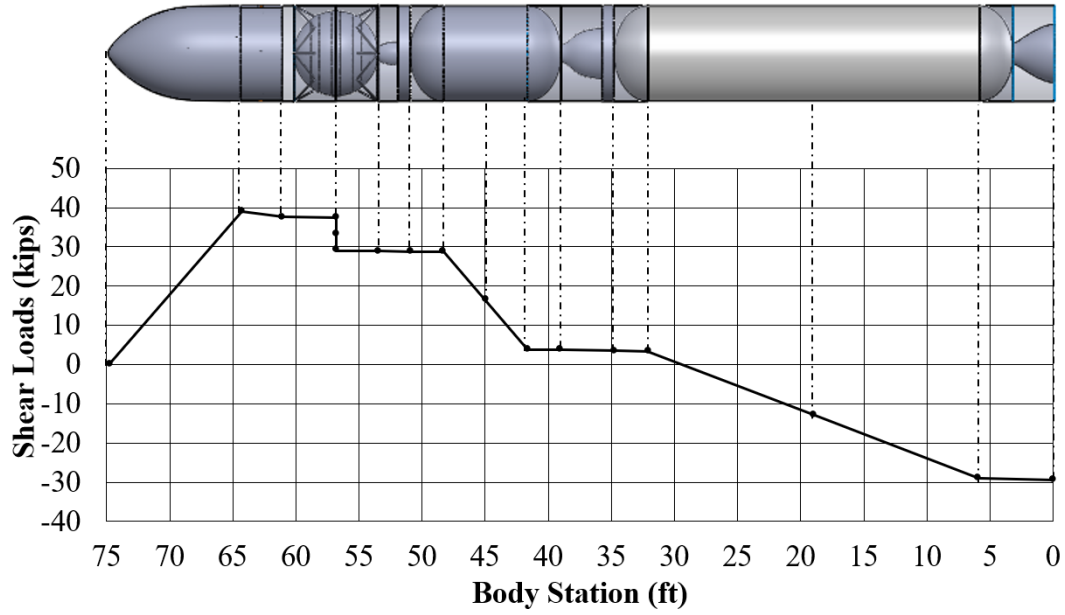


Figure 6.2-1 Max-q Shear Loads

Figure 6.2-2 shows the max-q bending loads along the ICBM. At the point where the slope of the bending load curve is zero, the shear load is close to zero. This is the expected relationship between shear and bending. Figure 6.2-3 shows the max-q axial loads along the ICBM.

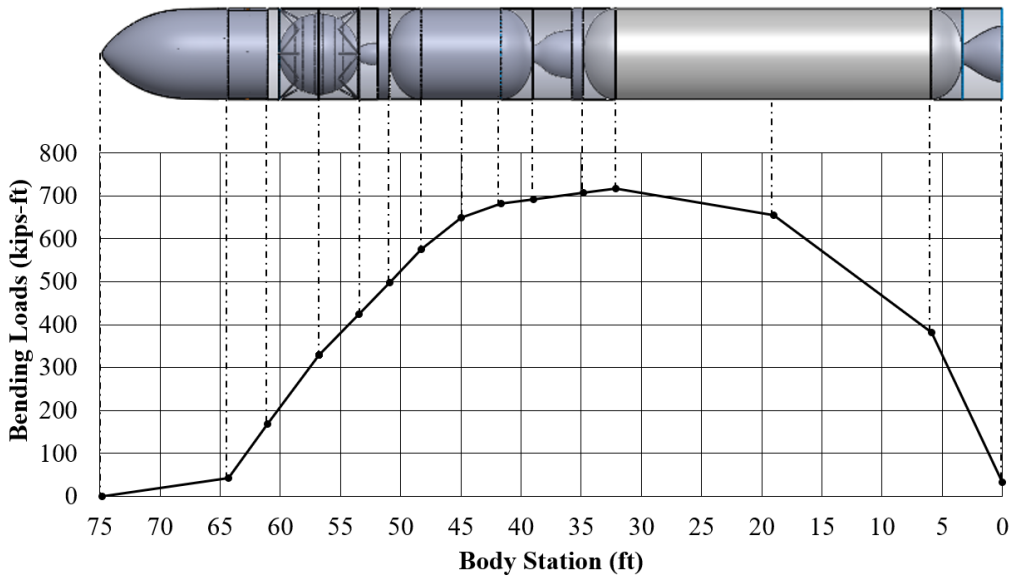


Figure 6.2-2 Max-q Bending Loads

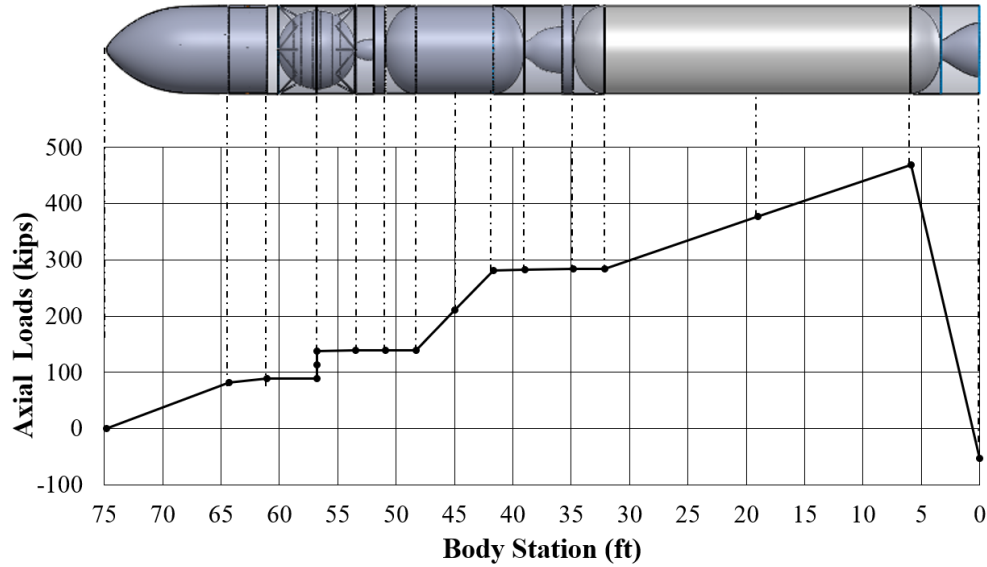


Figure 6.2-3 Max-q Axial Loads

6.3 Material Selection and Stress Analysis

6.3.1 Material Selection

Carbon epoxy composites were selected as the shroud and motor case material to reduce the structural weight of the ICBM. Table 6.3.1-1 outlines the material properties of the selected carbon epoxy composite (Ref 6.3.1-1).

Table 6.3.1-1 Carbon Epoxy Material Data

Carbon Epoxy Composite Material Data				
Material	Max Temp, °F (°C)	Density, lb _m /ft ³ (kg/m ³)	Elastic Modulus, ksi (MPa)	Min Ultimate Stress, ksi (MPa)
Carbon Epoxy Composite (T-500 12k/976)	250 (121)	99.3 (1,590)	152,000 (22.0)	1,470 (0.213)

The maximum temperature was determined from the glass transition temperature of the material. The shrouds and motor cases have an external protective laminate made of phenolic-nitrile resin and an elastomeric coating that provides impact resistance, thermal and rain protection, and is an electrical

insulator (Ref 6.3.1-2). Additionally, the inner surface of the PBV will be coated with barium sulfate to protect against x-rays and gamma rays (Ref 6.3.1-3).

When conducting the stress analysis described in the following section, only the thicknesses and material properties of the carbon composite layers were considered. This results in conservative factors of safety.

6.3.2 Stress Analysis

The shear, bending, and axial loads during pre-launch and max-q were used to calculate the total axial and shear stresses on the motor cases and shrouds. In addition, the stresses on the motor cases due to chamber pressure were calculated. For all three motor cases, the maximum stress was from the chamber pressure. For the shrouds, the maximum stress was from the total axial stress (from combined axial and bending loads) during max-q.

Table 6.3.2-1 outlines the thicknesses and factors of safety for critical locations along the ICBM. Some locations required the use of a minimum gauge thickness of 0.02-in which resulted in a high factor of safety.

Table 6.3.2-1 Stress Analysis Results

Stress Analysis Results			
Location	Thickness, in (mm)	Load Case	FS
Top of payload fairing	0.02 (0.5)	Max-q	-
Bottom of payload fairing/top of pbv	0.02 (0.5)	Max-q	11.47
Bottom of PBV	0.02 (0.5)	Max-q	6.69
Top of 3rd stage motor case	0.189 (4.8)	Chamber pressure	1.71
Middle of 3rd stage motor case	0.189 (4.8)	Chamber pressure	1.72
Bottom of 3rd stage motor case	0.189 (4.8)	Chamber pressure	1.73
Top of 3rd to 2nd stage interstage	0.02 (0.5)	Max-q	3.28

Bottom of 3rd to 2nd stage interstage	0.02 (0.5)	Max-q	2.96
Top of 2nd stage motor case	0.189 (4.8)	Chamber pressure	1.50
Middle of 2nd stage motor case	0.189 (4.8)	Chamber pressure	1.51
Bottom of 2nd stage motor case	0.189 (4.8)	Chamber pressure	1.52
Top of 2nd to 1st stage interstage	0.02 (0.5)	Max-q	1.84
Bottom of 2nd to 1st stage interstage	0.02 (0.5)	Max-q	1.81
Top of 3rd stage motor case	0.189 (4.8)	Chamber pressure	1.52
Middle of 1st stage motor case	0.189 (4.8)	Chamber pressure	1.52
Bottom of 1st stage motor case	0.189 (4.8)	Chamber pressure	1.59
Bottom of ground support	0.02 (0.5)	Max-q	17.07

The lowest factor of safety is 1.5 at the top of the second stage motor case.

6.4 Attitude Control System

The ICBM will utilize three inertial navigation systems (INS) and one celestial navigation system (CNS) per the RFP. Each INS uses three accelerometers and three gyroscopes to determine attitude, position, acceleration, and velocity. These measurements are updated at a quicker rate than the CNS but accumulate error over time. CNS uses star elevation measurements and a star database to determine attitude, position, and velocity. These measurements are highly accurate, but update at a slower rate than the INS. The solution to this problem is having the INS measurements fill in the gaps between CNS data. The CNS is a favorable over a GPS because it cannot be jammed. In case of CNS or INS failure, the systems will run through a voting system which will use probability and a dynamic model to take the most accurate data. The Kalman filter then calibrates the navigation systems in order for them to continue to provide accurate data. Once the vehicles attitude is decided, the system adjusts to the desired attitude

via thrust vectoring. The overall attitude control system in block diagram form can be viewed in Figure 6.4-1 (Ref 4.3.1-1). It is important to note the vehicle uses Lambert guidance during its third stage and post-boost phase for maximum accuracy during targeting.

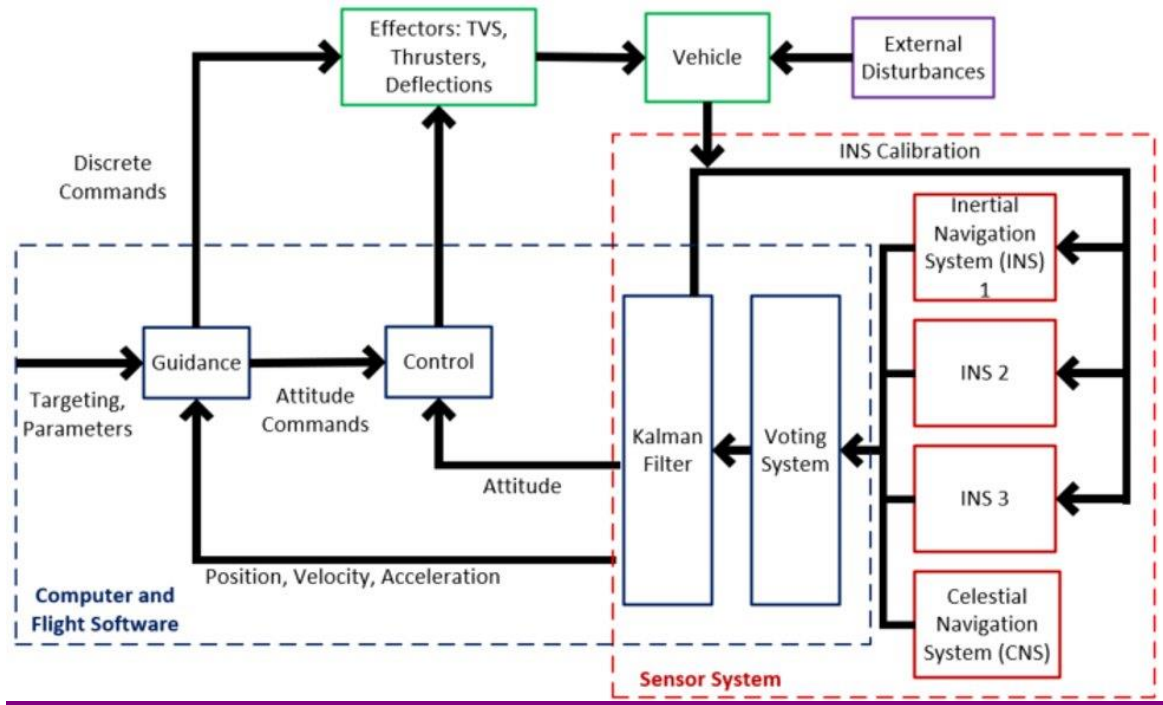


Figure 6.4-1 ICBM Attitude Control Block Diagram

6.5 Aerodynamic Stability

The aerodynamic stability of the ICBM was predicted using RASAero, a combined aerodynamic analysis and flight simulation software. It was used to estimate the aerodynamic coefficients during subsonic, transonic, supersonic, and hypersonic flight regimes, ranging from Mach 0.01 to Mach 25. The RASAero software has been calibrated using NACA and NASA wind tunnel data, free-flight test data, sounding rocket data, missile data, and professional engineering methods of analysis. RASAero has demonstrated an overall 3.38% average error equivalent numerical accuracy for altitude predictions. The various plots of aerodynamic capabilities are shown below (Figures 6.5-1 through 6.5-4).

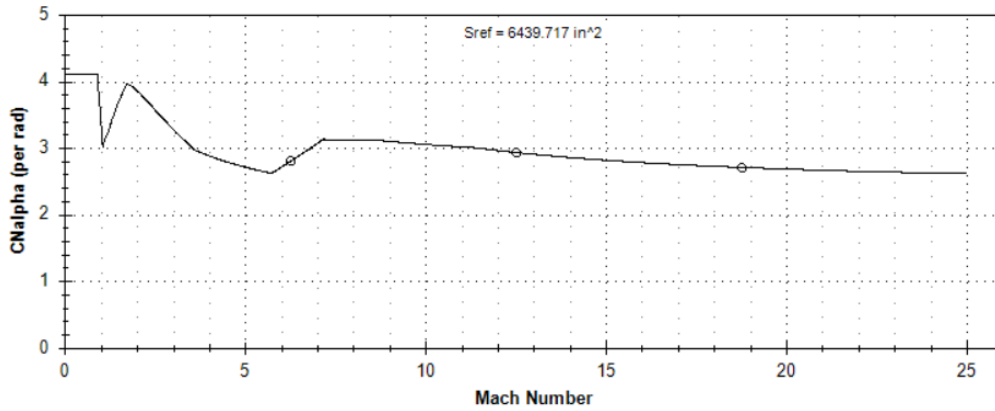


Figure 6.5-1 $C_{N\alpha}$ vs. Mach number

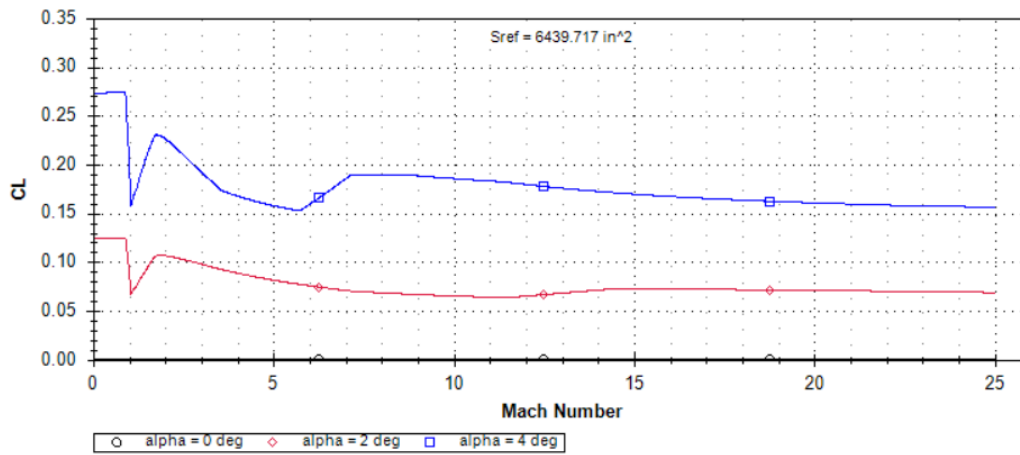


Figure 6.5-2 C_L vs. Mach number

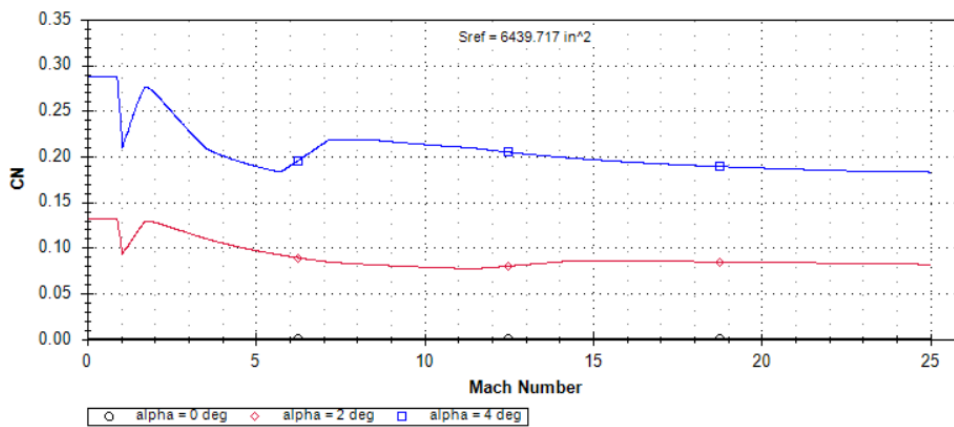


Figure 6.5-3 C_N vs. Mach number

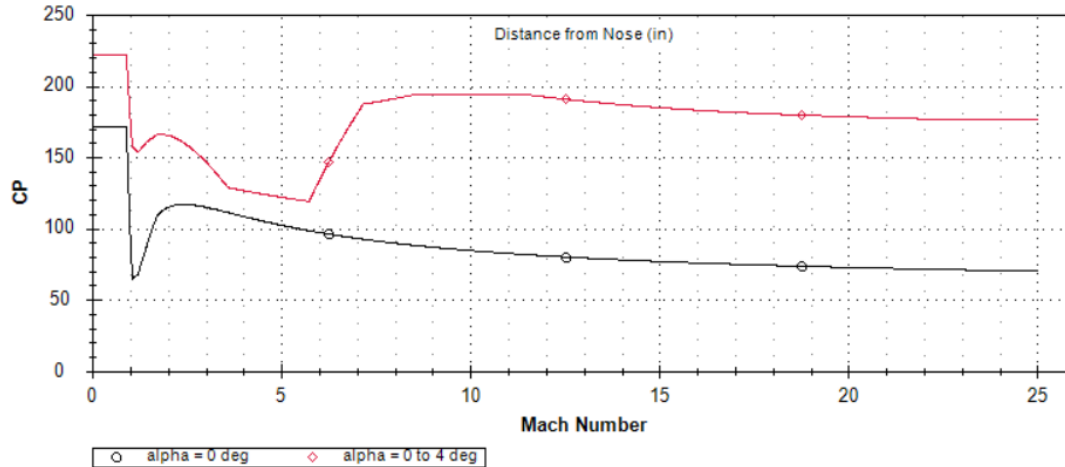


Figure 6.5-4 CP vs. Mach number

6.5.1 Static Stability

Since the CP is ahead of the CM, the vehicle is statically unstable, but grows more stable as the Mach number increases (Figure 6.5-4). Using preliminary time to double calculations the time to double was found to be 1.22 seconds using Equation 6.5.1-1 below (Ref 4.3.1-1).

$$T_{double} = \ln(2) \sqrt{I_y M_\alpha} \quad \text{(Equation 6.5.1-1)}$$

This is above the threshold of 0.5 seconds, meaning the vehicle can be stabilized. Taking the worst-case scenario when the CP is farthest from the CM and the highest destabilizing force is acting on the CP at max-Q, the equations of motion for the vehicle were found. This scenario is depicted below in Figure 6.5.1-1 with the letter P representing the CP, F representing the destabilizing force, l_a as the distance between the CM and CP, l is the distance from the CM to the top of the engine, T is the thrust, and the letter C representing the CM (Ref 4.3.1-1).

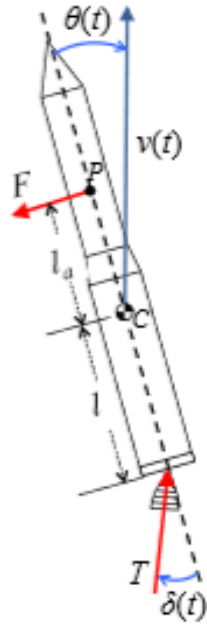


Figure 6.5.1-1 Free Body Diagram of Launch Vehicle

Assuming small angles and taking the Laplace transform, the transfer function of the ICBM was obtained. A rate feedback gain was added as an to attempt to stabilize the vehicle without a controls analysis. The transfer function of the vehicle is found below.

$$\text{Value:} \quad \frac{8.76e05}{1.035e07 s^2 - 1.752e06}$$

Figure 6.5.1-2 ICBM Transfer Function

Taking the transfer function into MATLAB and using the rlocus() function and bode() function, the closed loop root locus was found. As shown in Figure 6.5.1-3 the vehicle was unstable. The gain and phase margins did not have a stable frequency range. The gain margin was found to be 6.02 dB. A closed loop feedback controller needed to be added.

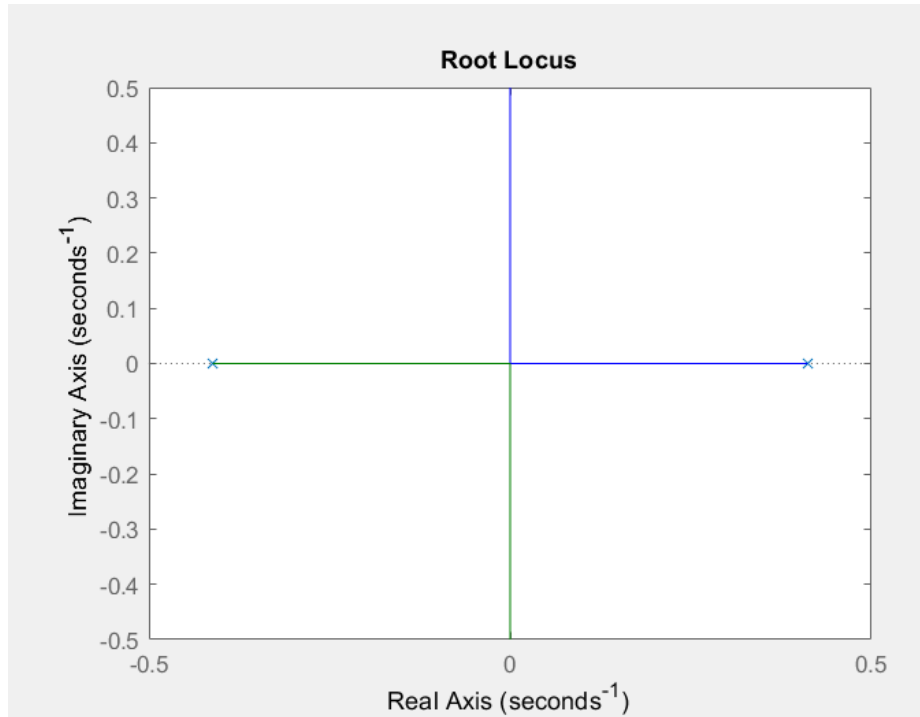


Figure 6.5.1-3 ICBM Closed Loop Root Locus with Rate Feedback Gain

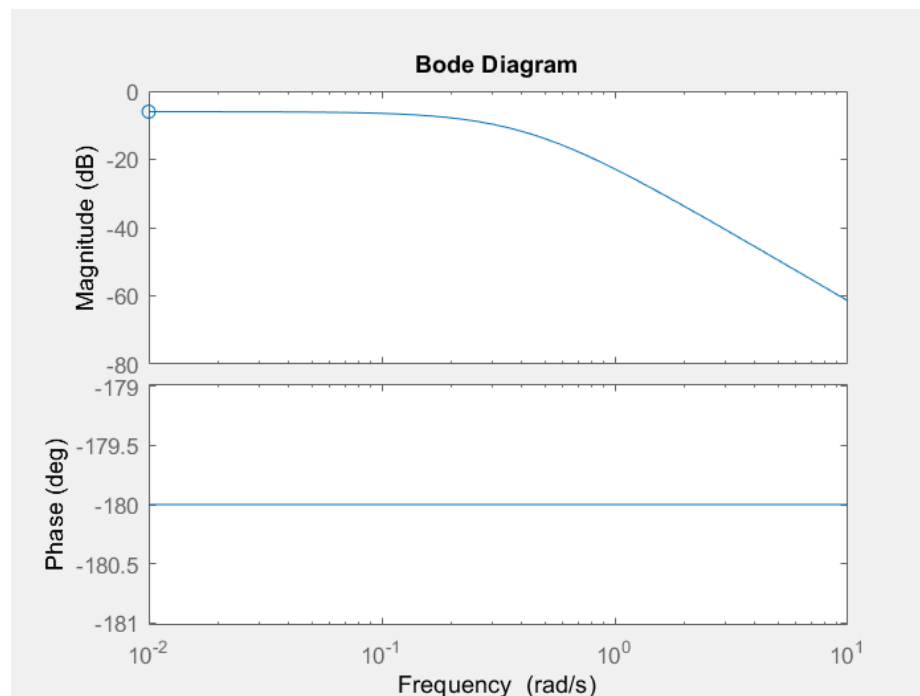


Figure 6.5.1-4 ICBM Bode Diagram with Rate Feedback Gain

6.5.2 Closed Loop Stability

A proportional–integral–derivative controller was to be designed to stabilize the vehicle. This process was undertaken using MATLAB’s application Control System Designer. Furthermore, a PID tuner within the application was used to optimize the step response. Final adjustments were made by changing the gain and phase margins within the bode editor. Overall, the results show a stable closed loop system for the ICBM. The controller transfer function is shown in Figure 6.5.2-1.

$$\text{Value:} \\ \frac{329.83 (s+0.6217) (s+0.1558)}{s}$$

Figure 6.5.2-1 PID Controller Transfer Function

Figure 6.5.2-2 shows the root locus which indicates a stable system.

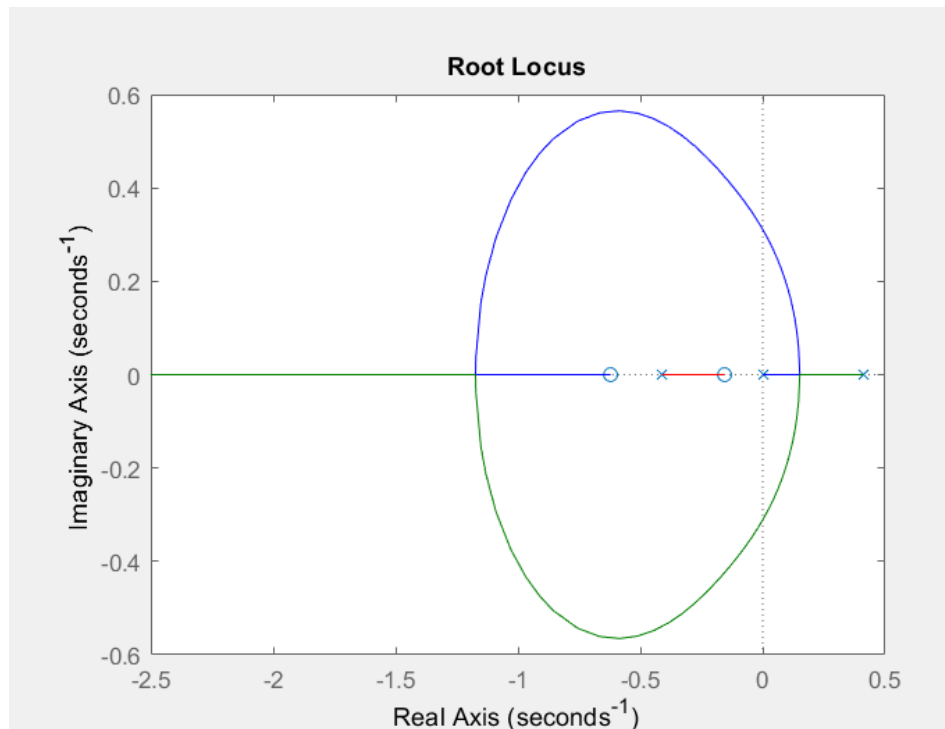


Figure 6.5.2-2 Root Locus with PID Controller

The final value of the transfer function for the PID controller is below. The step response shown in Figure 6.5.2-3 has a rise time of 0.0729 seconds, an overshoot of 2.59% at 0.289 seconds. It has a settling time of 0.921 seconds with no steady state error.

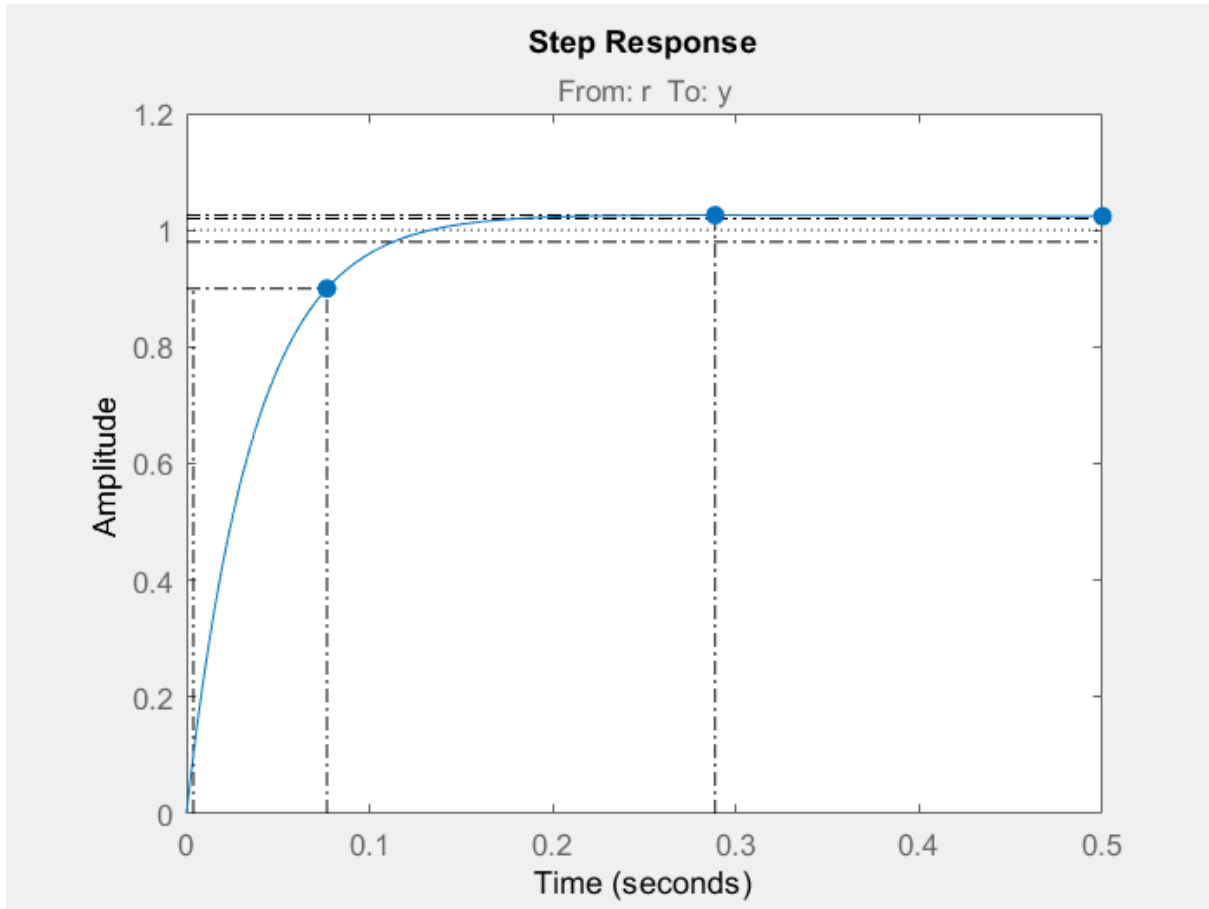


Figure 6.5.2-3 Step Response with PID Controller

The bode diagram is shown in Figure 6.5.2-4, the markers depict the stability margins. The gain margin is -38.2 dB at a frequency of 0.311 rad/s. The phase margin is 88.4° at a delay margin of 0.0553 seconds.

This occurs at frequency 27.9 rad/s.

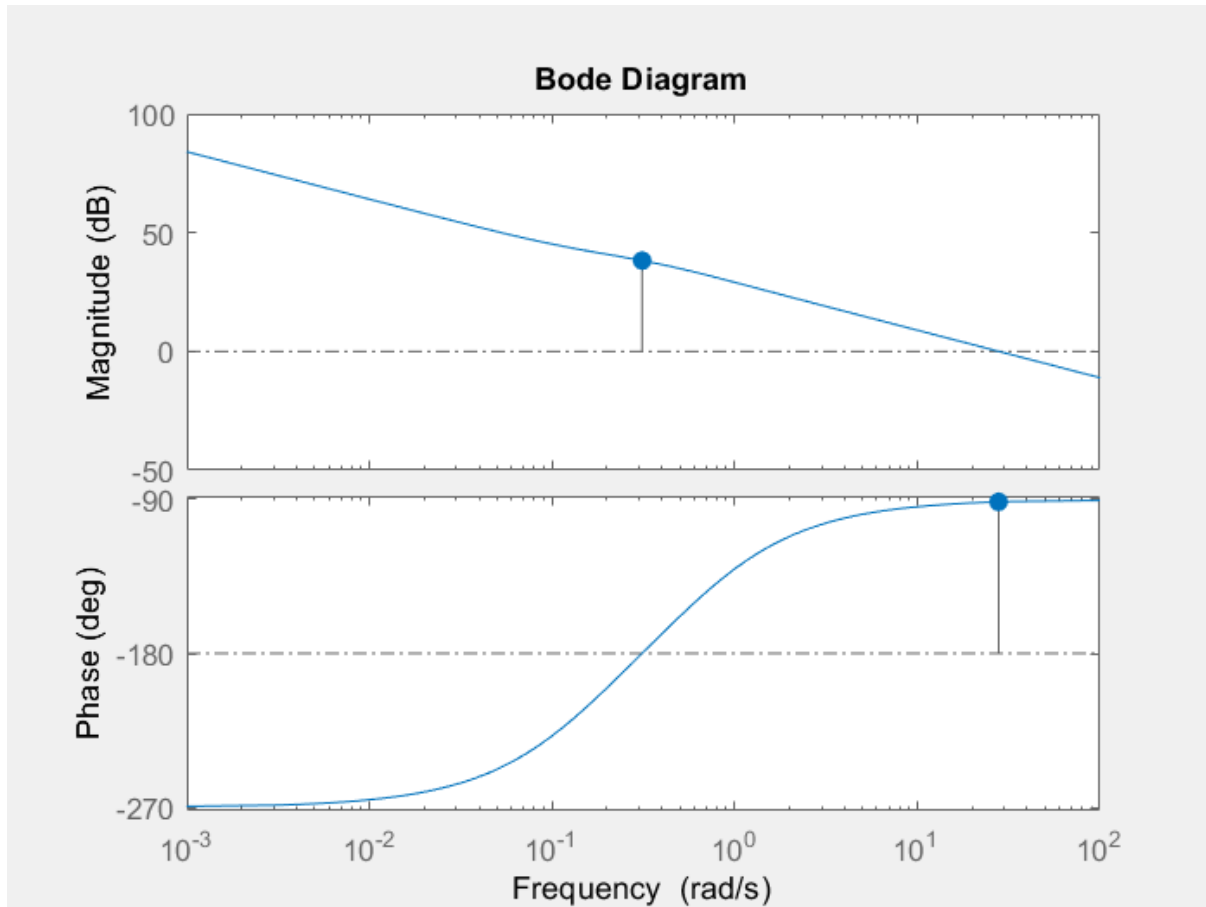


Figure 6.5.2-4 Bode Diagram with PID Controller

6.6 Software and Power Considerations

When considering software for the ICBM, Vega System was examined and resulted in an estimated 100,000 lines of code for the launch vehicle and the ballistic RV. The glide RV however has an estimated 1 million lines of code based on the Space Shuttle (Ref 4.3.1-1). The dramatic increase in code can be attributed to the software for attitude control, the advanced LQR control system required, and the software used to arm the payload.

Moving on to power considerations, the driving factor in deciding which power source to use fell with the maintenance requirement. Thermal batteries were chosen to power the avionics on board the launch vehicle, the PBV, and both the glide and ballistic RVs. Thermal batteries were chosen due to their 20 year or longer storage life, high energy density, and cost effectiveness. The batteries are made of lithium

silicon/iron disulfide couple for the highest capacity per unit volume. They are completely inert and non-reactive until activated. It is possible to activate without any preparation and supply full power almost immediately. These batteries may also be mass produced due to their automated production (Ref 6.6-1).

6.7 Reliability

Reliability design is ultimately a tradeoff between component/system redundancy and weight/volume. Risks and reliability analyses employ statistical methods to estimate the reliability of a system in order to mitigate risk. In this preliminary design, some risks were identified, and redundant systems were designed and considered, while reliability was calculated from empirical statistics on major subsystems. For qualitative system configurations, hot/cold spares, and diverse back ups are considered. Hot spares are identical redundant backups that are continuously powered for a smooth operation transition in the case the primary component fails. Cold spares are switched on when a component fails, to reduce the number of operating components when the system is operating nominally. It is important that during the detailed design, manufacturing, and testing phase of the system, that design choices, manufacturing methods, and testing methods are all NASA Technical Standard Compliant, particularly NPR 8705.6B – Safety and Mission Assurance Audits, Reviews, and Assessments, NASA – STD - 8739.8 – Software Assurance, and NPR 8715.3 – NASA General Safety Program Requirements. This allows Joust’s system to be compliant to government standards, reducing logistical errors and lead time of approving compliancy. In addition, it is important to continue the detailed design phase with NASA’s Continuous Risk Management (CRM) Process of inspecting, analyzing, and controlling risks.

To calculate the overall reliability of the system, each “unit” must be calculated for its reliability. For component reliability, some risks were identified and a redundant system was implemented. Assuming a successful mitigation of risk results in a 99.5% reliability, a minimum component reliability is calculated. This minimum component reliability can be used to obtain minimum requirement components from manufactures (i.e. Power supplies from Raytheon). Note the calculated component reliabilities are

assumed to be all the same for each set of components. The equations for parallel, and k-out-of-n system reliabilities are shown below, respectively:

$$R_{n_parallel} = 1 - (1 - R_A)(1 - R_B) \dots 1 - R_n \quad (\text{Equation 6.7-1})$$

$$R_{k-out-of-n} = \sum_{j=k}^n \binom{n}{j} R^j (1 - R)^{n-j} \triangleq \sum_{j=k}^n P(j) \quad (\text{Equation 6.7-2})$$

Five individual component failure modes were investigated; two electrical and three propulsion. The first electrical failure mode was a flight computer (FC) malfunction. To mitigate the possibility of a flight computer failure, three FCs in parallel will be implemented with a voting system, two with the same hardware and language, while the other with different hardware and language. This reduces the possibility of a single point of failure in the flight computers. Power supplies were the second electrical failure mode that was investigated. There will be four parallel power supplies for the flight avionics which will prevent a total loss of power if three out of four power supplies fail.

Table 6.7-1 Electrical System Minimum Component Reliability Requirements

Electrical System Minimum Component Reliability Requirements				
System(s)	Required Min. Reliability	Component Orientation	Number of Components	Total Chance of Success
Flight Computer	67%	Parallel	3	99.59%
Power Supply	60%	Parallel	4	99.58%

Above is a table summarizing the minimum component reliability to be obtained, to maintain a 99.5% subsystem reliability.

Three propulsion system components and their failure modes were investigated. The first failure mode is improper tank sealing. The solid motors will be sealed with three redundant o-ring seals and other sealing

surfaces. Failure to ignite the motor is considered a failure, therefore, an independently powered, double redundant ignition system will be implemented. Lastly, a motor depressurization system will be implemented with multiple redundancies to prevent any catastrophes at take-offs (CATOs). The table below summarizes the minimum component reliability to be acquired for the propulsion system.

Table 6.7-2 Solid Propulsion System Minimum Component Reliability Requirements

Solid Propulsion System Minimum Component Reliability Requirements				
System(s)	Required Min. Reliability	Component Orientation	Number of Components	Total Chance of Success
Tank Seals	74%	Series	3	99.54%
Ignition System	83%	Parallel	3	99.51%
Pressure Relief System	59%	Parallel	6	99.53%

To calculate the ICBM system lifetime reliability, each subsystem's reliability must be calculated. For the purpose of the preliminary design of the ICBM, an estimated reliability of each subsystem and individual components are calculated based on failure rates from various reliability handbooks and test data. For each subsystem reliability, the following equation is used:

$$R(t) = e^{-\lambda t} \quad \text{(Equation 6.7-3)}$$

where λ is the component/subsystem failure rate, obtained from Ref 6.7-3 and Ref 6.7-4.

To obtain a total system reliability, one must make an arbitrary Weibull Bathtub curve assumption of 20 years of operation. Due to the infancy of the design, these parameters are difficult to estimate, but as the detailed design and testing progress these values will become more apparent. An example Weibull Bathtub curve is shown below. For reference, the equation and variables used are:

$$\lambda(T) = k\lambda cT^{c-1} + (1-k)bT^{b-1} \beta e^{-(\beta T^b)} \quad \text{(Equation 6.7-1)}$$

Where $k = 0.99$, $c = 0.5$ (scale factor), $b = 1.025$ (scale factor), $\beta = 0.01$ (shape factor), and $\lambda = 0.0095$ (shape factor).

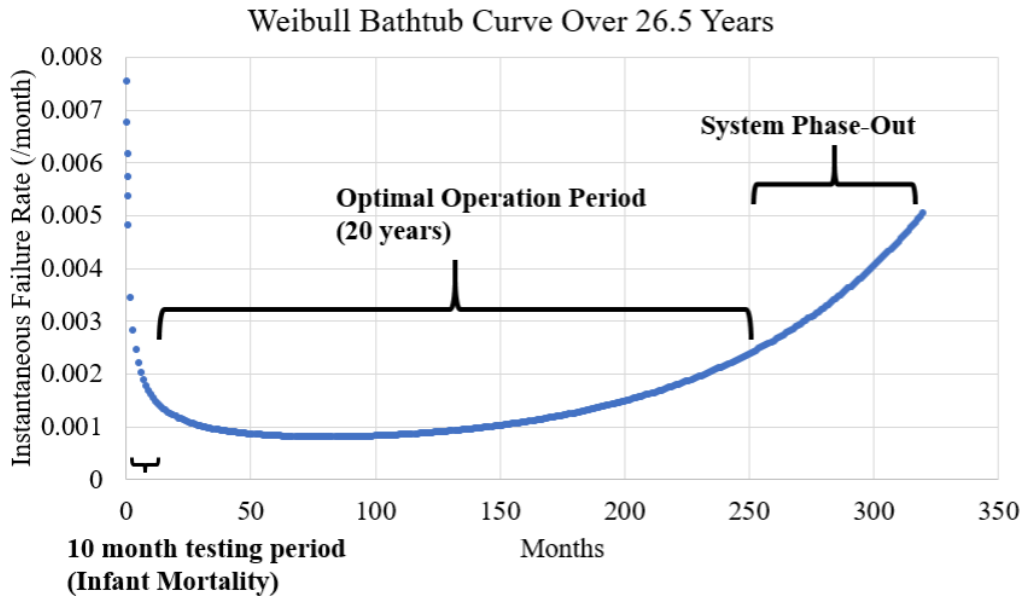


Figure 6.7-1 Weibull Bathtub curve depicting 3 life-cycle phases

Assuming the dormant reliability of each subsystem follows the optimal Weibull curve and that the operational period lies within a reasonably low failure rate, the subsystem failure rate can be found. The following table depicts the subsystem failure rates. Note the operation times are only allocated for inspection (i.e. turning on power supplies to ensure nominal functionality) and actual flight. This is due to the assumption that each inspection reveals and verifies that the reliability is 100% and the failure rate has not increased drastically, and that it remains towards the bottom of the bathtub curve.

Table 6.7-3 Subsystem Reliability and Total ICBM System Reliability

Subsystem	λ (/hr)	t (hr)	Reliability (R)
Avionics System	5.80×10^{-5}	60.9	99.65%
Power System	2.00×10^{-6}	60.9	99.99%
Propulsion System	8.80×10^{-7}	0.917	100.00%
Ignition System	5.66×10^{-6}	60.9	99.97%
Thrust Termination System	3.20×10^{-5}	60.9	99.81%
Total System Reliability			99.88%

6.8 Manufacturing and Maintenance

6.8.1 Manufacturing

As mentioned in Section 6.3.1, the fairing, shrouds, and motor cases will be made from carbon epoxy composites. They will be manufactured using filament winding. Due to the possibility of galvanic corrosion compromising the integrity of the structure, hydrolysable linkage resins will not be used in the manufacturing of any composite structures. However, the structures shall be constructed of aluminum extrusions for their low cost and ease of assembly. Lastly, the rocket motor nozzles will be 3-D printed out of Inconel 718 to lower the cost of manufacturing while increasing ease of assembly.

6.8.2 Maintenance

Per the RFP, the system will be able to go without maintenance for 20 years, however, inspection of components will be allowed. Therefore, inspection of the solid rocket motors will occur every 5 years, the missile suspension system will be inspected every 2 years, and the ignition cable(s) and ordnance tests will occur once every year. During the motors' inspections, the composite fibers of the motor cases and the propellant grains themselves will be examined with X-rays. Additionally, electronic components will be tested before installation to remove the infant mortality risk and the environmental control system will operate around the clock within the silo. Finally, the electronics will be hardened against EMP.

6.9 Launch System

6.9.1 Fixed vs. Mobile Launch System

Per the RFP, the ICBM must launch from either an existing Minuteman III silo or a mobile launch system. Table 6.9.1-1 shows the fixed versus mobile launch system trade study.

Table 6.9.1-1 Launch System Trade Study

Launch System Trade Study		
Criteria	Fixed Launch System (Minuteman III Silo)	Mobile Launch System
Added Cost	+ \$0	+ \$130B
Hardness (psi)	2,000-3,000	15-30
System Survivability (# of enemy re-entry vehicles required to destroy all 450 ICBMs)	1,200	120 - 10,000

The data in the table was obtained from Johns Hopkins Applied Physics Laboratory’s National Security Report (Ref 6.9.1-1). It is hard to assess the survivability of mobile ICBMs deploying from a garrison due to the uncertainties in numerous parameters. Given the significant costs of a mobile launch system and the uncertainty in system survivability, all ICBMs will be launched from existing Minuteman III silos.

6.9.2 Silo Survivability

The survivability of a silo-based ICBM system is shown in Figure 6.9.2-1 (Ref 6.9.1-1).

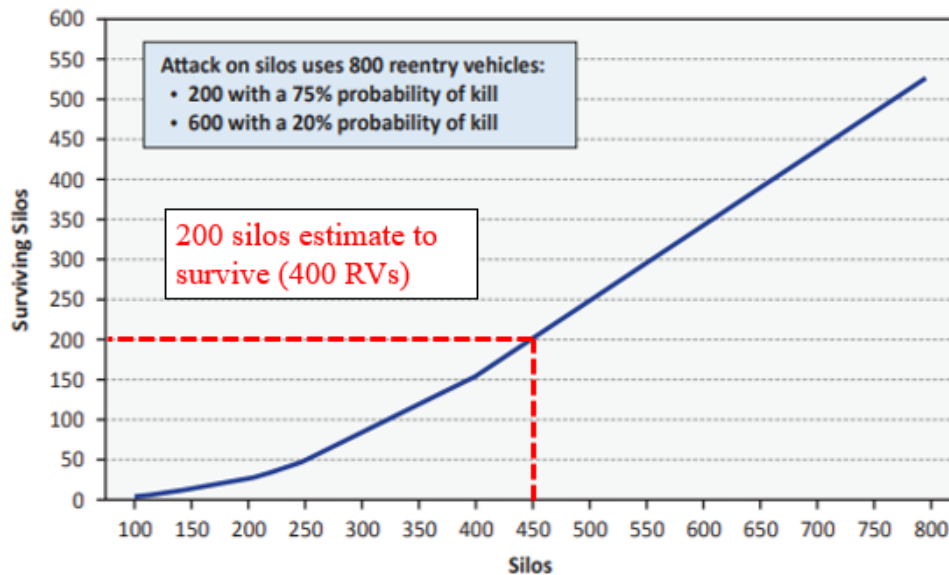


Figure 6.9.2-1 Silo Survivability

If all 450 ICBMs are housed in Minuteman III silos, 200 silos would survive in an attack using 800 RVs (200 with 75% probability to kill and 600 with a 20% probability of kill). This is enough to launch a significant counter-attack with 400 RVs, in addition to SLBMs and long-range nuclear-capable bombers.

The chart was also used to justify a completely silo-based ICBM force, instead of having a mix of both silo and mobile launched systems. As the amount of silos increase, the rate of increase of surviving silos also increases. Thus, replacing only some of the silos with a mobile launch platform would be detrimental to the system as a whole.

Figure 6.9.2-2 illustrates the enemy’s probability of kill against a Minuteman III silo.

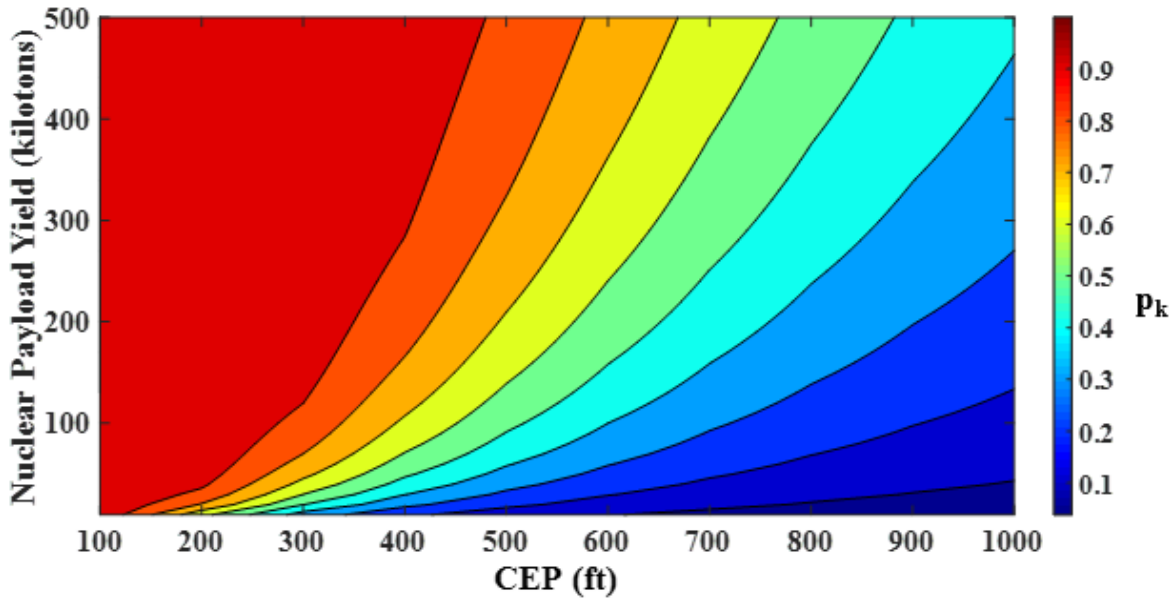


Figure 6.9.2-2 Probability of Kill Against Minuteman III Silo

The figure was generated from data calculated using Equation 6.9.2-1 (Ref 6.9.1-1).

$$p_k = 1 - 0.5 \frac{(1600)^2 Y^{2/3}}{H^{2/3} CEP^2} \quad \text{(Equation 6.9.1-1)}$$

Where p_k is the probability of kill, Y is the yield, and H is the hardness. It assumes 100% RV reliability.

For Figure 6.9.2-2, a hardness of 3,000 psi was used.

The probability of kill is high if the enemy RV's CEP is less than 200-ft or has a high yield nuclear payload. The figure also shows that the current ICBM design, with its 300 kt nuclear payload, only requires a CEP of 400-ft to have a probability of kill over 90%.

6.10 Mission Safety

To ensure mission safety there will be no ground communications with the ICBM during flight. This, combined with proper shielding and grounding of electronic components will prevent the ICBM from being hacked. An autonomous flight termination system will only be installed during testing. This ensures safe practices during the flight tests. Additionally, warheads will be armed during re-entry. This guarantees no armed warheads will be flying over non-enemy territory. The warheads attitude control system will also prevent the arming of the nuclear payload if the PBV cannot position the RV correctly. Due to unpredictable atmospheric conditions, this could lead to warheads being armed and sent in incorrect directions.

6.11 Disposal Concepts

The disposal of the Joust Aerospace system is based on one the most recent ICBM disposal. The Minuteman II missiles at Whiteman Air Force Base in Missouri were decommissioned in 1992, and the Joust Aerospace missiles will be disposed of in similar way, unless new treaties are signed that require different methods. The missiles will be disassembled onsite at the bases where they are located and prepared for transport by either truck or rail car. The solid rocket motors will be transported to Hill Air Force Base in Utah for either disposal or reuse. The classified material contained in the RV will be returned to the Department of Energy for disposal. Guidance and navigation systems will be transferred to the Pueblo Army Depot in Colorado where they will be disposed of.

6.12 End of Mission Repurposing

At the end of the system lifetime, it may be viable to repurpose the ICBM boost stages as launch vehicles. Through the simulation method described in Section 5.1, it has been demonstrated that the Lance system

can be used to launch small to medium satellites into low-earth orbit. A sample simulation showed the capability of the system to launch a 2,200 lbm payload into a 200 nmi circular orbit from Cape Canaveral (Table 6.12-1). A launch system of this magnitude is comparable to the Firefly Alpha launch vehicle (Ref 6.12-1), which is intended to cover the commercial small satellite market.

Table 6.12-1 Sample Burnout Results for Repurposed Vehicle

Solid-Fueled Launch Vehicle	
Payload Mass, lb _m (kg)	2,210 (1,000)
Altitude, nmi (km)	206 (382)
$Q, v^2/v_c^2$	1.08
Flight Path Angle, deg	1.40

Additionally, the system can be used to test future anti-ballistic missile system. This option would be more cost effective than small satellite repurposing, since the transition only involves the removal of RVs.

6.13 Cost Analysis

6.13.1 United States Air Force Space Planners Guide

The first cost estimation was done using the 1965 USAF Space Planners Guide. This method uses charts to estimate the cost of each component of the development and production of the system using inputs such as mass and engine thrust. The type of vehicle analyzed was a three-stage solid propellant launch vehicle with 455 total units produced. All values were adjusted for inflation from 1965, where \$1 has the buying power of \$8 in 2019. The total cost for development and production was found to be \$26.4 billion. Additionally, the unit cost for each missile was found to be \$21.6 million. The results of the analysis are presented in Table 6.13–1.

Table 6.13-1 USAF Space Planners Guide Cost Estimation

Total Launch Vehicle Program Cost			
	Description	1965 Cost (millions)	2019 Cost (millions)
1	Total DT&E	202	1,620
2	Total Facilities	5.8	46.4
3	Total AGE Production	9	72
4	Total Hardware Production	1,400	11,200
5	Total Operations	1,680	13,400
6	Total Launch Vehicle System Program	3,290	26,400

6.13.2 TRANCOST Analysis

The cost estimation method used was TRANCOST Analysis. This method uses equations based on the masses of certain aspects of the system such as propellant mass and payload mass. These factors are multiplied by weighting factors which vary based on aspects such as team experience and technology readiness. This allows for development and production costs to be determined using the units for work year. Work years were then converted to 2019 \$USD using the 2019 work year rate. The total development cost was found to be \$5.9 billion, with the production cost at \$33.5 billion. The unit cost for each missile was to be \$73.6 million. In total the TRANCOST model found the Joust Aerospace system would cost \$39.4 billion. The results of the analysis are presented in Table 6.13–1.

Table 6.13-1 TRANSCOST Analysis

Development Costs	
Solid Motor Costs	8,574 WYr
Propulsion Module Costs (PBV and RVs)	1,033 WYr
Total Development Cost	\$5.9 Billion
Production Costs	
Engine Production Costs	122.2 WYr
Propulsion Module Costs (PBV and RVs)	48.1 WYr
Cost Per Unit	\$73.6 Million
Total Production Cost (455 Units)	\$33.5 Billion
Total System Cost	\$39.4 Billion

6.13.3 Additional Costs and Cost Comparison

Additional facilities costs were also considered as neither cost estimation method accounted for silo-based launch vehicles. Using the Air Force estimates for the fifty-year life-cycle of the Ground Strategic Deterrent, it was estimated that the facilities operation costs would reach \$3 billion per year for the 450 silos. Additionally, based on 2014 estimates from the RAND Corporation, silo upgrade costs will amount to about \$6.6 billion, which is added to the launch vehicle costs. Compared to the Ground Based Strategic Deterrent, these cost estimations show a lower price for the Joust Aerospace system to replace the Minuteman III, where the lowest estimate for the replacement is \$62 billion. Because no unit cost is associated with GBSD, the next best comparison is the Minuteman III unit cost, which is approximately \$20 million adjusted for inflation. The USAF Space Planners Guide shows a slightly higher unit cost,

with TRANSCOST showing a unit cost about 3.5 times as high. These comparisons are presented in Table 6.13.3-1 and 2.

Table 6.13.3-1 Cost Estimation Comparison

Minuteman III Replacement Cost Estimates	
Joust Aerospace	
Space Planners Guide	\$33 Billion
TRANSCOST	\$46 Billion
Ground Based Strategic Deterrent	
Air Force Estimate	\$62 Billion
Pentagon Estimate	\$85 Billion
Other Air Force Estimates	\$140 Billion

Table 6.13.3-2 Unit Cost Estimation Comparison

ICBM Unit Cost Estimate	
Joust Aerospace	
Space Planners Guide	\$21.6 Million
TRANSCOST	\$73.3 Million
Minuteman III	
1970s Adjusted Cost	\$20 Million

6.14 Treaty Compliance

Two treaties were looked at to determine if Joust Aerospace was compliant with all of their provisions. The first was the Intermediate-Range Nuclear Forces Treaty, which eliminates the use of land-based missiles that have ranges of 310-3,240 miles. Although the treaty is currently suspended, if it were to be reinstated in the future, Joust Aerospace would be compliant as the missile range exceeds 3,240 miles.

The second treaty looked at was the New Strategic Arms Reduction Treaty. As Joust Aerospace will only be placing ICBMs in the 450 active Minuteman III silos, the system will be compliant with the treaty.

6.15 Development Schedule

Development on the Joust Aerospace system will begin in October 2020, as stated in the RFP. By mid-2022, production will begin on the first of the five test vehicles, with completion in 2025. During this time period component testing will take place, with emphasis placed on newer technologies that require maturation. This will lead into the first test flight in early 2027. This allows for over six years total of development and production for the new missile, compared to the Minuteman I, which had three years between development commencing and the first test flight. Subsequent test flights will occur over the next two years, with 1 per half-year until early 2029. Enough data from these test flights should be necessary to allow delivery of the missiles to each silo in late 2029, where initial operational capability will be reached in December 2029. Because of its new technology, the glide re-entry vehicle may require extra flight testing. If this is the case, additional ballistic re-entry vehicles will be produced and used in place of the glide vehicles until they are ready to ensure IOC in December 2029.

6.16 Derived Requirements

Table 6.16-1 outlines the derived requirements.

Table 6.16-1 Derived Requirements

Requirement Statement	Major Disciplines
Propellants must be storable for up to 20 years without maintenance	Propulsion, Maintenance
If mobile-launched, a mobile launching system must be designed to launch from a truck or train car	Launch Site Operation, Risk Analysis, Logistics
If mobile-launched, the mobile launching erection system must be able to carry the entire weight of the ICBM	Launch Site Operation, Structures
If mobile-launched, the mobile launching system must be able to carry the ICBM safely to a predetermined location	Launch Site Operation, Risk Analysis, Logistics
The missile will implement high efficiency propellants to increase the previous Minuteman III range by 3000 nm	Propulsion
If silo-launched, the missile diameter must be less than or equal to that of the Peacekeeper (2.3 m)	Launch Site Operation, Inboard Profile
If silo-launched the missile length must be less than or equal to 25.9 m (length of Peacekeeper launch canister)	Launch Site Operation, Inboard Profile
The system will utilize new GPS systems capable of reading m-code as a redundant navigational system	Guidance, Stability, and Control
Payload fairing must encapsulate the entirety of both re-entry vehicles with at least 1 inch of margin on all sides	Inboard Profile, Aerodynamics, Structures
The thrust to weight ratio at liftoff should exceed 2	Propulsion
The TVC must be able to provide a deflection angle of 3.2°	Controls, Aerodynamics

7.0 Project Schedule

The project was started on November 11, 2018. As shown in Figure 7.0-1, the team completed a Systems Definition Review (SDR) and Preliminary Design Review (PDR). The SDR was conducted at Northrop Grumman Innovation Systems in Chandler, AZ and the PDR was conducted at the Los Angeles Air Force Base.

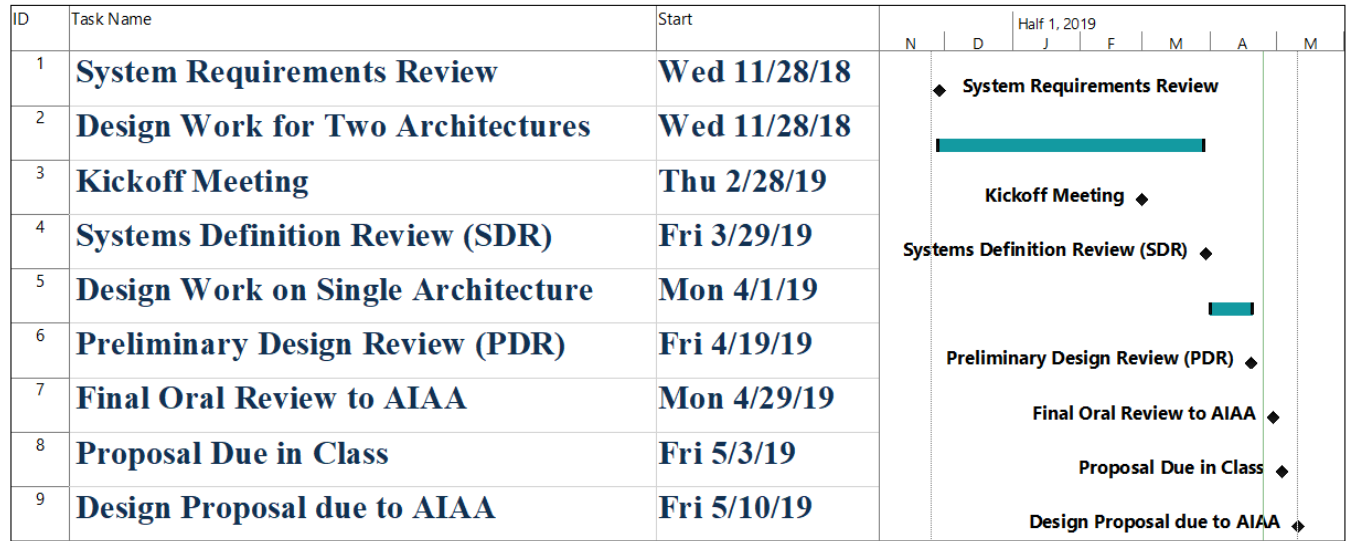


Figure 7.0-1 Project Schedule

8.0 Compliance Matrix

The compliance matrix is provided in Table 8.0-1. The design meets all requirements.

Table 8.0-1 Compliance Matrix

Requirement Statement	Compliant	Verification Method
The Long-Range Strategic Missile (LRSM) must be capable of carrying a minimum of two independently guided payloads in separate re-entry vehicles	Yes	Inspection
The LRSM will have the capability of being stored for 20 years without maintenance	Yes	Similarity
The LRSM will have a threshold range of 7,000 nmi and an objective range of 10,000 nmi	Yes	Trajectory Simulations (Range = 10,000 nmi)
Each of the two payloads has a weight of 1,000 lbs with a 22 in diameter and an 80 in length	Yes	Inspection
The circular error probability will have an objective range of 100 ft and threshold range of 150 ft with a 100 nmi footprint	Yes	Monte Carlo Simulations (CEP = 142 ft)
The LRSM will deploy its payload with an objective flight time of 60 min and threshold flight time of 90 min	Yes	Trajectory Simulation (t = 46 min)
Missile will be capable of launching from a ground-based silo, truck, or train car	Yes	Inspection
The re-entry vehicles must be designed to engage deeply buried hardened targets and soft target areas	Yes	Inspection
The weapon system shall use an IMU and celestial navigation to guide the re-entry vehicle to the separation point	Yes	Inspection
Each independently guided payload shall be GPS guided and have a backup navigation system in case of GPS denial	Yes	Inspection
Development will start in 2020 with operational capability in 2029	Yes	Scheduling
The cost estimate will include the cost of the missile, silo, and launching costs for 455 total units at 45 launcher sites	Yes	Cost Analysis

9.0 Conclusion

Joust Aerospace has designed an ICBM that is capable of meeting and exceeding the requirements listed in the RFP including objective range and time of flight. Project Lance is capable of completing any mission requirement due to its flexible payload configurations. The design combines the reliability of current ICBMs by using solid rocket motors and increases survivability through the use of both glide and ballistic RVs. Furthermore, Project Lance is cost effective in development and manufacturing costs based on current Air Force estimates. A summary of the key configurations of Project Lance are listed in Table 9.0-1.

Table 9.0-1 ICBM Summary Sheet

ICBM Summary Sheet	
Parameter	Result
Propellant	NEPE-75 (solid)
Length, ft (m)	74.8 (22.8)
Diameter, ft (m)	7.54 (2.3)
GLOM, Tons (Tonne)	107 (97.4)
Time of Flight, min	46
Max Range, nmi (km)	10,000 (18,500)
Max-Q, atm (kPa)	1.15 (117)
Cost/Unit (mil, 2019)	73.3

References

- Ref 1.3-1) Bate, R. R., Mueller, D. D., & White, J. E. *Fundamentals of Astrodynamics*. Courier Corporation.
- Ref 3.2-1) U.S. Congress, Office of Technology Assessment, *Ballistic Missile Defense Technologies, OTA-ISC-254* (Washington, DC: U.S. Government Printing Office, 1985).
- Ref 4.1-1) Kyle, E. (2017, August 29). Minotaur 4 Data Sheet. Retrieved from <https://www.spacelaunchreport.com/mintaur4.html>
- Ref 4.1-2) Sutton, George P. *Rocket Propulsion Elements: An Introduction to the Engineering of Rockets*. New York: Wiley, 1992. Print.
- Ref 4.1-3) Fleeman, E. L. (2012). *Missile design and system engineering*. Reston (Virginia): American Institute of Aeronautics and Astronautics.
- Ref 4.1-4) Vigor Yang, Thomas Brill, and Wu-Zhen Ren. *Solid Propellant Chemistry Combustion and Motor Interior Ballistics*.
- Ref 4.1-5) Taek Kim, Min & Song, Soonho & Jin Yim, Yoo & Wook Jang, Myung & Baek, Gookhyun. (2015). Comparative Study on Infrared Irradiance Emitted from Standard and Real Rocket Motor Plumes. *Propellants, Explosives, Pyrotechnics*. 40. 10.1002/prop.201400213.
- Ref 4.3.1-1) Edberg, D., & Costa, W. (2018). *Elements of Space Launch Vehicle Design*. Pomona, CA: Cognella.
- Ref 4.3.3.1-1) Frank J. Regan, *Dynamics of Atmospheric Re-Entry*, AIAA Educational Series
- Ref 4.3.3.2-1) Radcliffe, W.F, “Hypersonic Glide Vehicle Design Considerations”. Convair Astronautics
- Ref 5.1.2-1) Rogers, C.E. and Cooper, D. *Rogers Aerospace RASAero Aerodynamic Analysis and Flight Simulation Software*, 04 May 2019, from <http://www.rasaero.com/>
- Ref 5.2-1) Isaacson, J. A., & Vaughan, D. R. (1996). *Estimation and Prediction of Ballistic Missile Trajectories* (No. RAND/MR-737-AF). RAND CORP SANTA MONICA CA.
- Ref 5.2-2) Justus, C. G., & Woodrum, A. (1972). *Atmospheric pressure, density, temperature and wind variations between 50 and 200 km*.
- Ref 5.3.1-1) “What Is A Flight Termination System?” PacSci EMC, psemc.com/solutions/flight-termination/.
- Ref 5.3.1-2) *Effectiveness of Minuteman II Stage III Refurbishment Program*. apps.dtic.mil/dtic/tr/fulltext/u2/a363899.pdf.
- Ref 5.3.1-3) Vono, Charles. “Minuteman Thrust Termination.” *Charlie Vono, Retired Cold Warrior*, 10 June 2017, charlesvono.com/minuteman-thrust-termination/.
- Ref 5.3.2-1) Wellerstein, A. (n.d.). NUKEMAP. Retrieved April 16, 2019, from <http://www.nuclearsecrecy.com/nukemap/>
- Ref 5.3.3-1) Linderman, R. B., Rotx, J. V., & Yeh, G. C. (1974, September). *Design of Structures for Missile Impact*. Retrieved from inis.iaea.org/collection/NCLCollectionStore/_Public/06/178/6178001.pdf

Ref 5.3.4-1) Caston, Lauren, Robert S. Leonard, Christopher A. Mouton, Chad J. R. Ohlandt, Craig Moore, Raymond E. Conley, and Glenn Buchan, *The Future of the U.S. Intercontinental Ballistic Missile Force*. Santa Monica, CA: RAND Corporation, 2014.

<https://www.rand.org/pubs/monographs/MG1210.html>

Ref 6.1-1) *TPS Reinventing Thermal Protection in Aerospace Applications*, Amorim Cork Composites

<http://www.amorim-sealtex.com/AMORIM/UploadFiles/2013924152058965.pdf>

Ref 6.1-2) E.D. Smyly and C.D. Pears, *Properties of Ablation and Insulation Materials*, Southern Research Institute Birmingham, Alabama

<https://ntrs.nasa.gov/archive/nasa/casi.ntrs.nasa.gov/19710018270.pdf>

Ref 6.1-3) Lecture #1: Stagnation Point Heating

<https://tfaws.nasa.gov/TFAWS12/Proceedings/Aerothermodynamics%20Course.pdf>

Ref 6.3.1-1) Department of Defense. *Composite Materials Handbook*. Vol 2. 17 June 2002.

Ref 6.3.1-2) Hawkinson, Elden. *Laminated Shield for Missile Structures and Substructures*. patents.google.com/patent/US4428998

Ref 6.3.1-3) Seenappa and Manjunatha. *A Study of Shielding Properties of X-ray and Gamma in Barium Compounds*. *Journal of Radiation Protection and Research* 2017.

Ref 6.6-1) “Missile Batteries.” *Eagle Pitcher Technologies*, Eagle Pitcher Technologies, 2 Feb. 2019, www.eaglepitcher.com/markets/defense/missile-batteries/.

Ref 6.7-1) Motiwala, Samira A., Mathias, Donovan L., Mattenberger, Christopher J., *Conceptual Launch Vehicle and Spacecraft Design for Risk Assessment*, NASA

<https://ntrs.nasa.gov/archive/nasa/casi.ntrs.nasa.gov/20150000182.pdf>

Ref 6.7-2) Space Launch System Program (SLSP) Flight Software Application Software Assurance Plan (SAP), NASA

<https://archive.org/details/SPACELAUNCHSYSTEMPROGRAMSLSPFLIGHTSOFTWAREAPPLICATIONSOFTWAREASSURANCEPLANSAP/page/n5>

Ref 6.7-3) Component Reliability Data For Use In Probabilistic Safety Assessment, IAEA

https://www-pub.iaea.org/MTCD/Publications/PDF/te_478_web.pdf

Ref 6.7-4) *ELECTRONIC RELIABILITY DESIGN HANDBOOK, MILITARY HANDBOOK*

https://www.navsea.navy.mil/Portals/103/Documents/NSWC_Crane/SD-18/Test%20Methods/MILHDBK338B.pdf

Ref 6.9.1-1) Evans, D., & Schwalbe, J. (2017). *Intercontinental and Their Role In Future Nuclear Forces*. Retrieved from apps.dtic.mil/dtic/tr/fulltext/u2/1033589.pdf

Ref 6.12-1) “Firefly Alpha.” Wikipedia, Wikimedia Foundation, 12 Apr. 2019, en.wikipedia.org/wiki/Firefly_Alpha.

Appendix A: Using Solver to Optimize ΔV Ratios

1. Add Solver to the Excel's Data tab.

- Under Excel “Options,” go to the Add-ins tab, and click on the “Go...” button next to “Manage Excel Add-ins” (Figure A-1). Click the box next to the Solver Add-in option and click “Okay”.

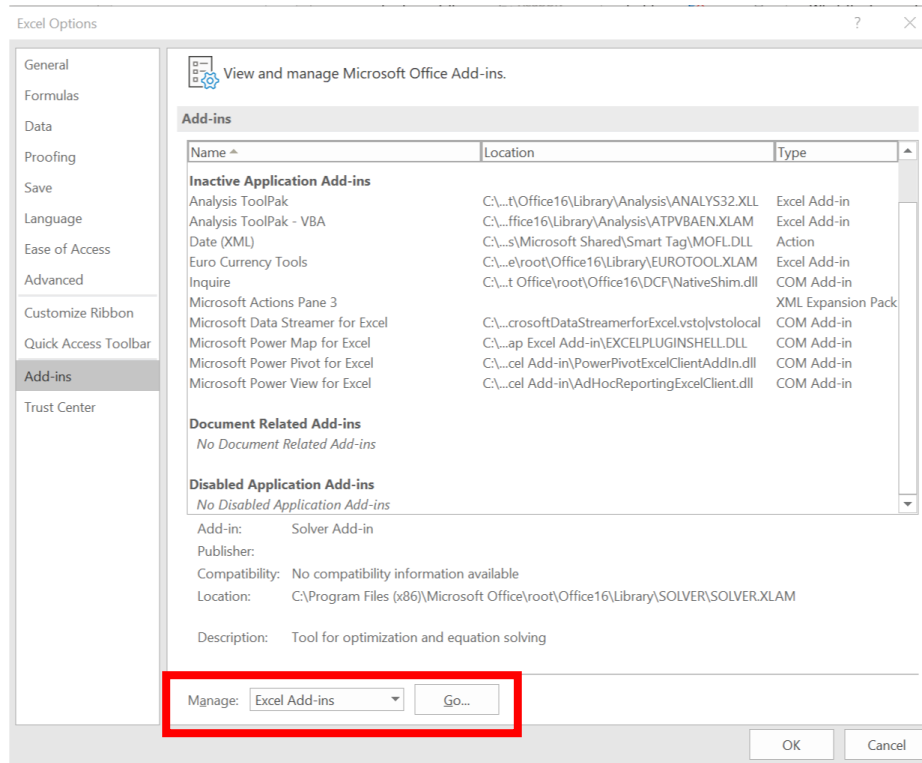


Figure A-1 Adding the Solver Add-in to Excel

2. Make a table that includes each step's I_{sp} and structural factor, g_0 , the required ΔV , and m_{pay} (Figure A-2).

Step No.	Propellant	Isp (s)	Struct, Mass Fraction σ
1	Solid	270	0.1
2	Solid	285	0.1
3	Solid	300	0.1
<hr/>			
g_0 (m/s ²)	9.80665		
<hr/>			
Required ΔV (m/s)	9360.8		
<hr/>			
Payload, RVs (kg)	907.20		
PBV (kg)	300.00		
Hardware, PAF (kg)	90.72		
Total m_{nav} (kg)	1297.92		

Figure A-2 Launch Vehicle Properties

3. Add a table that includes the ΔV for each stage, the total ΔV , and the ratio of each stage's ΔV to the total ΔV . The formula for the stage ΔV is the product of the ratio and the total ΔV . Make all three ratios zero (Figures A-3 and A-4).

Optimum Velocity Ratio			
ΔV_1	0.00	m/s	0.00%
ΔV_2	0.00	m/s	0.00%
ΔV_3	0.00	m/s	0.00%
ΔV_{total}	0.00	m/s	0.00%

Figure A-3 Optimum Velocity Ratio Table

Optimum Velocity Ratio			
ΔV_1	=Required_DV*ratio_1	m/s	0
ΔV_2	=Required_DV*ratio_1	m/s	0
ΔV_3	=Required_DV*ratio_1	m/s	0
ΔV_{total}	=SUM(C31:C33)	m/s	=SUM(E31:E33)

Figure A-4 Optimum Velocity Ratio Formulas

4. Add a table that includes the stage mass ratios, μ_k , initial mass, structural mass, and propellant mass for each step, plus the gross liftoff mass (GLOM). The mass ratios should be calculated using the rocket equation and the ΔV s in the optimum velocity ratio table. The remaining values should be calculated using the initial mass of each stage (Figures A-5 and A-6).

μ_1	1.00	-
μ_2	1.00	-
μ_3	1.00	-
m_{o3}	1442.13	kg
m_{o2}	0.00	kg
m_{o1}	0.00	kg
GLOM	2740.05	kg
m_{s3}	144.21	kg
m_{s2}	0.00	kg
m_{s1}	0.00	kg
m_{p1}	0.00	kg
m_{p2}	0.00	kg
m_{p3}	1297.92	kg

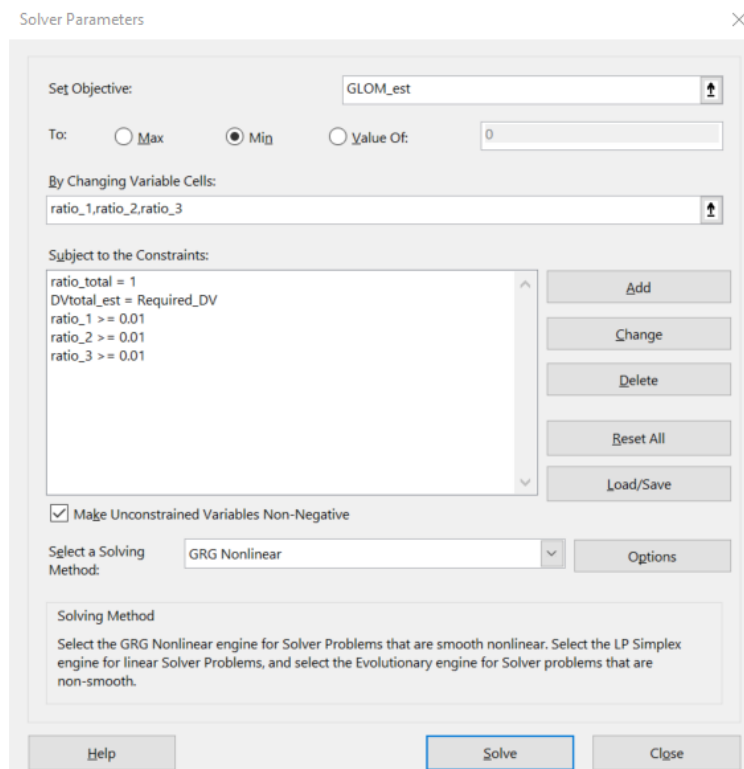
Figure A-5 Mass Ratios and GLOM Table

μ_1	=EXP(DV_1/(isp_1*g0))	-
μ_2	=EXP(DV_2/(isp_2*g0))	-
μ_3	=EXP(DV_3/(isp_3*g0))	-
m_{o3}	=(MR_3)*mpay_est/(1-((MR_3)*sigma_3))	kg
m_{o2}	(((MR_2)-1)*(mo3_est+mpay_est))/(1-((MR_2)*sigma_2))	kg
m_{o1}	(((MR_1)-1)*(mo3_est+mo2_est+mpay_est))/(1-((MR_1)*sigma_1))	kg
GLOM	=SUM(C19:C21)+mpay_est	kg
m_{s3}	=sigma_1*mo3_est	kg
m_{s2}	=sigma_2*mo2_est	kg
m_{s1}	=sigma_3*mo1_est	kg
m_{p1}	=mo1_est-ms1_est	kg
m_{p2}	=mo2_est-ms2_est	kg
m_{p3}	=mo3_est-ms3_est	kg

Figure A-6 Mass Ratios and GLOM Formulas

5. The Solver Add-in can be used to optimize the ΔV ratio of a multistage launch vehicle (Figure A-7).

- For “Set Objective”, click on the cell with the gross liftoff mass calculation.
- Click on the “Min” option in order to minimize the gross liftoff mass.
- Under the “By Changing Variable Cells” field, select the cells containing the velocity ratios for all stages.
- Add the following constraints:
- Make the calculated ΔV_{total} equal to the desired ΔV_{total} .
- For each stage, add a constraint so that the velocity ratio of the stage is greater than or equal to 0.01.
- Add a constraint so that the sum of the ratios is equal to 1.
- Keep the other settings unchanged.
- Click “Solve.” The program will vary the velocity ratios until the minimum gross liftoff mass is found for the vehicle that satisfies the ΔV requirement (Figure A-8).



Solver Parameters

Set Objective: GLOM_est

To: Max Min Value Of: 0

By Changing Variable Cells: ratio_1,ratio_2,ratio_3

Subject to the Constraints:

ratio_total = 1
 DVtotal_est = Required_DV
 ratio_1 >= 0.01
 ratio_2 >= 0.01
 ratio_3 >= 0.01

Make Unconstrained Variables Non-Negative

Select a Solving Method: GRG Nonlinear

Solving Method
 Select the GRG Nonlinear engine for Solver Problems that are smooth nonlinear. Select the LP Simplex engine for linear Solver Problems, and select the Evolutionary engine for Solver problems that are non-smooth.

Help Solve Close

Figure A-7 Solver Parameters for a Three-Stage Vehicle

μ_1	3.25	-	
μ_2	3.05	-	
μ_3	2.89	-	
m_{o3}	5270.75	kg	
m_{o2}	19422.86	kg	
m_{o1}	86602.47	kg	
GLOM	112594.00	kg	
m_{s3}	527.08	kg	
m_{s2}	1942.29	kg	
m_{s1}	8660.25	kg	
m_{p1}	77942.22	kg	
m_{p2}	17480.57	kg	
m_{p3}	4743.68	kg	
Optimum Velocity Ratio			
ΔV_1	3120.27	m/s	33.33%
ΔV_2	3120.27	m/s	33.33%
ΔV_3	3120.27	m/s	33.33%
ΔV_{total}	9360.80	m/s	100.00%

Figure A-8 Solver Results

Appendix B: Trajectory Simulation MATLAB Script Listing

Ascent Function:

```
function [ flight,range,time,burnout,orbit ] = ascent_simulation(
architecture,tstep,pitch_kick,pitch_time,latitude,direction,coast_time,drop_time,Tfrac
)
%% Euler-Integrated Ascent Simulation
% Author: J. David Montes
% Last Update: 05 Mar 2019

% Description: ---

%% Run Conditions
% Select Architecture:
arch = architecture; % 1 or 2
% Time Step:
dt = tstep; % ENTER A FRACTION WITH 1 IN THE NUMERATOR
% Pitch kick and time:
dpitch = deg2rad(pitch_kick);
time.pitch = pitch_time; %integer or multiple of dt
% Select Latitude:
Lat = latitude;
% Launch Direction Angle from Due East
Beta = direction;
% Select coast time and stage drop time:
time.coast = coast_time; %s
time.stage_drop = drop_time; %s

%% Load Data
engine = engine_data(arch,Tfrac);
rocket = stage_info(arch);
load('earth')
load('standard_atmosphere')
load('drag_profile')
%% Relevant Functions
CD = @(M) interp1(Mach,Drag,M); %Drag Coefficient
q = @(r,v) 0.5*r*(v^2); %Dynamic Pressure (Pa)
D = @(C,q) C*q*rocket.S; %Drag (N)
accel = @(T,D,m,g,f) (T/m) - (D/m) - g*sin(f); %Acceleration (m/s^2)
fpdot = @(g,v,h,f) -((g/v) - (v/(earth.R + h))*cos(f)); %Flight Path (rad)
Xdote = @(v,h,f) (earth.R/(earth.R + h))*v*cos(f); %Down-Range Vel. (m/s)
Hdote = @(v,f) v*sin(f); %Vertical Velocity (m/s)
Q = @(v,h) (norm([earth.v(Lat),0] + v*[cosd(Beta),sind(Beta)]).^2)*(earth.R + h)/earth.mu; %Orbital Parameter

%% Initial Calculations
% Stage Timing:
time.burnout = zeros(rocket.stages,1);
time.drop = zeros(rocket.stages,1);
time.start = zeros(rocket.stages,1);
for i = 1:rocket.stages
    if i == 1
        time.burnout(i) = rocket.mp(i)/engine.mdot(i);
        time.drop(i) = time.burnout(i) + time.stage_drop;
    else
        time.start(i) = time.burnout(i-1) + time.coast;
        time.burnout(i) = time.start(i) + rocket.mp(i)/engine.mdot(i);
        time.drop(i) = time.burnout(i) + time.stage_drop;
    end
end
end
```

```

%% Pre-allocate Flight Data Arrays
time.sim = floor(time.burnout(rocket.stages) + 1);
flight.t = (0:dt:time.sim)';
[N,~] = size(flight.t);
flight.m = zeros(N,1);
flight.a = zeros(N,1);
flight.fpdot = zeros(N,1);
flight.v = zeros(N,1);
flight.fp = zeros(N,1);
flight.Xdot = zeros(N,1);
flight.X = zeros(N,1);
flight.Hdot = zeros(N,1);
flight.H = zeros(N,1);
flight.rho = zeros(N,1);
flight.D = zeros(N,1);
flight.g = zeros(N,1);
flight.q = zeros(N,1);
flight.Q = zeros(N,1);
flight.M = zeros(N,1);
flight.T = zeros(N,1);

%% T0 Conditions
flight.m(1) = rocket.glom;
flight.T(1) = engine.T(1,0);
flight.a(1) = accel(flight.T(1),0,flight.m(1),earth.g0,pi/2);
flight.fpdot(1) = 0;
flight.v(1) = 0;
flight.fp(1) = pi/2;
flight.Xdot(1) = 0;
flight.X(1) = 0;
flight.Hdot(1) = 0;
flight.H(1) = 0;
flight.rho(1) = atm.rho(0);
flight.D(1) = 0;
flight.g(1) = earth.g0;
flight.q(1) = 0;
flight.Q(1) = 0;
flight.M(1) = 0;

%% Simulation
stage = 1;
atm_limit = 84900;
for i = 2:N
    %Rely on previous time-step:
    flight.v(i) = flight.v(i-1) + flight.a(i-1)*dt;
    flight.H(i) = flight.H(i-1) + flight.Hdot(i-1)*dt;
    flight.X(i) = flight.X(i-1) + flight.Xdot(i-1)*dt;
    if flight.t(i) == time.pitch
        flight.fp(i) = flight.fp(i-1) - dpitch;
    else
        flight.fp(i) = flight.fp(i-1) + flight.fpdot(i-1)*dt;
    end
    %Rely on current time-step:
    if flight.H(i) > atm_limit
        flight.rho(i) = 0;
        flight.M(i) = flight.M(i-1);
        flight.T(i) = engine.T(stage,atm_limit);
    else
        flight.rho(i) = atm.rho(flight.H(i));
        flight.M(i) = flight.v(i)/atm.a(flight.H(i));
        flight.T(i) = engine.T(stage,flight.H(i));
    end
end

```



```

flight.q(i) = q(flight.rho(i), flight.v(i));
flight.D(i) = D(CD(flight.M(i)), flight.q(i));
flight.g(i) = earth.g(flight.H(i));
flight.fpdot(i) = fpdot(flight.g(i), flight.v(i), flight.H(i), flight.fp(i));
flight.Xdot(i) = Xdot(flight.v(i), flight.H(i), flight.fp(i));
flight.Hdot(i) = Hdot(flight.v(i), flight.fp(i));
flight.Q(i) = Q(flight.v(i), flight.H(i));
%Engine Staging Conditions
if flight.t(i) < time.burnout(stage)
    flight.m(i) = flight.m(i-1) - engine.mdot(stage)*dt;
    if flight.H(i) > atm_limit
        flight.T(i) = engine.T(stage, atm_limit);
    else
        flight.T(i) = engine.T(stage, flight.H(i));
    end
elseif (flight.t(i) > time.burnout(stage)) && (flight.t(i) < (time.burnout(stage)
+ time.coast))
    if abs(flight.t(i) - time.drop(stage)) < (dt/2)
        flight.m(i) = flight.m(i-1) - rocket.ms(stage);
    else
        flight.m(i) = flight.m(i-1);
    end
    flight.T(i) = 0;
elseif (stage == rocket.stages) && (flight.t(i) > time.burnout(stage))
    flight.m(i) = flight.m(i-1);
    flight.T(i) = 0;
elseif (abs(flight.t(i) - time.start(stage+1)) < (dt/2)) || (flight.t(i) >
time.start(stage+1))
    stage = stage + 1;
    flight.m(i) = flight.m(i-1) - engine.mdot(stage)*dt;
    if flight.H(i) > atm_limit
        flight.T(i) = engine.T(stage, atm_limit);
    else
        flight.T(i) = engine.T(stage, flight.H(i));
    end
end
flight.a(i) = accel(flight.T(i), flight.D(i), flight.m(i), flight.g(i), flight.fp(i));
end
burnout.Q = flight.Q(end);
burnout.fp = flight.fp(end);
burnout.R = (earth.R + flight.H(end)); %m

orbit.e = sqrt(1 + burnout.Q*(burnout.Q - 2)*(cos(burnout.fp)^2));
orbit.a = burnout.R/(2 - burnout.Q);
orbit.re.r = earth.R + atm_limit;

r = @(a,e,t) a*((1 - e^2)./(1 + e*cos(t)));
rbo = @(t) r(orbit.a, orbit.e, t) - burnout.R;
rre = @(t) r(orbit.a, orbit.e, t) - orbit.re.r;
BOA = fzero(rbo, pi);
REA = fzero(rre, 2*pi);

range.angle.FF = abs(REA - BOA);

% range.angle.FF = 2*acos((1 - burnout.Q*(cos(burnout.fp)^2))/sqrt(1 +
burnout.Q*(burnout.Q - 2)*(cos(burnout.fp)^2)));
range.angle.PW = flight.X(end)/earth.R;
range.sym.angle = range.angle.FF + range.angle.PW;
range.sym.km = range.sym.angle*earth.R/1000;
range.sym.nm = range.sym.angle*3440;

```

```

orbit.E1 = acos((orbit.e - cos(range.angle.FF/2))/(1 -
orbit.e*cos(range.angle.FF/2)));
orbit.flight_time = 2*sqrt((orbit.a^3)/earth.mu)*(pi - orbit.E1 +
orbit.e*sin(orbit.E1));
time.sym.total_flight = (orbit.flight_time + 2*flight.t(end))/60;
if Beta == 0
    range.sym.spin_nm = -earth.rot*3440*orbit.flight_time;
    range.sym.spin_km = -(earth.rot*earth.R/1000)*orbit.flight_time;
elseif Beta == 180
    range.sym.spin_nm = earth.rot*3440*orbit.flight_time;
    range.sym.spin_km = (earth.rot*earth.R/1000)*orbit.flight_time;
end
range.sym.tot_km = range.sym.km + range.sym.spin_km;

orbit.re.h = atm_limit;
orbit.re.v = sqrt(2*earth.mu*(1/orbit.re.r - 1/(2*orbit.a)));
orbit.re.Q = 2 - orbit.re.r/orbit.a;
orbit.re.fp = -acos(sqrt((orbit.e^2 - 1)/(orbit.re.Q*(orbit.re.Q - 2))));
end

```

Re-entry function:

```

function [ fli,ran,tim ] = re_entry( re_entry_vehicle,time_step,det_alt,entry_pitch )
%% Euler-Integrated Re-entry Simulation
% Author: J. David Montes
% Last Update: 10 Apr 2019

% Description: ---

%% Run Conditions
% Time Step:
dt = time_step; % ENTER A FRACTION WITH 1 IN THE NUMERATOR
% Simulation time:
sim_time = 500;
% Alt at Detonation:
det_H = det_alt;
% RV Parameters
rv = re_entry_vehicle;

%% Load Data
load('earth')
load('standard_atmosphere')
load('drag_rv')
load('flightdata')
time.asc = time.sim;

%% Relevant Functions
CD = @(M) interp1(Mach,Drag,M); %Drag Coefficient
CL = @(M) rv.LD*CD(M);
q = @(r,v) 0.5*r*(v^2); %Dynamic Pressure (Pa)
D = @(C,q) C*q*rv.S; %Drag (N)
L = @(C,q) C*q*rv.S;
heat = @(r,R,v) (1.7415e-4)*((r/R)^0.5)*v^3;
temp = @(q) (q/(0.75*5.67e-8))^0.25;
accel = @(T,D,m,g,f) (T/m) - (D/m) - g*sin(f); %Acceleration (m/s^2)
fpdot = @(L,m,g,v,h,f) (L/(m*v)) - ((g/v) - (v/(earth.R + h)))*cos(f); %Flight
Path (rad)
Xdote = @(v,h,f) (earth.R/(earth.R + h))*v*cos(f); %Down-Range Vel. (m/s)
Hdote = @(v,f) v*sin(f); %Vertical Velocity (m/s)

```

```

%% Pre-allocate Flight Data Arrays
time.sim = sim_time;
flight.t = (0:dt:time.sim)';
[N,~] = size(flight.t);
flight.a = zeros(N,1);
flight.fpdot = zeros(N,1);
flight.v = zeros(N,1);
flight.fp = zeros(N,1);
flight.Xdot = zeros(N,1);
flight.X = zeros(N,1);
flight.Hdot = zeros(N,1);
flight.H = zeros(N,1);
flight.rho = zeros(N,1);
flight.D = zeros(N,1);
flight.L = zeros(N,1);
flight.g = zeros(N,1);
flight.q = zeros(N,1);
flight.Q = zeros(N,1);
flight.M = zeros(N,1);
flight.T = zeros(N,1);
flight.heat = zeros(N,1);
flight.m = rv.m*ones(N,1);

%% T0 Conditions
flight.v(1) = orbit.re.v;
flight.H(1) = orbit.re.h;
flight.fp(1) = orbit.re.fp - deg2rad(entry_pitch);
flight.rho(1) = atm.rho(flight.H(1));
flight.q(1) = q(flight.rho(1),flight.v(1));
flight.g(1) = earth.g(flight.H(1));
flight.Hdot(1) = Hdot(flight.v(1),flight.fp(1));
flight.Xdot(1) = Xdot(flight.v(1),flight.H(1),flight.fp(1));
flight.M(1) = flight.v(1)/atm.a(flight.H(1));
flight.D(1) = D(CD(flight.M(1)),flight.q(1));
flight.L(1) = L(CL(flight.M(1)),flight.q(1));
flight.fpdot(1) =
fpdot(flight.L(1),rv.m,flight.g(1),flight.v(1),flight.H(1),flight.fp(1));
flight.a(1) = accel(0,flight.D(1),rv.m,flight.g(1),flight.fp(1));

Rn = 0.03;
%% Simulation
J = 0;
maneuver = 0;
for i = 2:N
    flight.v(i) = flight.v(i-1) + flight.a(i-1)*dt;
    flight.H(i) = flight.H(i-1) + flight.Hdot(i-1)*dt;
    if ((abs(flight.H(i)) < det_H) || (flight.H(i) < 0)) && (J == 0)
        J = i;
    end
    flight.X(i) = flight.X(i-1) + flight.Xdot(i-1)*dt;
    flight.fp(i) = flight.fp(i-1) + flight.fpdot(i-1)*dt;

    if (flight.fp(i) > rv.fp_limits(2)) && (rv.LD > 0) && (maneuver < rv.maneuvers)
        rv.LD = -rv.LD;
        CL = @(M) rv.LD*CD(M);
        maneuver = maneuver + 1;
    elseif (flight.fp(i) < rv.fp_limits(1)) && (rv.LD < 0) && (maneuver <
rv.maneuvers)
        rv.LD = -rv.LD;
        CL = @(M) rv.LD*CD(M);
        maneuver = maneuver + 1;
    elseif (flight.fp(i) < rv.fp_limits(1)) && (maneuver == rv.maneuvers)
        rv.LD = 0;

```

```

        CL = @(M) rv.LD*CD(M);
    end

    flight.rho(i) = atm.rho(flight.H(i));
    flight.heat(i) = heat(flight.rho(i),Rn,flight.v(i));
    flight.T(i) = temp(flight.heat(i));
    flight.M(i) = flight.v(i)/atm.a(flight.H(i));
    flight.q(i) = q(flight.rho(i),flight.v(i));
    flight.D(i) = D(CD(flight.M(i)),flight.q(i));
    flight.L(i) = L(CL(flight.M(i)),flight.q(i));
    flight.g(i) = earth.g(flight.H(i));
    flight.fpdot(i) =
fpdot(flight.L(i),rv.m,flight.g(i),flight.v(i),flight.H(i),flight.fp(i));
    flight.Xdot(i) = Xdot(flight.v(i),flight.H(i),flight.fp(i));
    flight.Hdot(i) = Hdot(flight.v(i),flight.fp(i));

    flight.a(i) = accel(flight.T(i),flight.D(i),flight.m(i),flight.g(i),flight.fp(i));
end
if J > 0
    flight.v = flight.v(1:J);
    flight.H = flight.H(1:J);
    flight.X = flight.X(1:J);
    flight.fp = flight.fp(1:J);
    flight.rho = flight.rho(1:J);
    flight.M = flight.M(1:J);
    flight.D = flight.D(1:J);
    flight.L = flight.L(1:J);
    flight.g = flight.g(1:J);
    flight.fpdot = flight.fpdot(1:J);
    flight.Xdot = flight.Xdot(1:J);
    flight.Hdot = flight.Hdot(1:J);
    flight.a = flight.a(1:J);
    flight.q = flight.q(1:J);
    flight.t = flight.t(1:J);
    flight.T = flight.T(1:J);
    flight.heat = flight.heat(1:J);
end

time.entry = flight.t(end);
time.to_target = time.asc + orbit.flight_time + time.entry;
range.true.km = ((range.angle.FF + range.angle.PW)*earth.R + flight.X(end))/1000 +
range.sym.spin_km;
range.true.nm = (range.angle.FF + range.angle.PW)*3440 + flight.X(end)*0.000539957 +
range.sym.spin_nm;

fli = flight;
ran = range;
tim = time;

end

```